

We put science to work.™



**Savannah River  
National Laboratory™**

OPERATED BY SAVANNAH RIVER NUCLEAR SOLUTIONS

A U.S. DEPARTMENT OF ENERGY NATIONAL LABORATORY • SAVANNAH RIVER SITE • AIKEN, SC

# FY13 Glycolic-Nitric Acid Flowsheet Demonstrations of the DWPF Chemical Process Cell with Simulants

D. P. Lambert  
J. R. Zamecnik  
D. R. Best

SRNL-STI-2013-00343, Revision 0  
March 2014

Prepared for the U.S. Department of Energy  
under contract number DE-AC09-08SR22470.

SRNL.DOE.GOV

**DISCLAIMER**

This work was prepared under an agreement with and funded by the U.S. Government. Neither the U.S. Government or its employees, nor any of its contractors, subcontractors or their employees, makes any express or implied:

1. warranty or assumes any legal liability for the accuracy, completeness, or for the use or results of such use of any information, product, or process disclosed; or
2. representation that such use or results of such use would not infringe privately owned rights; or
3. endorsement or recommendation of any specifically identified commercial product, process, or service.

Any views and opinions of authors expressed in this work do not necessarily state or reflect those of the United States Government, or its contractors, or subcontractors.

**Printed in the United States of America**

**Prepared for  
U.S. Department of Energy**

We put science to work.™



**Savannah River  
National Laboratory™**

OPERATED BY SAVANNAH RIVER NUCLEAR SOLUTIONS

A U.S. DEPARTMENT OF ENERGY NATIONAL LABORATORY • SAVANNAH RIVER SITE • AIKEN, SC

# FY13 Glycolic-Nitric Acid Flowsheet Demonstrations of the DWPF Chemical Process Cell with Simulants

D. P. Lambert  
J. R. Zamecnik  
D. R. Best

SRNL-STI-2013-00343, Revision 0  
March 2014

Prepared for the U.S. Department of Energy  
under contract number DE-AC09-08SR22470.

SRNL.DOE.GOV

## REVIEWS AND APPROVALS

## AUTHORS:

Don Lambert 3/13/14  
 D. P. Lambert, Process Technology Programs Date

DPL for J.R. Zamecnik 3/14/14  
 J. R. Zamecnik, Process Technology Programs Date

David Best 3/13/14  
 D. R. Best, Process Technology Programs Date

## TECHNICAL REVIEW:

J.D. Newell 3/14/14  
 J. D. Newell, Process Technology Programs Date

DPL for M.E. Stone 3/14/14  
 M. E. Stone, Process Technology Programs Date

## APPROVAL:

D.H. McGuire 3/17/14  
 D. H. McGuire, Manager Date  
 Process Technology Programs

Sharon Marra 3/24/14  
 S. L. Marra, Manager Date  
 Environmental & Chemical Process Technology Research Programs

E.J. Freed 4-1-14  
 E. J. Freed, Manager Date  
 Waste Solidification Engineering

## **PREFACE OR ACKNOWLEDGEMENTS**

The experiments documented in this report were complicated and required the support of many people. A special thanks to the following for their significant support:

- The experiments were completed around the clock for twelve days, with the only break being the weekend. Jon Duvall, Phyllis Workman, Vickie Williams, and David Healy provided the coverage with Vern Bush and Wanda Matthews filling in as needed. Their excellent work is greatly appreciated.
- These experiments generated 150 samples; most were analyzed by PSAL. Special thanks to David Best, Whitney Riley, Beverly Wall, and Kim Wyszynski for all the sample results. Thanks also to Tom White, Steve Crump, and Amy Ekechukwu of AD with their support for anion, cation, carbon, and volatile organic analysis.
- These experiments used three offgas analyzers, which greatly increased our understanding of the offgas during processing. Special thanks to Frances Williams and John Pareizs for preparing the GCs for these runs and reprocessing the post run data. Thanks also to Jack Zamecnik for setting up, calibrating, running and interpreting the data from the FTIR and Mass Spec.
- Thanks to Tom Peters for providing the Next Generation Solvent for the SRAT cycles.
- Thanks to David Newell for providing the ARP simulant for the SRAT cycles.

## EXECUTIVE SUMMARY

Savannah River Remediation is evaluating changes to its current Defense Waste Processing Facility flowsheet to replace formic acid with glycolic acid in order to improve processing cycle times and decrease by approximately 100x the production of hydrogen, a potentially flammable gas. Higher throughput is needed in the Chemical Processing Cell since the installation of the bubblers into the melter has increased melt rate. Due to the significant maintenance required for the safety significant gas chromatographs and the potential for production of flammable quantities of hydrogen, eliminating the use of formic acid is highly desirable. Previous testing at the Savannah River National Laboratory has shown that replacing formic acid with glycolic acid allows the reduction and removal of mercury without significant catalytic hydrogen generation.

Five back-to-back Sludge Receipt and Adjustment Tank (SRAT) cycles and four back-to-back Slurry Mix Evaporator (SME) cycles were successful in demonstrating the viability of the nitric/glycolic acid flowsheet. The testing was completed in FY13 to determine the impact of process heels (approximately 25% of the material is left behind after transfers). In addition, back-to-back experiments might identify longer-term processing problems. The testing was designed to be prototypic by including sludge simulant, Actinide Removal Product simulant, nitric acid, glycolic acid, and Strip Effluent simulant containing Next Generation Solvent in the SRAT processing and SRAT product simulant, decontamination frit slurry, and process frit slurry in the SME processing. A heel was produced in the first cycle and each subsequent cycle utilized the remaining heel from the previous cycle. Lower SRAT purges were utilized due to the low hydrogen generation. Design basis addition rates and boilup rates were used so the processing time was shorter than current processing rates.

Significant processing findings identified in the five SRAT cycles include:

- Low hydrogen generation (<0.0005 lb/hr hydrogen peak, <0.077% of SRAT limit of 0.65 lb/hr). This is 0.25% of the Lower Flammability Limit.
- Complete destruction of nitrite in SRAT cycle
- Stable SRAT slurry pH post acid addition (<5)
- Several small foamovers were noted
- No fouling of heating rods (similar to steam coils)
- There was less elemental mercury and more dark crystalline mercury recovered in subsequent cycles. Some of the mercury, likely a mercury film on a gas bubble, floated and some bypassed the Mercury Water Wash Tank without being collected. This has not been noted in previous simulant testing.
- No dimethyl mercury generation was detected by the mass spectrometer
- Hexamethyldisiloxane, an antifoam degradation product, was detected by the mass spectrometer and Fourier Transformed InfraRed analyzer. This may be useful in determining the effectiveness of the antifoam
- Oxygen was completely consumed in 3 of the 5 cycles, just after initiating boiling
- The REDOX measured in the glass product made by combining the SRAT product with frit at 36% waste loading was 0.46 – 0.55  $\text{Fe}^{2+}/\Sigma\text{Fe}$ , much higher than the 0.1 target.
- No detectable ammonia was removed by the Ammonia Scrubber

Significant processing findings identified in the four SME cycles include:

- Low hydrogen generation (<0.0076 lb/hr hydrogen peak, 3.4% of SME limit of 0.228 lb/hr). This is 0.63% of the Lower Flammability Limit.
- Stable pH throughout SME processing (<5)

- The heating rods (similar to steam coils) were fouled by thick deposits during the later decon water evaporation and frit dewater stages of the SME cycle.
- The REDOX measured in glass made from SME Product was (0.22 – 0.28  $\text{Fe}^{2+}/\Sigma\text{Fe}$ ). There was no REDOX target for the SME cycles as the ratio of oxidants and reductants was established by the SRAT product used for this testing. No nitric acid or glycolic acid was used in this testing.
- No detectable ammonia was removed by the Ammonia Scrubber

#### Recommendations for Improving R&D testing

- Complete the SRAT cycles using the same recipe as a previous successful experiment. In these experiments, the REDOX was high and this could have been prevented by completing a series of SRAT cycles first and using the conditions from the optimum experiment for the back-to-back experiments. In addition, the product from the optimum experiment could serve as the heel so that each experiment would include a heel.
- Videotaping the experiments throughout is also recommended. This would help to identify when foamovers happen and help to understand the collection of mercury in the MWWT. In addition, making sure a camera was present in the lab for still photos is essential in documenting interesting observations.
- This testing was completed at design basis conditions. Future testing should be completed at prototypic processing conditions. This will lengthen the testing but will be more realistic as it would duplicate the time at temperature, which affects antifoam degradation, antifoam addition amount, anion destruction, and steam stripping.
- Varying the conditions for the five runs will allow gathering more information in an attempt to better understand DWPF SRAT processing. Runs GN61-64 were identical. For example, varying the SRAT dewater amount would allow testing at various slurry rheologies to help in understanding rheological impacts such as fouling of coils.
- Digestion and analysis of the collected MWWT mercury would help in determining the mass of Hg collected. The mass of mercury is likely overestimated, as the assumption is that it is elemental Hg. For example, if some of the mercury is present as calomel ( $\text{Hg}_2\text{Cl}_2$ ) or mercuric oxide, the Hg mass can be overestimated by 15%. Although the mercury is dried out in the dessicator, there is likely some water, sludge solids and antifoam present with the mercury. Identification of the forms of mercury is also suggested.
- DWPF rarely transfers mercury or drains the Mercury Water Wash Tank. Consider returning the contents of the Mercury Water Wash Tank after previous run to better simulate processing conditions instead of starting with a clean vessel and distilled water.
- The presence of ARP and MCU strip effluent make a huge difference in processing. These should be included in future experiments as much as possible. However, the organic added with the strip effluent likely has no impact on processing and could be eliminated. The solvent was added to the kettles as planned in only two of the five experiments – in two of the experiments it was added too slowly and then sped up and in a third experiment the syringe pump was bumped, adding the remaining contents faster than planned. Elimination of the solvent feed would also simplify the experiments without losing significant processing information.

#### Recommendations to improve the project or plant operations

- An improved REDOX equation is needed to produce melter feed with the appropriate REDOX ratio.

- At the conclusion of ARP and strip effluent additions, the steam flow should be reduced to keep from overheating vessel contents. This is likely the cause of some foamovers in DWPF.
- A good practice to minimize coil fouling is to monitor the steam pressure and steam flow. There should be a direct correlation between flow and pressure. When it takes more pressure to get the same flow, the slurry is either very thick or the coils are starting to foul.
- Another good practice is to calculate the steam coil heat transfer coefficient and monitor this during boiling. It would be expected to decrease slightly as the slurry is concentrated but recovering to the same value after each decon blast or frit slurry addition.

## TABLE OF CONTENTS

LIST OF TABLES .....	xi
LIST OF FIGURES .....	xii
LIST OF ABBREVIATIONS .....	xiv
1.0 Introduction .....	1
2.0 Experimental Procedure .....	1
2.1 CPC Simulation Details .....	1
2.2 Sludge, SRAT Product, ARP and MCU Slurries Used in Testing .....	4
2.3 Process Assumptions .....	8
2.3.1 Back to Back SRAT Process Assumptions .....	8
2.3.2 Back to Back SME Process Assumptions .....	9
2.4 Analytical Methods.....	10
2.4.1 Slurry Analytical Methods .....	10
2.4.2 Offgas Methods.....	10
3.0 Results and Discussion.....	13
Back to Back SME simulations using SRAT Product Blend and Frit 418 .....	13
3.1 GN60-64 Back to Back SRAT Simulations with heels with ARP and MCU.....	13
3.1.1 GN60-64 SRAT Products .....	13
3.1.1.1 GN60-64 SRAT Product Elemental Results by ICP-AES .....	14
3.1.1.2 GN60-64 SRAT Product Solids, Density and pH .....	16
3.1.1.3 GN60-64 SRAT Product Anion Results .....	16
3.1.2 GN60-64 MWWT .....	17
3.1.3 GN60-64 Post Run FAVC, Dewater, and SMECT samples .....	19
3.1.3.1 GN60-64 Post Run FAVC Sample Results.....	20
3.1.3.2 GN60-64 Post Run SMECT Sample Results .....	20
3.1.3.3 GN60-64 Post Run Dewater Sample Results.....	20
3.1.4 GN60-64 Offgas.....	20
3.1.4.1 GN60-64 Gas Chromatograph .....	20
3.1.4.2 GN60-64 Mass Spec and FTIR .....	23
3.1.5 GN60-64 pH.....	36
3.1.6 GN60-64 ARP.....	37
3.1.7 GN60-64 MCU.....	39
3.1.8 GN60-64 SRAT Heating Rod Heat Transfer .....	40
3.1.9 GN60-64 REDOX.....	42

3.1.10 GN60-64 Ammonia Scrubber .....	42
20.....	43
<10 .....	43
22.....	43
3.1.11 GN60-64 Lessons Learned.....	43
3.2 GN65-68 Back to Back SME Simulations using GN SRAT Product Blend and Frit 418...	44
3.2.1 GN65-68 SME Product.....	44
3.2.2 GN65-68 Dewater Samples.....	48
3.2.3 GN65-68 In Process Supernate Samples.....	49
3.2.4 GN66-68 Post Run FAVC, and SMECT samples.....	53
3.2.4.1 GN65-68 Post Run FAVC Sample Results.....	53
3.2.4.2 GN65-68 Post Run CondensateSample Results.....	53
3.2.5 GN65-68 Offgas.....	53
3.2.6 GN65-68 pH.....	56
3.2.7 GN65-68 SME Heating Rod Heat Transfer .....	56
3.2.8 GN65-68 SME Foaming .....	58
3.2.9 GN65-68 SME Anion Destruction.....	58
3.2.10 GN65-68 SME REDOX.....	59
3.2.11 GN65-68 Ammonia Scrubber .....	59
3.2.12 GN65-68 Lessons Learned.....	59
4.0 Conclusions .....	61
5.0 Recommendations, Path Forward or Future Work.....	62
6.0 References .....	64

## LIST OF TABLES

Table 2-1. SB6I Sludge Simulant Composition .....	5
Table 2-2. SB6 SRAT Product Blend Composition .....	6
Table 2-3. ARP Simulant Composition.....	7
Table 2-4. MCU Simulant Composition .....	7
Table 2-5. MCU Solvent Composition.....	7
Table 2-6. Nitric and Glycolic Acid Concentration .....	8
Table 2-7. Frit 418.....	8
Table 2-8. GN60-64 Process Assumptions.....	9
Table 2-9. GN60-64 Process Assumptions.....	10
Table 2-10. Mass Spectrometer Calibration Gases .....	11
Table 3-1. Summary of Runs Performed.....	13
Table 3-2. SRAT Processing Time Line .....	13
Table 3-3: SRAT Product Slurry Cation Concentration, wt % calcined solids.....	14
Table 3-4: SRAT Product Supernate Cation Concentration, mg/L.....	15
Table 3-5: SRAT Product Cation Solubility, % .....	15
Table 3-6: SRAT Product Solids, Density and pH.....	16
Table 3-7: SRAT Product Slurry Anions, mg/kg .....	16
Table 3-8: SRAT Product Supernate Anions, mg/L.....	17
Table 3-9: SRAT Product Anion Solubility, % .....	17
Table 3-10: Peak Off Gas Generation Rates (lb/hr) .....	23
Table 3-11. Solvent Component Mass Balance.....	40
Table 3-12. Ammonia Scrubbers Sample Results .....	43
Table 3-13. SME Processing Time Line .....	44
Table 3-14. SME Product Slurry Cation Composition, wt % Calcined Solids .....	45
Table 3-15. SME Product Slurry Anion Results .....	45
Table 3-16. SME Product Solids, pH and Density Compositions.....	46
Table 3-17. SME Product Supernate Cation Composition, mg/L .....	46

Table 3-18. SME Product Supernate Anion Composition, mg/L.....	47
Table 3-19. SME Product Anion Solubility, % .....	47
Table 3-20. SME Product Anion Solubility, % .....	48
Table 3-21. Inprocess Dewater Analysis by ICP-AES, mg/L .....	49
Table 3-22. In Process Supernate Analysis by IC, mg/L.....	51
Table 3-23. In Pprocess Supernate Analysis by ICP-AES, mg/L.....	52
Table 3-24. SME Cycle Anion Destruction .....	59
Table 3-25. SME REDOX.....	59
Table 3-26. Ammonia Scrubbers Sample Results .....	59

## LIST OF FIGURES

Figure 2-1. Sketch of Experimental Setup .....	2
Figure 3-1. Black Solids Coating Drain Leg from Condenser to MWWT.....	18
Figure 3-2. Floating Bubbles with Solids in MWWT .....	18
Figure 3-3. Foamover in MWWT during SRAT Cycle GN64.....	19
Figure 3-4. Mercury in MWWT at Completion of Five Back-to-Back SRAT Cycles.....	19
Figure 3-5: Measured CO <sub>2</sub> Concentration .....	21
Figure 3-6: Measured N <sub>2</sub> O Concentration.....	22
Figure 3-7: Measured O <sub>2</sub> Concentration.....	22
Figure 3-8: Structure of hexamethyldisiloxane (HMDSO) .....	23
Figure 3-9: Structure of trimethylsilanol (TMS).....	23
Figure 3-10: Structure of hexamethylcyclotrisiloxane (D3) or octamethyltrisiloxane (L3).....	24
Figure 3-11: IR Spectra of Gas Sample, HMDSO, Isooctane, Hexadecane, and Dodecane .....	24
Figure 3-12: Sample from GN62 Subtracting HMDSO at 750-1300 cm <sup>-1</sup> .....	25
Figure 3-13: Sample from GN62 Subtracting HMDSO – Effect at 2800-3000 cm <sup>-1</sup> .....	25
Figure 3-14: Sample from GN62 Subtracting Isooctane at 2800-3000 cm <sup>-1</sup> .....	26
Figure 3-15: Sample from GN62 Subtracting n-Dodecane at 2800-3000 cm <sup>-1</sup> .....	26

Figure 3-16: Subtraction of HMDSO from Sample Spectrum .....	27
Figure 3-17: Subtraction of TMS from Sample Spectrum .....	27
Figure 3-18: Mass Spectrum of Dimethylmercury .....	28
Figure 3-19: Dimethylmercury Mass Signal Intensities Compared to Background.....	28
Figure 3-20: GN60 Isopar, HMDSO, and CO <sub>2</sub> Concentration.....	29
Figure 3-21: GN60 NO, NO <sub>2</sub> , N <sub>2</sub> O, and CO <sub>2</sub> Concentration .....	30
Figure 3-22: GN61 HMDSO, Isooctane, C <sub>4</sub> H <sub>9</sub> fragment, and CO <sub>2</sub> Concentration .....	31
Figure 3-23: GN61 Mass Spec Masses 50, 57, 105, 122, and 137.....	32
Figure 3-24: GN62 Isopar, Isooctane, C <sub>4</sub> H <sub>9</sub> , C <sub>5</sub> H <sub>11</sub> , HMDSO, and CO <sub>2</sub> Concentration .....	33
Figure 3-25: GN62 FTIR NO, NO <sub>2</sub> , N <sub>2</sub> O, and CO <sub>2</sub> Concentration.....	33
Figure 3-26: GN63 HMDSO, Isopar-L, and CO <sub>2</sub> Concentration .....	34
Figure 3-27: GN63 Isopar, Isooctane, C <sub>4</sub> H <sub>9</sub> , G <sub>5</sub> H <sub>11</sub> , HMDSO, and CO <sub>2</sub> Concentration.....	34
Figure 3-28: GN63 NO, NO <sub>2</sub> , N <sub>2</sub> O, N <sub>y</sub> O <sub>x</sub> , and CO <sub>2</sub> Concentration .....	35
Figure 3-29: GN64 Isopar, Isooctane, C <sub>4</sub> H <sub>9</sub> , G <sub>5</sub> H <sub>11</sub> , HMDSO, and CO <sub>2</sub> Concentration.....	35
Figure 3-30: GN64 NO, NO <sub>2</sub> , N <sub>2</sub> O, and CO <sub>2</sub> Concentration .....	36
Figure 3-31. SRAT Cycle pH Profile .....	37
Figure 3-32. GN62 SRAT Cycle Condenser Temperature Profile.....	39
Figure 3-33. SRAT Heat Transfer Coefficient Profile .....	41
Figure 3-34. SRAT Power Input Profile.....	42
Figure 3-35. SME Formate Concentration, mg/kg .....	50
Figure 3-36. SME Nitrate, Glycolate Concentration, mg/kg.....	50
Figure 3-37: SME Measured Hydrogen Concentration, volume % .....	54
Figure 3-38: SME Measured Carbon Dioxide Concentration, volume % .....	54
Figure 3-39: SME Nitrogen versus Oxygen Concentration, volume % .....	55
Figure 3-40: SME cycle pH.....	56
Figure 3-41: SME Cycle Heat Transfer Coefficient Profile.....	57
Figure 3-42: SME Cycle Fouled Rod Deposits .....	58

## LIST OF ABBREVIATIONS

AD	Analytical Development
ARP	Actinide Removal Process
BDL	Below Detection Limit
BobCalix	Calix[4]arene-bis(t-octylbenzo-crown-6)
CPC	Chemical Process Cell
DMM	Dimethylmercury
DWPF	Defense Waste Processing Facility
FAVC	Formic Acid Vent Condenser
FTIR	Fourier Transform InfraRed
GC	Gas Chromatograph
GN	Glycolic Acid/Nitric Acid
HMDSO	Hexamethyldisiloxane
IC	Ion Chromatography
ICP-AES	Inductively Coupled Plasma-Atomic Emission Spectroscopy
KAMA	Koopman Acid Minimum Amount
LFL	Lower Flammability Limit
MaxCalix	1,3- <i>alt</i> -25,27-Bis(3,7-dimethyloctyl-1-oxy)calix[4]arene-benzocrown-6
MCU	Modular Caustic-side Solvent Extraction Unit
Modifier	1-(2,2,3,3-Tetrafluoropropoxy)-3-(4- <i>sec</i> -butylphenoxy)-2-propanol
MS	Mass Spectrometer
MWWT	Mercury Water Wash Tank
NM	Not Measured
PSAL	Process Science Analytical Laboratory
REDOX	Reduction/Oxidation
SME	Slurry Mix Evaporator
SMECT	Slurry Mix Evaporator Condensate Tank
SRAT	Sludge Receipt and Adjustment Tank
SRNL	Savannah River National Laboratory
SRR	Savannah River Remediation
TIC	Total Inorganic Carbon Analysis
TIDG	N,N',N''-tris(3,7-dimethyloctyl)guanidine
TOC	Total Organic Carbon Analysis
TT&QAP	Task Technical and Quality Assurance Plan

## 1.0 Introduction

Savannah River Remediation (SRR) is evaluating changes to its current Defense Waste Processing Facility (DWPF) flowsheet to reduce facility hazards and improve processing cycle times. The focus of the project is to reduce facility hazards related to formic acid, to improve pH stability, rheological control, and have lower offgas production compared to the nitric-formic acid flowsheet. It will also enable the facility to have a greater ability to support higher canister production while maximizing waste loading. Higher throughput is needed in the Chemical Processing Cell (CPC) since the installation of the bubblers into the melter has increased melt rate. Due to the significant maintenance required for the DWPF gas chromatographs (GC) and the potential for production of flammable quantities of hydrogen, eliminating the use of formic acid in the CPC is being developed. Work at Savannah River National Laboratory (SRNL) has shown that replacing formic acid with glycolic acid allows the reduction and removal of mercury in the SRAT without any significant catalytic hydrogen generation.<sup>1,2,3,4</sup>

The objective of the testing detailed in this document is to determine the viability of the nitric-glycolic acid flowsheet in processing sludge in back to back runs as requested by DWPF<sup>5</sup>. This work was performed under the guidance of Task Technical and Quality Assurance Plan (TT&QAP)<sup>6</sup>.

## 2.0 Experimental Procedure

The experimental apparatus used in these experiments is typical for DWPF SRAT and SME testing. The experiments were performed in 4-L kettles. The test equipment included a GC to measure off-gas composition, an ammonia scrubber, and a pH meter. In all runs, the SRNL acid calculation spreadsheet used the Koopman equation<sup>7</sup> to determine acid addition quantities and dewater targets. In the SRAT testing, a Fourier Transformed InfraRed (FTIR) and Mass Spectrometer (MS) were used to monitor the offgas composition.

### 2.1 CPC Simulation Details

The back-to-back SRAT cycles (GN60-64) used a single SRAT 4-L rig that was assembled following the guidelines of SRNL-3100-2011-00127.<sup>8</sup> A glass kettle is used to replicate the SRAT, and it is connected to the SRAT Condenser, the Mercury Water Wash Tank (MWWT), and the Formic Acid Vent Condenser (FAVC). The Slurry Mix Evaporator Condensate Tank (SMECT) is represented by a sampling bottle that is used to remove condensate through the MWWT. For the purposes of this paper, the condensers and MWWT are referred to as the off-gas components. A sketch of the experimental setup is given in Figure 2-1.

The back-to-back SME cycles (GN65-68) used a similar set up with an empty MWWT. A glass kettle is used to replicate the SME, and it is connected to the SME Condenser, and the FAVC. The Slurry Mix Evaporator Condensate Tank (SMECT) is represented by a sampling bottle that is used to remove condensate through the MWWT.

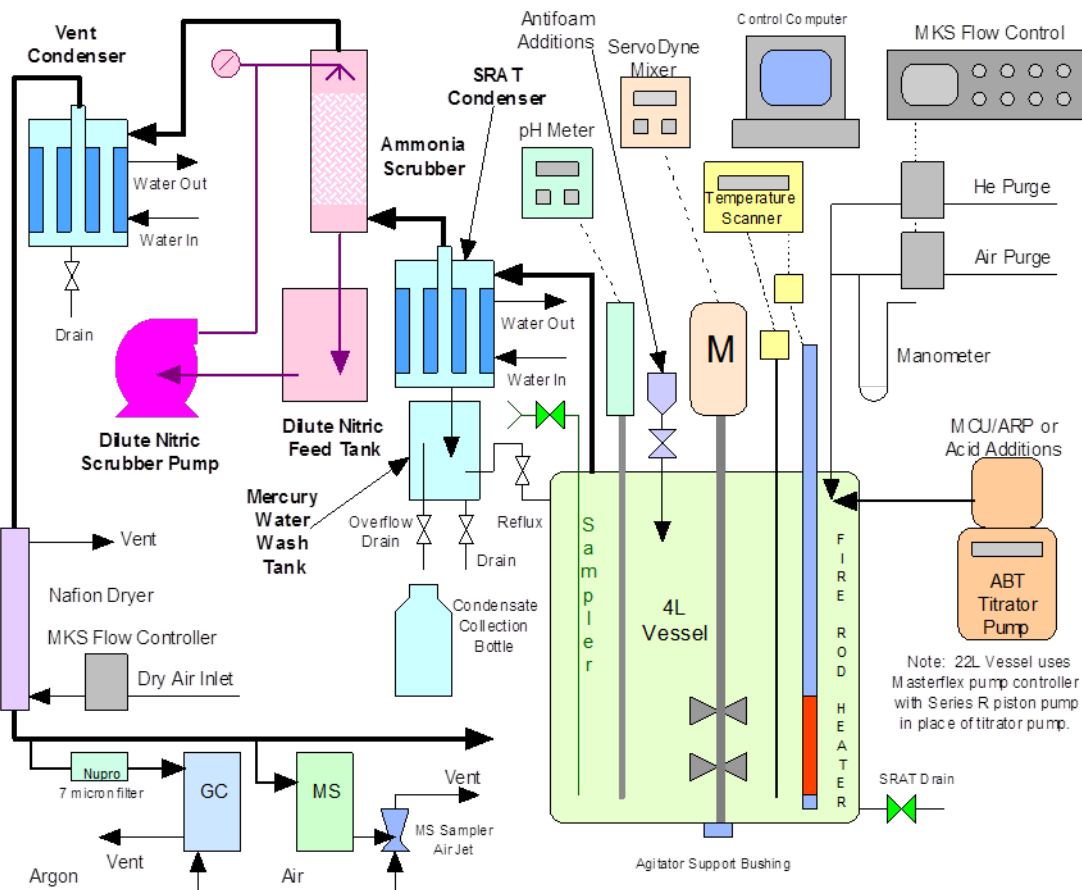


**Figure 2-1. Sketch of Experimental Setup**

The runs were performed using the guidance of Procedure ITS-0094 (“Laboratory Scale Chemical Process Cell Simulations”) of Manual L29<sup>9</sup>. Off-gas hydrogen, oxygen, nitrogen, nitrous oxide, and carbon dioxide concentrations were measured during the experiments using in-line instrumentation. Helium was introduced at a concentration of 0.5% of the total air purge as an inert tracer gas so that total amounts of generated gas and peak generation rates could be calculated. This approach eliminates the impact of fugitive gas losses through small leaks on the calculated outlet gas flowrates. During the runs, the kettle was visually monitored to observe process behavior including foaming, air entrainment, rheology changes, loss of heat transfer capabilities, and off-gas carryover. Observations were recorded on data sheets, scanned and imported into laboratory enotebooks<sup>10,11</sup>.

Quality control measures were in place to qualify the data in this report. Helium and air purges were controlled using mass flow controllers calibrated by the SRNL Standards Lab using traceable standards and methods. Thermocouples were calibrated using a calibrated dry block calibrator. The GCs were calibrated with standard calibration gases before and after the runs and the data reprocessed based on these data. The pH probes were calibrated with pH 4 and pH 10 buffer solutions and rechecked at the conclusion of each run using pH 4, 7 and 10 buffer solutions.

The automated data acquisition system developed for the 4-L rigs was used to collect data electronically. Data included slurry temperature, bath temperatures for the cooling water to the condenser and FAVC, slurry pH, heating rod temperature and watts, mixer speed and torque, and air and helium purge flows. Cumulative acid addition flowrate and volume data are calculated from the acid pump rotation speed. Raw GC data were acquired on a computer dedicated to the GCs.

Dual column Agilent 3000A micro GC's were used on both runs. The GC's were baked out before and between runs. Column-A can collect data related to He, H<sub>2</sub>, O<sub>2</sub>, N<sub>2</sub>, NO, and CO, while column-B can collect data related to CO<sub>2</sub>, N<sub>2</sub>O, and water. Calibrations were performed using a standard calibration gas containing 0.499 vol% He, 1.000 vol% H<sub>2</sub>, 20.00 vol% O<sub>2</sub>, 51.0 vol% N<sub>2</sub>, 25.0 vol% CO<sub>2</sub> and 2.50 vol% N<sub>2</sub>O. Instrument calibration was verified prior to starting the SRAT cycle. Room air was used to give a two-point calibration for N<sub>2</sub>. Calibration status was rechecked following all SRAT or SME cycles.

Concentrated nitric acid (~50 wt %) and glycolic acid (~70 wt %) were used to acidify the sludge and perform neutralization and reduction reactions during processing. The total amount of acid (in moles) to add for each run was determined using the Koopman acid equation (KAMA)<sup>7</sup>. The KAMA used a 110% stoichiometric factor (117% Hsu Stoichiometry).

In Runs GN60-64, the acid mix was partitioned between nitric and glycolic acid by targeting a ratio of glycolate plus formate in the SRAT product divided by glycolate plus nitrate in the SRAT product =0.380 in an attempt to target a Reduction/Oxidation (REDOX) ( $Fe^{2+}/\Sigma Fe$ ) of 0.1. Process assumptions were made to predict SME product anion concentrations. In addition to the standard assumptions needed for formate and oxalate loss and nitrite to nitrate conversion, a factor was added to the acid calculation for glycolate loss. Process assumptions for the stoichiometric window testing were adjusted based on results from earlier testing.

The ammonia scrubber used in this testing is not prototypic of DWPF. All condensate from the DWPF SRAT, SME and FAVC drains to the SMECT and is recirculated through all three ammonia scrubbers. In this testing, 750 mL of a 0.01 M nitric acid solution (pH 2, 620 mg/L nitrate) is recirculated through the SRAT ammonia scrubber. The condensate generated is drained to sample bottles and is not recirculated through the ammonia scrubbers. In the case of a foamover, the slurry would be collected in the condensate sample bottle and was not recirculated through the scrubber. As a result, the ammonia scrubber is virtually solids free. However, it does scrub anions such as nitrate from the offgas. The standard 4-L apparatus ammonia scrubber was used for both the SRAT and SME simulations. The scrubber solution consisted of 749 g of de-ionized water and 1 g of 50-wt% nitric acid. The solution was recirculated through the column by a MasterFlex pump at 300 mL/min through a spray nozzle at the top of the packed section. Glass rings were used as packing and did not significantly add to the backpressure on the kettle.

The offgas system consisted of the ammonia scrubber and two condensers. The cooling water to the SRAT or SME condenser was maintained at 25 °C during the run, while chilled water to the vent condenser was maintained at 4 °C.

100 mg/kg antifoam was added at four points during each SRAT cycle (before ARP addition, before nitric acid addition, before glycolic acid addition, and prior to boiling. This is significantly less antifoam than is used in DWPF.

In Runs GN60-64, both an Actinide Removal Process (ARP) and Modular Caustic-side Solvent Extraction Unit (MCU) simulant were added to each experiment. The stirred ARP simulant was

added during boiling (before acid addition). The MCU solvent used was a blend of Bob Calix and Max Calix designed to simulate the expected solvent composition after the switchover to Max Calix without draining out the existing solvent. The MCU solvent was combined at a concentration of 87 mg/kg with a 0.01 M boric acid solution during boiling (post acid addition). The MCU solution was added during boiling (after acid addition). The offgas was monitored using the MS, FTIR and activated carbon tubes to collect any organic in the offgas. The carbon tubes were extracted with carbon disulfide and the extractant was analyzed by SVOA and VOA.

In Runs GN65-68, DI water was added to a blended SRAT product in five equal additions to simulate the addition of the scaled equivalent of 5,000 gallons of water created by decontaminating five canisters. After this water had been removed via evaporation, two equal additions of frit and water (without added formic acid) were made to the SME and water was removed by evaporation to reach a total solids target.

## 2.2 Sludge, SRAT Product, ARP and MCU Slurries Used in Testing

The sludge used in these process demonstrations was an SB6I simulant prepared for SRNL by Blue Grass Chemical Specialties, LLC. The measured sludge simulant composition is summarized in Table 2-1.

The SRAT product used in these process simulations was a blend of approximately ten GN SRAT products, all produced from SB6 sludge. All these SRAT products contained mercury and noble metals. The measured SRAT Product composition is summarized in Table 2-2.

The ARP simulant composition is summarized in Table 2-3. This ARP simulant recipe was developed to reflect the composition of ARP as measured in DWPF after the MST concentration in ARP has been decreased from 0.4 to 0.2 g MST/L.

The MCU simulant was a blend of 0.01 M boric acid solution with 87 mg/kg solvent. The MCU aqueous stream composition is summarize in Table 2-4. The solvent composition is summarized in Table 2-5.

**Table 2-1. SB6I Sludge Simulant Composition**

Analyte	Concentration	Units
Total Solids	17.92%	wt % slurry basis
Insoluble Solids	12.94%	wt % slurry basis
Soluble Solids	4.99%	wt % slurry basis
Calcined Solids	12.90%	wt % slurry basis
Filtrate Solids	5.73%	wt % slurry basis
pH	12.5	Unitless
Slurry Density	1.1197	g/mL
Supernate Density	1.0426	g/mL
Al	14.3	wt % calcined solids basis
Ba	0.135	wt % calcined solids basis
Ca	1.25	wt % calcined solids basis
Ce	0.189	wt % calcined solids basis
Cr	0.184	wt % calcined solids basis
Cu	0.130	wt % calcined solids basis
Fe	22.2	wt % calcined solids basis
K	0.246	wt % calcined solids basis
Mg	0.946	wt % calcined solids basis
Mn	7.08	wt % calcined solids basis
Na	13.1	wt % calcined solids basis
Ni	3.08	wt % calcined solids basis
P	0.131	wt % calcined solids basis
Pb	<0.010	wt % calcined solids basis
S	0.251	wt % calcined solids basis
Si	1.28	wt % calcined solids basis
Ti	<0.100	wt % calcined solids basis
Zn	0.114	wt % calcined solids basis
Zr	0.264	wt % calcined solids basis
F	<100	mg/kg slurry
Cl	<100	mg/kg slurry
NO <sub>2</sub> <sup>-</sup>	4,775	mg/kg slurry
NO <sub>3</sub> <sup>-</sup>	5,305	mg/kg slurry
SO <sub>4</sub> <sup>2-</sup>	652	mg/kg slurry
C <sub>2</sub> O <sub>4</sub> <sup>2-</sup>	156.5	mg/kg slurry
HCO <sub>2</sub> <sup>-</sup>	<100	mg/kg slurry
PO <sub>4</sub> <sup>3-</sup>	<100	mg/kg slurry
Total Base to pH 7	0.444	mol/L slurry
Total Base to pH 5.5	0.515	mol/L slurry
Al	854	mg/L filtrate
Ca	1.32	mg/L filtrate
Cr	1.09	mg/L filtrate
K	549.5	mg/L filtrate
Na	20,950	mg/L filtrate
P	46.0	mg/L filtrate
S	542	mg/L filtrate
Total Inorganic Carbon (TIC)	1,005	mg/kg slurry
Total Inorganic Carbon (TIC)	876	mg/L filtrate

Ba, Ce, Cu, Fe, Mg, Mn, Ni, Pb, Si, Ti, Zn in filtrate are below detection limits.

**Table 2-2. SB6 SRAT Product Blend Composition**

<b>Analyte</b>	<b>Supernate Concentration, mg/L</b>	<b>Slurry Concentration, wt % Calcined Solids</b>	<b>% Soluble</b>
Al	1760	15.1	5.70%
B	1.25	0.10085	0.60%
Ba	2.19	0.0689	1.55%
Ca	3,100	2.040	74.1%
Cr	41.4	0.13735	14.7%
Cu	39.2	0.09995	19.1%
Fe	710	22.80	1.52%
K	409	0.099	201%
Li	<10.0	<0.100	NA
Mg	1,490	1.281	56.6%
Mn	5,880	3.47	82.6%
Na	31,400	14.315	107%
Ni	871	1.83	23.2%
P	0.926	<0.100	NA
Pd	<0.100	<0.100	NA
Rh	10.2	Not Measured	NA
Ru	86.4	Not Measured	NA
S	694	0.3172	106%
Si	75.3	1.34	2.74%
Sn	20.4	0.04	22.1%
Ti	<0.100	<0.100	NA
Zn	22.5	0.05425	20.2%
Zr	39.9	0.107	18.1%
<b>Analyte</b>	<b>Supernate Concentration, mg/L</b>	<b>Slurry Concentration, mg/kg</b>	<b>% Soluble</b>
F	<500	<500	NA
Cl	<500	<500	NA
NO2	<500	<500	NA
NO3	92,600	65,400	109%
C2H3O3	39,900	28,500	107%
SO4	2,690	1,900	108%
C2O4	2,010	1,920	80.3%
HCO2	4,450	3,250	105%
PO4	<500	<500	NA
Total Solids	16.19 wt %	28.60 wt %	NA
Insoluble Solids	NA	14.80 wt %	NA
Calcined Solids	Not Measured	15.75 wt %	NA
Soluble Solids	NA	13.80 wt %	NA
pH	Not Measured	4.10	NA
Density	1.1110 g/mL	1.1431 g/mL	NA

**Table 2-3. ARP Simulant Composition**

<b>Analyses</b>	<b>Concentration</b>	<b>Units</b>
Weight % Total Solids	6.96	wt%
Weight % Calcined Solids	4.93	wt%
Weight % Insoluble Solids	1.51	wt%
Density	1.0535	kg / L slurry
Supernate density	1.04	kg / L supernate
Nitrite	2,960	mg/kg slurry
Nitrate	13,400	mg/kg slurry
Oxalate	6,090	mg/kg slurry
Sulfate (mg/kg)	882	mg/kg slurry
Slurry TIC (treated as carbonate)	476	mg/kg slurry
Supernate TIC (treated as carbonate)	498	mg/L supernate
Hydroxide (Base Equivalents) pH = 7	0.4673	Equiv Moles Base/L slurry
Sodium (% of Calcined Solids)	40.97	wt % calcined basis
Potassium (% of Calcined Solids)	0.927	wt % calcined basis

**Table 2-4. MCU Simulant Composition**

<b>Analyses</b>	<b>Concentration</b>	<b>Units</b>
Total Solids	0.062	Wt % Slurry Basis
Calcined Solids	0.059	Wt % Slurry Basis
Supernate density	0.999	g/mL
Acid Normality (Acid Equivalents, pH = 7)	0.03	N
Boric Acid Concentration	0.01	M
Next Generation Solvent Concentration	87	mg/kg

**Table 2-5. MCU Solvent Composition**

<b>Component</b>	<b>MW</b>	<b>Concentration</b>	<b>Units</b>	<b>Concentration</b>	<b>Units</b>
Target					
Isopar L				73.8	Wt %
MaxCalix	955.36	46.5	mM	5.31	Wt %
BobCalix	1150	3.5	mM	0.48	Wt %
Modifier	338.35	0.5	M	20.2	Wt %
TIDG	515.5	3.0	mM	0.18	Wt %
Trioctylamine	353	1.5	mM	0.06	Wt %
Measured					
Isopar L		650,000	mg/L	77.62	Wt %
Modifier	338.35	130,000	mg/L	15.52	Wt %
Density		0.8374	g/mL		

The concentration of the acids used was estimated using a density measurement for the acids. The concentration of the acids is calculated using correlations and the results are reported below. The glycolic acid used was provided by DuPont, Glycolic Acid 70% SOLN TECH, Batch/Lot No. 03121306 The data sheet stated that the acid is 71.50 % glycolic acid, 0.13 % Formic acid 68-ppm sulfate.

**Table 2-6. Nitric and Glycolic Acid Concentration**

Component	Temperature, °C	Density, g/mL	Concentration, wt %	Concentration, M
Glycolic Acid	20	1.2667	71.65	11.93
Glycolic Acid	50	1.2409		
Nitric Acid	20	1.3072	49.49	10.26

**Table 2-7. Frit 418**

Element	Concentration, wt %	Oxide	Concentration, wt %	Target, wt%
Si	34.83	SiO <sub>2</sub>	74.51	76
Na	5.942	Na <sub>2</sub> O	8.01	8
Li	3.720	Li <sub>2</sub> O	7.99	8
B	2.398	BO <sub>3</sub>	7.72	8

### 2.3 Process Assumptions

A number of process assumptions were made both for the back-to-back SRAT (GN60-64) and back to back, SME runs. The following assumptions are discussed and summarized in the following sections.

#### 2.3.1 *Back to Back SRAT Process Assumptions*

Five back-to-back SRAT cycles were performed, primarily to understand the effectiveness of the glycolic-nitric flowsheet with a heel leftover from the previous run. DWPF leaves a heel of approximately 1500 gallons behind after each batch and combines it with approximately 6000 gallons of fresh sludge. In addition, both ARP and MCU were added, as this is typical for DWPF processing. It should be noted that although DWPF pulls a sample from the SRAT after ARP addition, no post ARP sample was used to calculate the acid requirement. Instead, the composition of the sludge and ARP product were combined in the acid calculation spreadsheet and used to calculate the acid requirement. This allowed processing to continue without stopping throughout the SRAT cycle.

Design basis boilup rates were used which shortened the time at temperature during the SRAT cycle compared to typical DWPF processing rates. In addition, time saving process changes which have been implemented for the glycolic-nitric acid flowsheet were used; namely faster volumetric acid flowrates to achieve the same molar flowrate as formic acid and adding nitric acid during heatup. Much of the nitric acid addition is a free hydroxide neutralization, which produces sodium nitrate and water and later carbonate decomposition, generating carbon dioxide. It does not matter what temperature the neutralization occurs so it can be completed at room temperature, during heatup, or at 93°C. It is recommended that the SRAT temperature be at 93°C before beginning the glycolic acid addition.

The first of the back-to-back runs, GN60, was completed with no heel. After Run GN60 was complete, the SRAT kettle was not completely emptied, leaving approximately a 600 g heel behind for the subsequent run. No analysis of the blend of heel and fresh sludge was completed. Instead, the heel was ignored in the acid calc and only the fresh sludge mass was used to calculate the acid quantities needed for the run. Runs GN61-64 all had the same process assumptions,

although some of the assumptions were different for Run GN60 since it had more fresh sludge. The assumptions are summarized in Table 2-8.

**Table 2-8. GN60-64 Process Assumptions**

Assumption	GN60	GN61-GN64	Units
Heel Mass	0	600	g
Fresh Sludge Mass	3000	2,400	g
ARP Mass	940.6	752.5	g (752.5 g = 1,800 gal ARP)
MCU Mass	4,459	3,567	g (3,567 g = 8,920 gal MCU)
Solvent Mass	0.388	0.310	g
DWPF Scale	1:7,280	1:9,090	Scale to 6000 gallon DWPF
Nitric Acid Mass	222.77	181.87	g 49.4 wt %
Glycolic Acid Mass	246.23	197.24	g 71.29 wt %
Nitrite to Nitrate Conversion	50.0	50.0	gmol NO <sub>3</sub> <sup>-</sup> /100 gmol NO <sub>2</sub> <sup>-</sup>
Nitrite Destruction	100	100	% of starting nitrite destroyed
Glycolate Destruction	23.0	23.0	% glycolate converted to CO <sub>2</sub> etc.
Glycolate Conversion to Formate	2.00	2.00	mol% glycolate converted to formate
Glycolate Conversion to Oxalate	3.00	3.00	mol % glycolate converted to oxalate
Destruction of Oxalate charged	0.00	0.00	% of total oxalate destroyed
Percent Excess Acid	110	110	%
SRAT Product Target Solids	27.0	27.0	%
Redox Target	0.20	0.20	Fe <sup>+2</sup> / ΣFe
Trimmed Sludge Ag target	0.0012	0.0012	total wt% dry basis after trim
Trimmed Sludge Hg target	1.3408	1.3408	total wt% dry basis after trim
Trimmed Sludge Pd target	0.0706	0.0706	total wt% dry basis after trim
Trimmed Sludge Rh target	0.0339	0.0339	total wt% dry basis after trim
Trimmed Sludge Ru target	0.1940	0.1940	total wt% dry basis after trim
Nitric Acid Addition Rate	2.392	1.916	mL/min (4.601 gpm DWPF)
Glycolic Acid Addition Rate	2.066	1.655	mL/min (3.973 gpm DWPF)
Air Purge	363	363	sccm (93.7 scfm DWPF)
Helium Purge	1.81	1.82	sccm
Boilup Rate	5.2	4.2	g/min (5000 lb/hr DWPF)

### 2.3.2 Back to Back SME Process Assumptions

Four back-to-back SME cycles were performed, primarily to understand the effectiveness of the glycolic-nitric flowsheet with a heel leftover from the previous run. DWPF leaves a heel of approximately 1500 gallons behind after each batch and combines it with approximately 4500 gallons of SRAT Product. In addition, scaled equivalent of 6,000 gallons of water was added to simulate the water generated from the decontamination of six canisters, as this is typical for DWPF processing. Two process frit additions were made. It should be noted that no formic acid was added with the frit slurry as the use of formic acid has been eliminated from this flowsheet.

Design basis boilup rates were used which shortened the time at temperature during the SME cycle compared to typical DWPF processing rates.

The first of the back-to-back runs, GN65, was completed with no heel. After Run GN65 was complete, the SME kettle was not completely emptied, leaving approximately a 750 g heel behind for the subsequent run. No analysis of the blend of heel and fresh SRAT product was completed. Instead, calcined solids in the SRAT product and heel were summed and the result was used to

calculate the frit needed for the run. Runs GN66-68 all had the same process assumptions, except as noted. The assumptions are summarized in Table 2-8.

**Table 2-9. GN60-64 Process Assumptions**

<b>Assumption</b>	<b>GN60-</b>	<b>GN61-GN64</b>	<b>Units</b>
Heel Mass	0	750	g
Fresh Sludge Mass	3000	2,250	g
Decon Water Mass	3380	3380	g (3380 g = 6,000 gal water)
Decon Dewater Mass	3380	3380	g
Frit Water Mass	839	629	g (629 g = x gal water)
Frit Mass	839	629	g (629 g = 4,227 kg frit)
SME Scale	1:6,720	1:6,720	Scale to 6000 gallon DWPF
SME Product Target Solids	50	45-50*	%
Waste Loading	36	36	%
Air Purge	310	310	sccm (93.7 scfm DWPF)
Helium Purge	1.55	1.55	sccm
Boilup Rate	5.6	5.6	g/min (5000 lb/hr DWPF)

\* GN66 targeted a total solids target of 50-wt%. After breaking the glassware, GN67 and GN68 were completed with a total solids target of 45-wt%.

## 2.4 Analytical Methods

This section discusses the slurry and offgas analytical methods used in these experiments.

### 2.4.1 Slurry Analytical Methods

Process samples were analyzed by various methods. Slurry and supernate elemental compositions were measured by inductively coupled plasma-atomic emission spectroscopy (ICP-AES) at Process Science Analytical Laboratory (PSAL). Soluble anion concentrations were measured by Ion Chromatography (IC). Mercury concentration was measured by ICP-AES. Ammonium ion concentration on selected samples was measured by cation chromatography by SRNL Analytical Development (AD). Slurry and supernate densities were measured using an Anton-Parr instrument at PSAL. Dewater and condensate samples were submitted to PSAL for IC analysis. A gradient method using the Dionex AG-11HC and AS-11HC, 2mm microbore columns was used to analyze fluoride, glycolate, formate, chloride, nitrite, nitrate, sulfate, oxalate and phosphate on SRAT/SME samples.<sup>12</sup>

SME product samples (or SRAT products combined with Frit 418) were vitrified in nepheline-sealed crucibles, and the resulting glasses were measured for REDOX ( $\text{Fe}^{2+}/\Sigma\text{Fe}$ ).<sup>13</sup> The REDOX target for the SRAT simulations in this study was 0.1 (there was no REDOX target for the SME cycle as the acids have already been added and there is no way to control this). The target is achieved by predicting the SME product anion concentrations and adjusting the split of acids between nitric and glycolic. Therefore, the ability to control REDOX at the target value is highly dependent on being able to accurately predict anion behavior in the SRAT and SME cycles. Inserting the actual SRAT product data into the latest REDOX correlation gave a “predicted” REDOX that was different from the target. It should be noted that frit 418 was used for all runs.

### 2.4.2 Offgas Methods

Agilent<sup>®</sup> 3000A micro GC's were used for all runs. The GC's were baked out before and between runs. Column-A can collect data related to He, H<sub>2</sub>, O<sub>2</sub>, N<sub>2</sub>, NO, and CO, while column-B can collect data related to CO<sub>2</sub>, N<sub>2</sub>O, and water. GC's were calibrated with a standard calibration gas containing 0.510 vol% He, 1.000 vol% H<sub>2</sub>, 20.10 vol% O<sub>2</sub>, 50.77 vol% N<sub>2</sub>, 25.1 vol% CO<sub>2</sub> and

2.52 vol% N<sub>2</sub>O. The calibration was verified prior to starting the SRAT cycle and after completing the SME cycle. Room air was used to give a two-point calibration for N<sub>2</sub>. No evidence for CO generation was obtained while examining the region of the chromatogram where it would elute. The chilled off-gas leaving the FAVC was passed through a Nafion<sup>®</sup> dryer in counter-current flow with a dried air stream to reduce the moisture content at the GC inlet. The dried, chilled off-gas stream was sampled by a GC from the beginning of heat-up to temperature to start the SRAT cycle through most of the cool down following the SME cycle.

Gas chromatograph off-gas data were scaled to DWPF flow rates. The calculation methodology has been previously documented.<sup>14</sup> An internal standard flow is usually established with helium. Other gas flow rates are determined relative to helium by taking the ratio of the two gas volume percentages times the helium standard flow. The result is scaled by the ratio of 6,000 gallons of fresh sludge divided by the volume of fresh sludge in the simulant SRAT charge.

Two new instruments, an Extrel<sup>®</sup> MAX300LG Mass Spectrometer (MS) and an MKS MG2030 Fourier Transform InfraRed (FTIR) Analyzer were used in the SRAT cycles.

The Extrel<sup>®</sup> MS samples were pulled through the MS using a single diaphragm sample pump on the outlet of the MS sampling port. MS was calibrated with a series of calibration gases as described in the next paragraph. The MS measured the composition of the sample approximately every 7 seconds (or 24 sample results during the 2.87-minute period).

Process mass spectrometry measures the intensity of ion signals and converts these signals to concentrations using the calibration data. Because some gases have interfering ions (e.g., N<sub>2</sub> is measured at mass/charge (m/z) of 28 (N<sub>2</sub><sup>+</sup>); CO<sub>2</sub> is measured at m/z 44, and has an interfering ion fragment at m/z of 28 from CO<sup>+</sup> that must be subtracted from the total signal at m/z 28 to give the correct signal for N<sub>2</sub>. This ‘fragment’ calibration is done using a calibration gas, in this case CO<sub>2</sub> in Ar. The gases NO<sub>2</sub>, NO, N<sub>2</sub>O, and CO<sub>2</sub> all have fragments that interfere at other m/z values. The signals are calibrated with calibration gases; the calibration factors determined are termed “sensitivity”. Background signals at each measurement m/z were measured in pure N<sub>2</sub> and Ar. The calibration gases used are summarized in Table 2-10.

**Table 2-10. Mass Spectrometer Calibration Gases**

Gas	Purpose
Ar	background signals at m/z 28 & 30
N <sub>2</sub>	background signals at m/z 2, 4, 32, 40, 44, 46
20% CO <sub>2</sub> in Ar	CO <sub>2</sub> fragment at m/z 28
5% NO <sub>2</sub> in N <sub>2</sub> + O <sub>2</sub>	NO <sub>2</sub> fragment at m/z 30, calibration for NO <sub>2</sub> m/z 46
2% H <sub>2</sub> , 1% He, 20% O <sub>2</sub> , 10% CO <sub>2</sub> , 1% Ar, 66% N <sub>2</sub>	calibration of each gas (m/z 2, 4, 32, 44, 40, respectively); N <sub>2</sub> sensitivity = 1.000 by definition)
2% NO in Ar	calibration for NO at m/z 30

The presence of N<sub>2</sub>O in the process gas introduces error in the measurements of CO<sub>2</sub>, NO, and N<sub>2</sub> because it has fragments with m/z at the measurement masses of each of these gases. The MS cannot be calibrated for N<sub>2</sub>O, because the relative amount of N<sub>2</sub>O to the other gases is too small to give a reliable calibration. The presence of 1.2% N<sub>2</sub>O (the highest measured by GC) would result in the measurement of N<sub>2</sub> being high by about 0.12%, NO being high by about 0.24%, and CO<sub>2</sub> being high by about 0.86%.

About twice per hour, the MS was set to scan the mass spectrum from 48 to 250 to detect any larger species. The purpose of this was to search for components that were not being measured by the GCs. The ion  $\text{CF}_3^+$  was consistently found, but this was due to the turbomolecular pump seal oil. The presence of hexamethyldisiloxane (HMDSO) was seen in several of the mass spectra. No other species were detected.

The FTIR was used to measure the gas composition of one of the two SRAT rigs during each concurrent run. The sample location was the same as used for the GC and MS. The FTIR uses factory calibration data for the infrared spectra and does not need to be calibrated; it automatically adjusts for changes in signal strength. The gases measured by the FTIR were  $\text{CO}_2$ ,  $\text{N}_2\text{O}$ ,  $\text{NO}$ ,  $\text{NO}_2$ , and HMDSO. It also had the ability to detect  $\text{CO}$ ,  $\text{NH}_3$ , nitric acid, formic acid, and water, but no significant amounts were detected. Low ppm amounts of nitric and formic acids were detected during nitric and glycolic acid additions, but these values may have been due to interferences.

In general, the FTIR values matched the GC and MS values reasonably well. Note that the concentrations in the process for  $\text{NO}$ ,  $\text{NO}_2$ , and  $\text{CO}_2$  significantly exceeded the calibration data, so the FTIR values are extrapolations of the calibration curves. The raw spectral data will be analyzed for the presence of species not in the calibration library at a future date. Antifoam breakdown products such as trimethylsilanol and siloxanes larger than six carbons are possible species that could be found from the spectra by further analysis.

### 3.0 Results and Discussion

Five back to back SRAT simulations with SB6I slurry, ARP and MCU, and four back to back SME simulations with blended SRAT products were completed to demonstrate the feasibility the nitric acid/glycolic acid flowsheet with heels in SRAT and SME processing. Each of these sets of runs will be discussed in a separate subsection of this report. All of the SRAT simulations were completed using the SB6I simulant, which is a rheologically thin simulant. The SME cycles were completed using a blend of GN products. The run objectives are summarized in Table 3-1.

**Table 3-1. Summary of Runs Performed**

Run	Objective	Section
GN60-64	Back to Back SRAT simulations with ARP and MCU	3.1
GN65-68	Back to Back SME simulations using SRAT Product Blend and Frit 418	3.2

#### 3.1 GN60-64 Back to Back SRAT Simulations with heels with ARP and MCU

No GN Flowsheet experiments have been completed utilizing a heel and no back-to-back experiments had been completed prior to this testing. In all previous GN experiments, each experiment began with a clean SRAT vessel, clean offgas equipment (SRAT condenser and FAVC), and a clean MWWT filled to overflow with DI water.

In this series of experiments, the first SRAT cycle began with clean glassware and no heel. However, the other four experiments were completed in the same uncleaned glassware and with a 600 g heel left behind. The SRAT cycles were performed around the clock; although experiment GN62 was interrupted (there was no technician coverage on the first weekend). GN62 was restarted on the second week and the rest of the SRAT cycles were completed without interruption. The time line for these experiments is summarized in Table 3-2. Different aspects of the run are discussed in the following subsections.

**Table 3-2. SRAT Processing Time Line**

Process Step	GN60	GN61	GN62	GN63	GN64
Heat on	3/12/13 9:25	3/13/13 17:00	3/14/13 23:31	3/19/13 3:30	3/20/13 5:30
Start ARP	3/12/13 9:49	3/13/13 18:05	3/15/13 0:40	3/19/13 0:28	3/20/13 6:38
Stop ARP	3/12/13 12:15	3/13/13 20:00	3/15/13 2:20	3/19/13 2:09	3/20/13 8:22
Start Nitric	3/12/13 13:19	3/13/13 21:02	3/15/13 3:59	3/19/13 3:40	3/20/13 9:41
Stop Nitric	3/12/13 14:34	3/13/13 22:18	3/15/13 5:12	3/19/13 4:56	3/20/13 10:55
Start Glycolic	3/12/13 14:46	3/13/13 22:28	3/15/13 5:24	3/19/13 5:11	3/20/13 11:16
Stop Glycolic	3/12/13 16:24	3/14/13 0:05	3/15/13 7:04	3/19/13 6:47	3/20/13 12:58
Start Boiling	3/12/13 16:50	3/14/13 0:20	3/15/13 7:30	3/19/13 7:25	3/20/13 13:23
Finish Dewater/Start MCU	3/12/13 20:08	3/14/13 3:40	3/15/13 10:50	3/19/13 10:25	3/20/13 16:26
End SRAT	3/13/13 12:31	3/14/13 18:00	3/18/13 19:42	3/20/13 1:25	3/21/13 7:10
ARP Addition Time, hrs	2.4	1.9	1.7	1.7	1.7
Nitric Addition Time, hrs	1.3	1.3	1.2	1.3	1.2
Glycolic Addition Time, hrs	1.6	1.6	1.7	1.6	1.7
Dewater Time, hrs	3.3	3.3	3.3	3.0	3.0
MCU Addition Time, hrs	16.4	14.3	14.7	15.0	14.7
Conflux Time, hrs	19.7	17.7	18.0	18.0	17.8

#### 3.1.1 *GN60-64 SRAT Products*

The SRAT product samples were analyzed after completion of the extraction by AD. The results are summarizing in this section.

3.1.1.1 GN60-64 SRAT Product Elemental Results by ICP-AES

The analytical results for the slurry and supernate are summarized in Table 3-3 and Table 3-4. This data was used to calculate the solubility for each of these elements and the results are summarized in Table 3-5. It should be noted that the Al was highest and Na lowest in runs 60 and 64. This would be consistent with the presence of less supernate and more insoluble solids in runs 60 and 64. However, other cations such as iron were not significantly higher as would be expected from poorly mixed samples. The samples are fast settling so pulling well-mixed samples can be a challenge.

**Table 3-3: SRAT Product Slurry Cation Concentration, wt % calcined solids**

Analyte Run	GN60	GN61	GN62	GN63	GN64
Al	10.7	8.47	8.53	9.52	11.0
B	<0.100	<0.100	<0.100	<0.100	<0.100
Ba	0.132	0.102	0.094	0.094	0.093
Ca	1.14	1.16	1.18	1.13	1.12
Ce	0.178	0.158	0.133	0.120	0.115
Cr	0.187	0.135	0.129	0.126	0.125
Cu	0.092	0.079	0.086	0.082	0.076
Fe	19.8	19.1	19.4	19.6	19.4
K	0.222	0.231	0.226	0.202	0.170
Mg	0.858	0.847	0.807	0.727	0.667
Mn	6.80	7.50	7.43	7.01	6.49
Na	17.5	20.2	20.5	19.2	17.8
Ni	2.77	2.79	2.81	2.75	2.70
P	<0.100	<0.100	<0.100	<0.100	<0.100
Pb	<0.100	<0.100	<0.100	<0.100	<0.100
S	0.364	0.362	0.349	0.316	0.273
Si	1.18	1.07	1.11	1.12	1.17
Ti	2.06	2.02	2.02	2.00	1.93
Zn	0.098	0.088	0.085	0.082	0.077
Zr	<0.100	<0.100	<0.100	<0.100	<0.100

**Table 3-4: SRAT Product Supernate Cation Concentration, mg/L**

Analyte Run	GN60	GN61	GN62	GN63	GN64
Al	614	504	599	682	683
B	222	217	222	221	215
Ba	2.47	1.85	2.23	2.07	2.05
Ca	1,120	810	792	973	971
Cr	2.42	1.54	1.75	2.09	2.07
Cu	75.5	46.2	66.1	89.0	87.9
Fe	676	503	611	733	737
K	989	992	1000	977	976
Li	<1.00	<1.00	<1.00	<1.00	<1.00
Mg	1306	1269	1316	1357	1358
Mn	10,200	9685	9875	9980	10,000
Na	30,050	30,800	31,500	31,350	30,650
Ni	1,810	1,580	1,770	2,060	2,075
P	<10.0	<10.0	<10.0	<10.0	<10.0
Pd	<1.00	<1.00	<1.00	<1.00	<1.00
Rh	8.21	13.3	20.1	22.1	22.0
Ru	24.9	131	160	171	170
S	789	791	810	797	797
Si	29.7	28.9	42.4	39.2	39.1
Sn	8.62	7.89	8.04	8.30	8.21
Ti	160	110	124	149	149
Zn	35.6	29.3	35.3	46.8	46.7
Zr	<0.100	<0.100	<0.100	<0.100	<0.100

**Table 3-5: SRAT Product Cation Solubility, %**

Analyte Run	GN60	GN61	GN62	GN63	GN64
Al	3.43%	4.12%	4.84%	4.66%	3.73%
Ba	1.12%	1.26%	1.63%	1.44%	1.33%
Ca	59.0%	48.5%	46.2%	56.0%	52.3%
Cr	0.775%	0.790%	0.939%	1.08%	1.00%
Cu	49.5%	40.7%	52.8%	70.7%	69.7%
Fe	2.05%	1.82%	2.17%	2.43%	2.29%
K	267%	297%	305%	315%	346%
Mg	91.3%	104%	112%	121%	123%
Mn	89.9%	89.5%	91.6%	92.5%	92.9%
Na	102.9%	105.9%	106.0%	106.2%	103.8%
Ni	39.2%	39.2%	43.4%	48.6%	46.3%
S	130%	152%	160%	164%	176%
Si	1.52%	1.88%	2.64%	2.27%	2.02%
Ti	0.251%	0.271%	0.274%	0.270%	0.257%
Zn	97.5%	86.4%	101%	118%	116%

### 3.1.1.2 GN60-64 SRAT Product Solids, Density and pH

The analytical results for the slurry and supernate are summarized in Table 3-6. The targeted total solids was 27.0 wt % so all the total, insoluble and calcined solids results are lower than planned. The most likely explanation is the thin rheology of the slurry, which makes the slurry difficult to sample as the solids settle so quickly. Other possible explanations include missing the concentration endpoints and over estimating the total solids concentration of the SB6I sludge simulant. The final SRAT product pH was approximately five, which was expected.

**Table 3-6: SRAT Product Solids, Density and pH**

Analyte Run	GN60	GN61	GN62	GN63	GN64
Total Solids, wt %	25.1	23.0	23.1	23.8	25.0
Insoluble Solids, wt %	10.2	8.01	7.81	8.53	9.87
Calcined Solids, wt %	13.5	12.0	12.0	12.6	13.4
Soluble Solids, wt %	14.9	14.9	15.2	15.3	15.1
pH	4.7	5.2	5.0	5.0	4.7
Slurry Density, g/mL	1.1972	1.1934	1.1841	1.1820	1.1882
Supernate Density, g/mL	1.1124	1.1093	1.1116	1.1138	1.1142

### 3.1.1.3 GN60-64 SRAT Product Anion Results

The analytical results for the slurry and supernate anions are summarized in Table 3-7 and Table 3-8. The predicted concentration for nitrite, nitrate, glycolate, and formate are also listed in Table 3-7. The glycolate was approximately 10% higher than projected and the oxalate was approximately 50% higher than expected. This led to higher REDOX result than planned.

The anion data from Table 3-7 and Table 3-8 was used to calculate the solubility for each of these anions and the results are summarized in Table 3-9. As expected, the solubility of all the anions is approximately 100%, except for oxalate.

**Table 3-7: SRAT Product Slurry Anions, mg/kg**

Analyte Run	Predicted	GN60	GN61	GN62	GN63	GN64
F <sup>-</sup>	NA	<500	<500	<500	<500	<500
Cl <sup>-</sup>	421-1,060 <sup>1</sup>	772	762	776	768	759
NO <sub>2</sub> <sup>-</sup>	0	<500	<500	<500	<500	<500
NO <sub>3</sub> <sup>-</sup>	54,100	54,400	52,300	54,150	53,700	55,300
C <sub>2</sub> H <sub>3</sub> O <sub>3</sub> <sup>-</sup>	44,600	50,100	48,100	47,900	48,000	49,300
SO <sub>4</sub> <sup>2-</sup>	1,340	1,770	1,740	1,760	1,780	1,820
C <sub>2</sub> O <sub>4</sub> <sup>2-</sup>	2,400	3,500	3,560	4,010	3,840	4,430
HCO <sub>2</sub> <sup>-</sup>	0-700	<500	<500	<500	<500	<500
PO <sub>4</sub> <sup>3-</sup>	0	<500	<500	<500	<500	<500

<sup>1</sup> Estimate of chloride concentration assuming no chloride in sludge and 1.25-1.67 g of chloride added with RuCl<sub>3</sub>. Even though no chloride was detected in sludge (<500 mg/kg), some chloride was present.

**Table 3-8: SRAT Product Supernate Anions, mg/L**

Analyte Run	GN60	GN61	GN62	GN63	GN64
F <sup>-</sup>	<500	<500	<500	<500	<500
Cl <sup>-</sup>	1,010	1,010	1,010	995	1,000
NO <sub>2</sub> <sup>-</sup>	<500	<500	<500	<500	<500
NO <sub>3</sub> <sup>-</sup>	75,000	69,900	74,500	74,500	74,500
C <sub>2</sub> H <sub>3</sub> O <sub>3</sub> <sup>-</sup>	60,100	60,600	60,200	62,500	62,800
SO <sub>4</sub> <sup>2-</sup>	2,310	2,300	2,340	2,360	2,390
C <sub>2</sub> O <sub>4</sub> <sup>2-</sup>	3,720	3,140	3,170	4,330	4,450
HCO <sub>2</sub> <sup>-</sup>	<500	<500	<500	<500	<500
PO <sub>4</sub> <sup>3-</sup>	<500	<500	<500	<500	<500

**Table 3-9: SRAT Product Anion Solubility, %**

Analyte Run	GN60	GN61	GN62	GN63	GN64
Cl <sup>-</sup>	106	107	109	107	110
NO <sub>3</sub> <sup>-</sup>	112	108	115	114	112
C <sub>2</sub> H <sub>3</sub> O <sub>3</sub> <sup>-</sup>	97	101	105	107	106
SO <sub>4</sub> <sup>2-</sup>	106	107	111	109	109
C <sub>2</sub> O <sub>4</sub> <sup>2-</sup>	86.0	71.0	66.1	92.7	83.6

### 3.1.2 GN60-64 MWWT

A total of 37.49 g of mercury oxide (34.72 g elemental Hg) was added during runs GN60-64. One of the most interesting observations in these experiments was the operation of the MWWT. In experiment GN60, the MWWT started with DI water. Throughout the rest of the four subsequent SRAT cycles, the MWWT continued to operate without draining the mercury or the aqueous through the bottom drain. Some observations regarding the MWWT included:

- At the completion of Run 60, the mercury was silvery and shiny
- During Run 61 ARP addition, it was noted that there was black mercury on top of the shiny, silvery mercury. This was likely due to cleaning these black mercury particles from the SRAT condenser during ARP boiling. The black particles were very fine and some of these particles were “suspended” in the MWWT. In addition, the black particles covered the SRAT condenser drain leg to the MWWT (Figure 3-1).
- Throughout the SRAT dewater and MCU addition, the SRAT condenser tubes were slowly coated with black particles.
- By the last run (GN64), some of the mercury was buoyant and appeared to dance due to disturbances in the MWWT caused by draining condensate. Photographs were taken of this are included in Figure 3-2. It should be noted that some solids bypassed the MWWT (overflowed to the SMECT) before they had a chance to be collected in the MWWT.
- In Run GN64, there was a foamover. It was not obvious at first, as very fine green/brown solids seemed to fill the bottom half of the MWWT (Figure 3-3), making the MWWT aqueous look like there were two layers. After several hours, the solids settled and were collected in the MWWT mercury layer.
- The MWWT mercury seemed to have more black particles over time.



**Figure 3-1. Black Solids Coating Drain Leg from Condenser to MWWT**

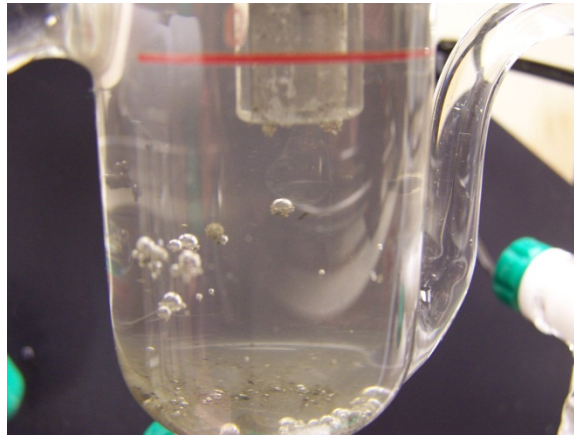


**Figure 3-2. Floating Bubbles with Solids in MWWT**



**Figure 3-3. Foamover in MWWT during SRAT Cycle GN64**



**Figure 3-4. Mercury in MWWT at Completion of Five Back-to-Back SRAT Cycles**

### 3.1.3 GN60-64 Post Run FAVC, Dewater, and SMECT samples

Samples were pulled at the completion of each run from the combined SRAT dewater, the SMECT (nitric acid circulated through ammonia scrubber, and FAVC. The samples were

analyzed by IC for anions and ICP-AES for cations. The results are summarized in the following subsections.

#### *3.1.3.1 GN60-64 Post Run FAVC Sample Results*

The FAVC sample is a very small sample (3-5 g) that is historically high in nitric and reducing acids. Only Si had a concentration above 10 mg/L, with a concentration from 27.5-111 mg/L. This is likely an antifoam degradation product. Because of the small sample size and large anion concentration, only the glycolate anion was quantified in the sample. The glycolate concentration ranged from 292,000 mg/L to 378,000 mg/L.

#### *3.1.3.2 GN60-64 Post Run SMECT Sample Results*

The SMECT samples are expected to be very low in anions and cations, unless there has been a foamover. Si had the highest concentration from 7.35-36.6 mg/L. This is likely an antifoam degradation product. Sodium, manganese, iron, and nickel were detected in the last two runs. Note that the foamover in GN64 (a small foamover) had very little impact on the SMECT concentration, likely because the solids settled in the MWWT instead of being transferred to the SMECT.

Only glycolate and formate were above the 100-ppm detection limit. Formate was above the detection limit in the last run (198 mg/L). Glycolate was above detection limits in runs GN61 (371 mg/L), GN62 (675 mg/L), GN63 (641 mg/L) and GN64 (608 mg/L).

#### *3.1.3.3 GN60-64 Post Run Dewater Sample Results*

The Dewater samples are expected to be very low in anions and cations, unless there has been a foamover. Only Si had a concentration above 1 mg/L, with a concentration from 130-280 mg/L. This is likely an antifoam degradation product. Glycolate was above the 100 ppm detection limit in runs GN60 (327 mg/L), GN61 (5,830 mg/L) and GN64 (4,500 mg/L). Formate was above the detection limit in GN61 (143 mg/L).

#### *3.1.4 GN60-64 Offgas*

Three offgas analyzers were used during these experiments. A GC was used to monitor helium, hydrogen, oxygen, nitrogen, carbon dioxide, nitric oxide, and nitrous oxide throughout the runs. The mass spec and FTIR were used to monitor a variety of species. The results are discussed in the subsections below.

##### *3.1.4.1 GN60-64 Gas Chromatograph*

Helium, hydrogen, oxygen, nitrogen, carbon dioxide, nitric oxide, and nitrous oxide were measured throughout the runs using GCs. Carbon dioxide was the first detected gas followed by the generation of nitrous oxide (Figure 3-5 and Figure 3-6). Carbon dioxide peaked at approximately 40-volume % near the end of nitric acid addition for the runs with heels. In these runs, there were three peaks, one during nitric acid addition, one during glycolic acid addition, and a third just after the initiation of boiling. In the first run (no heel), the peak was delayed by about 40 minutes and only reached 35 volume %. In addition, there were only two peaks. The acceleration of the CO<sub>2</sub> in the runs with heels was caused by the high acidity in the heel. In back-to-back runs with the baseline flowsheet, the SRAT product pH is usually close to neutral so has minimal impact on processing, while the Glycolic Flowsheet SRAT product has a pH of 4.5, which is much more acidic.

As carbon dioxide and nitrous oxide were generated, oxygen was depleted (Figure 3-7). After acid addition was completed, oxygen concentration continued to decrease and was close to zero

for approximately 30 minutes. By three hours into boiling, the oxygen concentration had returned to normal and stayed there throughout the SRAT cycle. For the most part, little gas was generated three hours past the end of acid addition in all of the runs. Note that the oxygen depletion coincides with the  $\text{NO}_2$  peak (see Figure 3-21). It is likely that the oxygen is reacting with  $\text{NO}$  to produce  $\text{NO}_2$ . This has been seen in all glycolic flowsheet runs and the depletion is greater in runs with a lower purge.

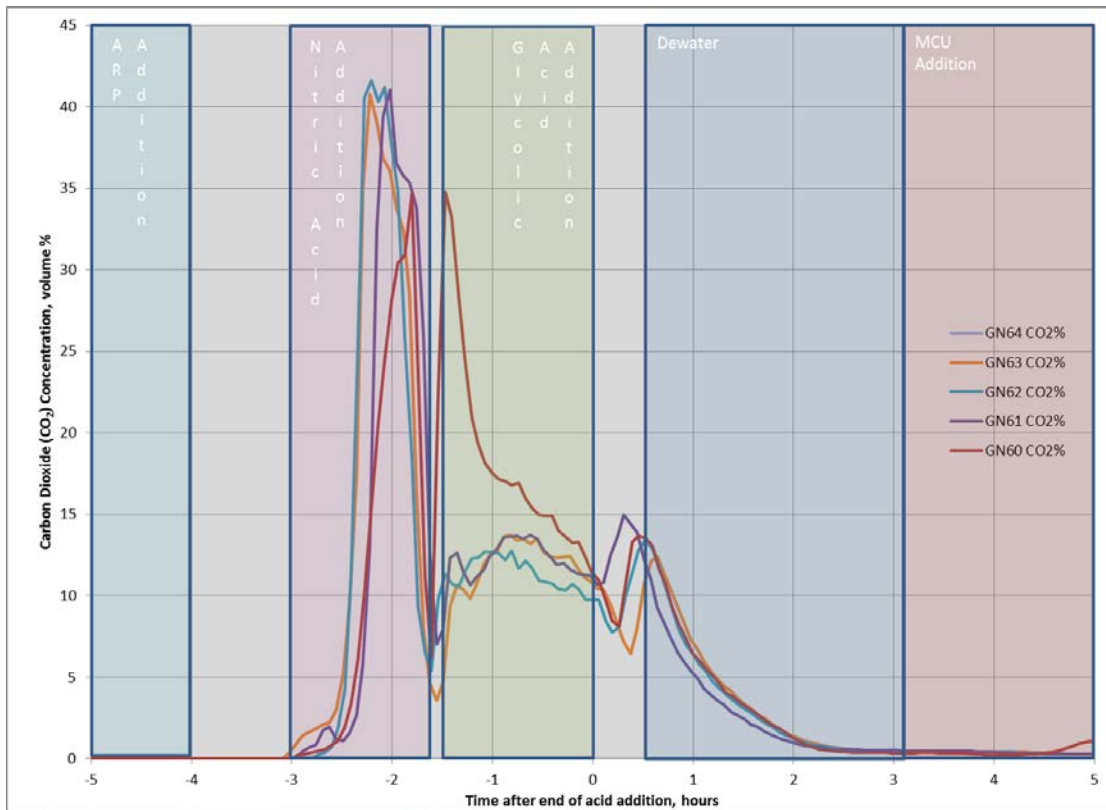


**Figure 3-5: Measured  $\text{CO}_2$  Concentration**

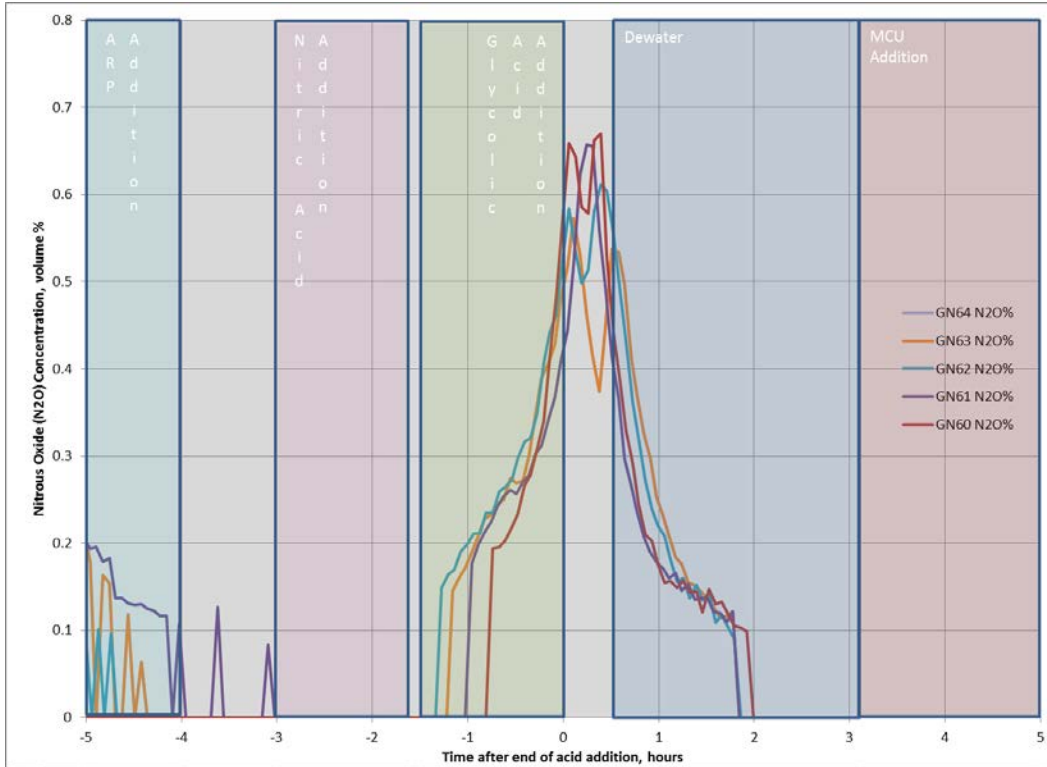


Figure 3-6: Measured N<sub>2</sub>O Concentration

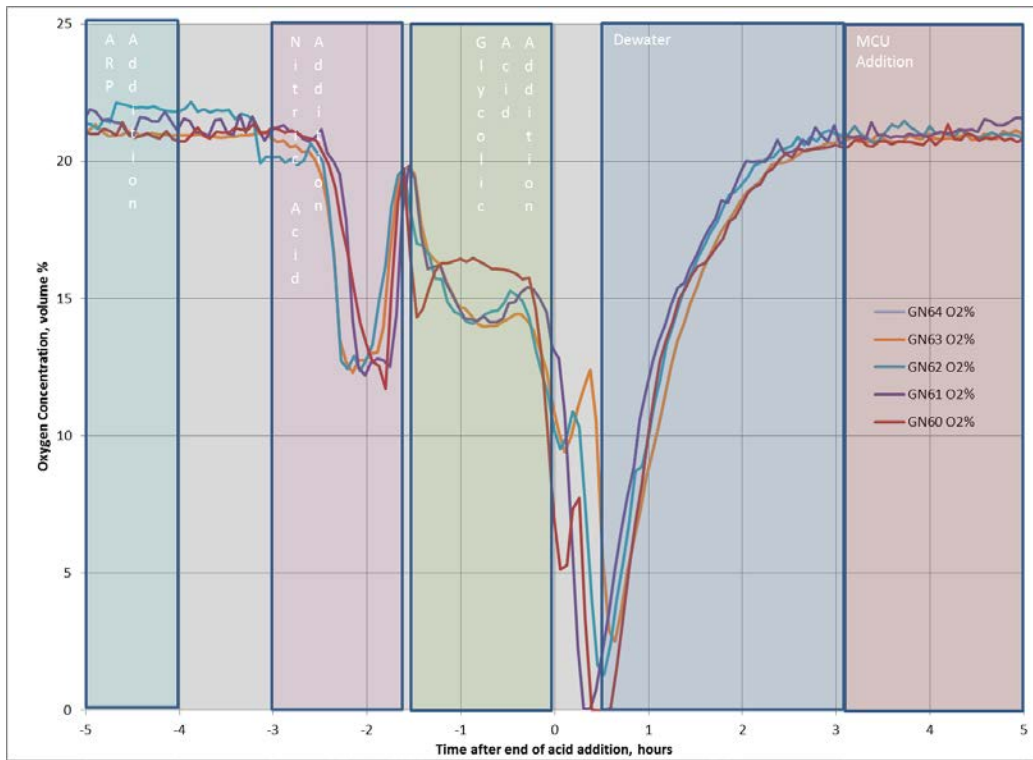


Figure 3-7: Measured O<sub>2</sub> Concentration

The GC measured peak offgas generation rates are summarized in Table 3-10. The H<sub>2</sub> and NO were not detected by the GC. The estimated detection limit is 1.45E-3 volume % H<sub>2</sub> or 4.17E-4 lb/hr, which is 0.064% of the hydrogen limit.

**Table 3-10: Peak Offgas Generation Rates (lb/hr)**

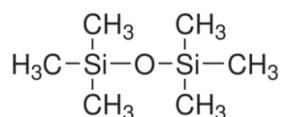
<b>RUN</b>	<b>Peak CO<sub>2</sub></b>	<b>Peak NO</b>	<b>Peak N<sub>2</sub>O</b>	<b>Peak H<sub>2</sub></b>
GN60	316	BDL	4.04	BDL
GN61	399	BDL	3.89	BDL
GN62	415	BDL	3.56	BDL
GN63	404	BDL	3.58	BDL
GN64	440	BDL	3.51	BDL

Figure A-1 through Figure A - 5 of Appendix A contain plots of the GC data from the individual runs.

#### 3.1.4.2 GN60-64 Mass Spec and FTIR

The Mass Spec and FTIR were used to monitor the offgas during the SRAT experiments. The analysis of the fixed gases NO, NO<sub>2</sub>, N<sub>2</sub>O, CO<sub>2</sub>, and H<sub>2</sub>O by FTIR is straightforward. Reference spectra are used to quantify these gases in the sample. In addition, detection of many other possible species is also straightforward because these species have very distinctive spectra. Sample spectra were qualitatively examined for the presence of nitric acid, nitrous acid, formic acid, acetic acid, hydrochloric acid, and hydrofluoric acid. Only hydrofluoric acid was found; it was found at <10 ppm levels during boiling.

Other organic species, such as Isopar™ L components and antifoam breakdown products such as hexamethyldisiloxane (HMDSO) Figure 3-8 are more difficult to quantify. The FTIR database contains limited reference species.



**Figure 3-8: Structure of hexamethyldisiloxane (HMDSO)**

The IIT-747 antifoam contains end groups containing three methyl groups attached to a Si atom that is bonded to an oxygen atom (trimethylsiloxy group) which can form trimethylsilanol (TMS), Figure 3-9:

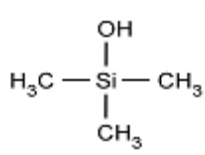


**Figure 3-9: Structure of trimethylsilanol (TMS)**

Figure 3-11 compares the spectra of a gas sample containing both HMDSO and Isopar™ L to the spectra of HMDSO, isooctane, hexadecane, and dodecane. The FTIR database also contains more complex siloxane species (see structure in Figure 3-10) that have spectra similar to HMDSO, such as hexamethylcyclotrisiloxane (D3) or octamethyltrisiloxane (L3):

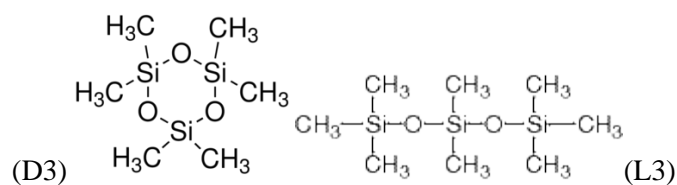


**Figure 3-10: Structure of hexamethylcyclotrisiloxane (D3) or octamethyltrisiloxane (L3)**

The spectra of such species are similar, but appear to be sufficiently different to eliminate these more complex siloxanes from consideration.

Isopar™ L is a mixture of isoparaffinic hydrocarbons with 11-13 carbons. Examples would be 3-methyl-undecane (C<sub>12</sub>H<sub>26</sub>) and 4-ethyl-decane (C<sub>12</sub>H<sub>26</sub>). The FTIR database does not contain C11-C13 isoparaffins; the closest matches are the linear n-hexadecane (C<sub>16</sub>H<sub>34</sub>) and n-dodecane, and isooctane (2,2,4 trimethylpentane). The three peaks from 750-1300 cm<sup>-1</sup> identify HMDSO very conclusively (Figure 3-11).

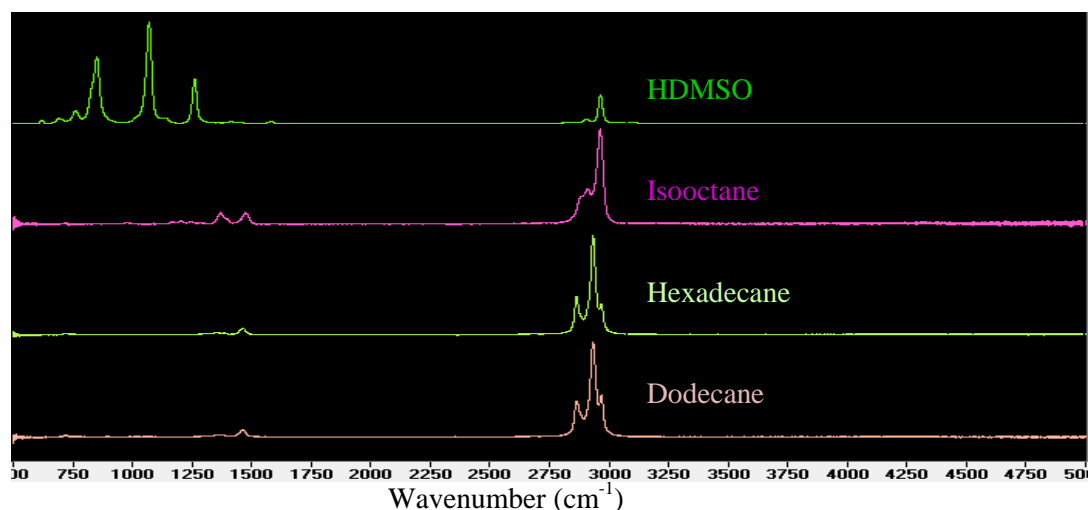


**Figure 3-11: IR Spectra of Gas Sample, HMDSO, Isooctane, Hexadecane, and Dodecane**

The subtraction of HMDSO from a spectrum taken during the GN62 run is shown in Figure 3-12. The top display shows the reference HMDSO peaks and the bottom shows the result of the subtraction. In Figure 3, the effect of the HMDSO at the higher wavenumbers where Isopar™ L has peaks is shown.

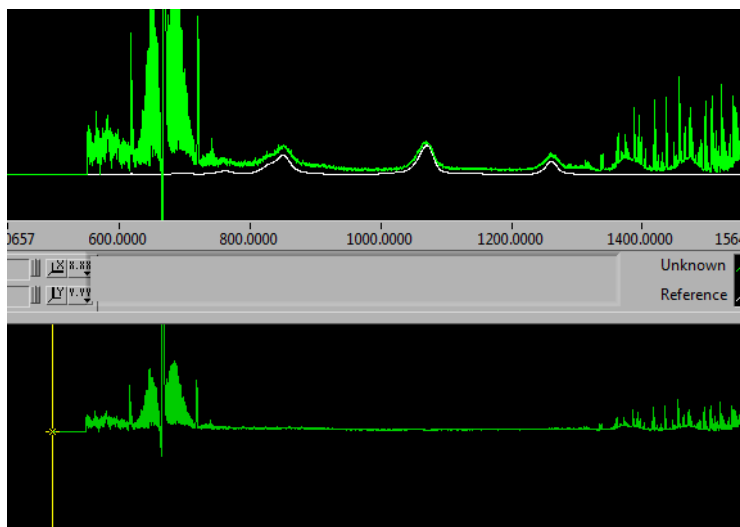


**Figure 3-12: Sample from GN62 Subtracting HMDSO at 750-1300  $\text{cm}^{-1}$**

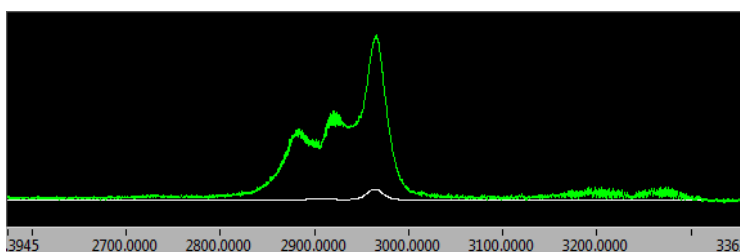


**Figure 3-13: Sample from GN62 Subtracting HMDSO – Effect at 2800-3000  $\text{cm}^{-1}$**

Figure 3-14 shows that subtracting isooctane from the spectrum almost completely accounts for the peaks in this region. Subtraction of the n-dodecane spectrum from the sample spectrum is shown to not work in Figure 3-15, so n-alkane (normal paraffin) spectra do not account for the peaks seen. Isopar™ L does not contain isooctane, but these data show that the peaks at 2800-3000 match the isoparaffin spectra better than the n-alkane spectra. Although the reference spectra match the sample spectra reasonably well, the calculated concentrations will not necessarily be correct because actual Isopar™ L spectra were not used (and are not available).

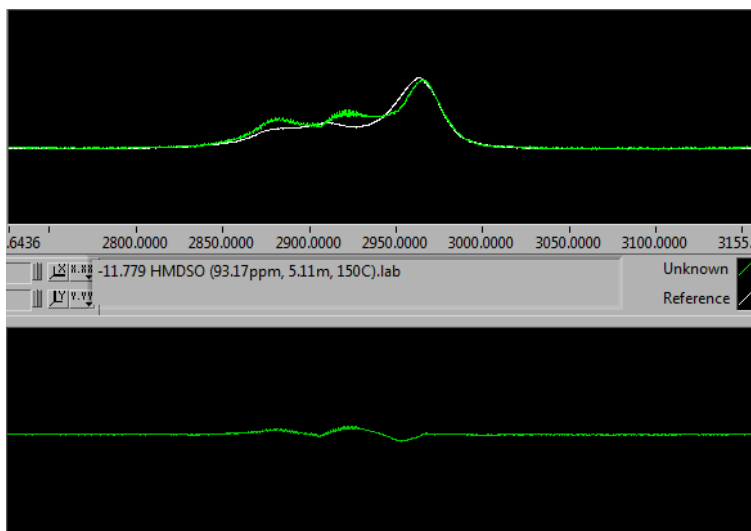


**Figure 3-14: Sample from GN62 Subtracting Isooctane at 2800-3000  $\text{cm}^{-1}$**

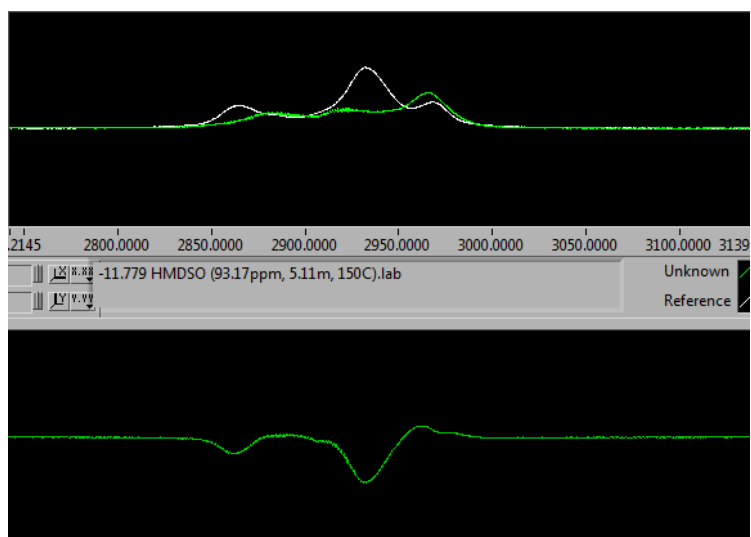


**Figure 3-15: Sample from GN62 Subtracting n-Dodecane at 2800-3000  $\text{cm}^{-1}$**

No attempts were made to measure by FTIR the Cs-7SB modifier or the guanidine based suppressor concentrations or any decomposition products from these. There are no available reference spectra that would be similar to these species.

Comparison of sample spectra to HMDSO and TMS show that TMS is not found in the offgas samples. Figure 3-16 shows that subtraction of the HMDSO spectrum from the sample spectrum accounts for all the peaks from 750-1300  $\text{cm}^{-1}$ . As shown in Figure 3-17, the TMS spectrum does not account for the peaks seen, so the peaks are not due to TMS. There could still be very small amounts present that would not significantly affect the spectra.

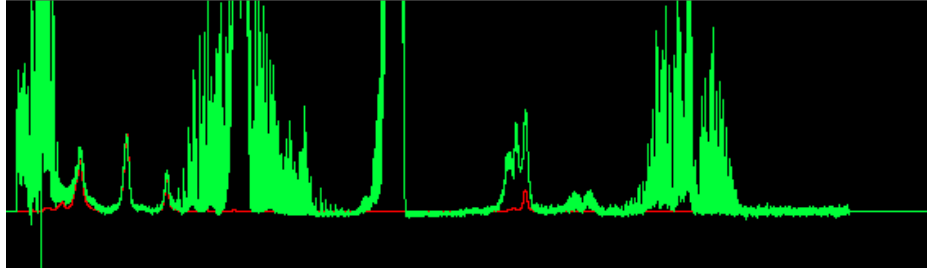


**Figure 3-16: Subtraction of HMDSO from Sample Spectrum**

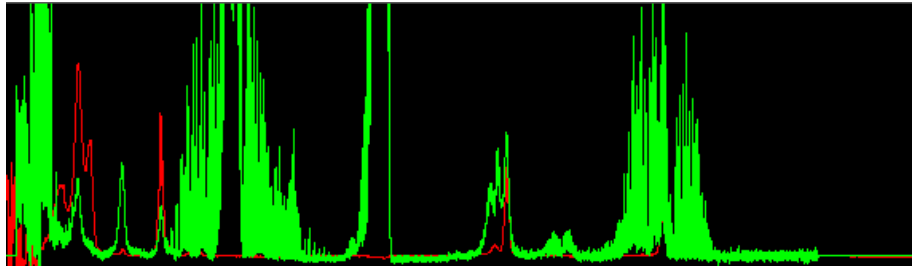
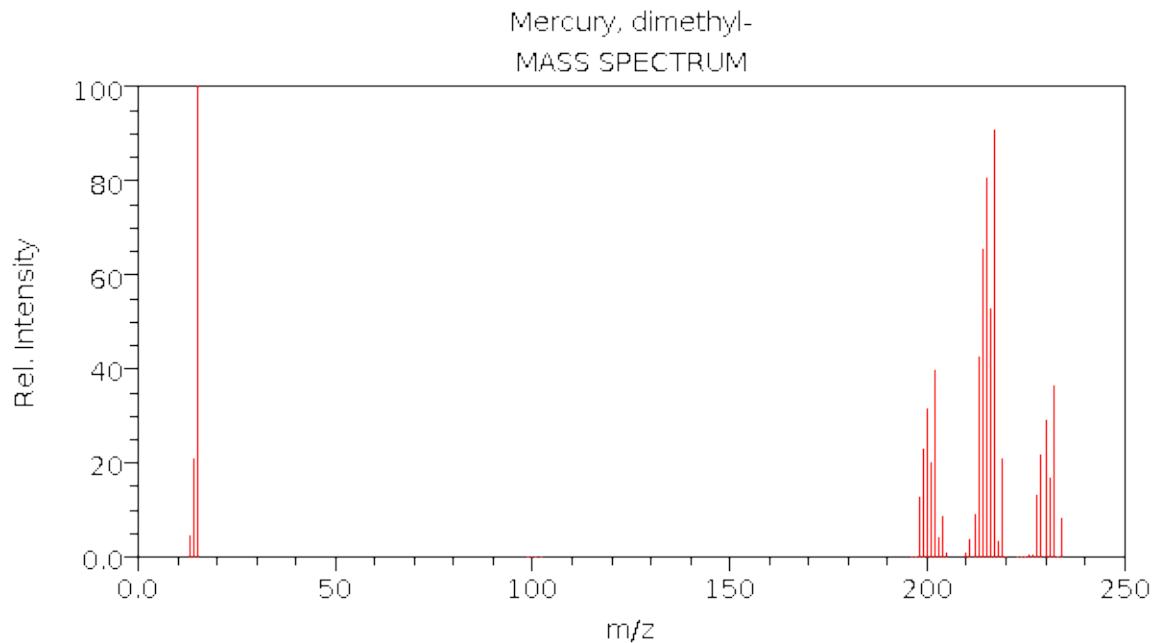


**Figure 3-17: Subtraction of TMS from Sample Spectrum**

#### Dimethylmercury (DMM)

In runs GN60-61, the MS was used to monitor masses (actually the mass to charge ratio  $m/z$ ; 'mass' will be used here to mean  $m/z$ ) where dimethylmercury is known to have signals. The masses monitored were 202, 213, 214, 215, 216, 217, 230, and 232. For comparison to background, masses 175 and 240 where no signals are expected were also monitored. The electron multiplier was used to increase the signals at these masses. The mass spectrum of dimethylmercury is shown in Figure 3-18.



NIST Chemistry WebBook (<http://webbook.nist.gov/chemistry>)

**Figure 3-18: Mass Spectrum of Dimethylmercury**

The signals from the measured masses and the background masses are plotted versus time in Figure 3-19. The data show that the signal intensities at the DMM masses are no different from the background signals at 175 and 240, so it can be concluded that no DMM was present.

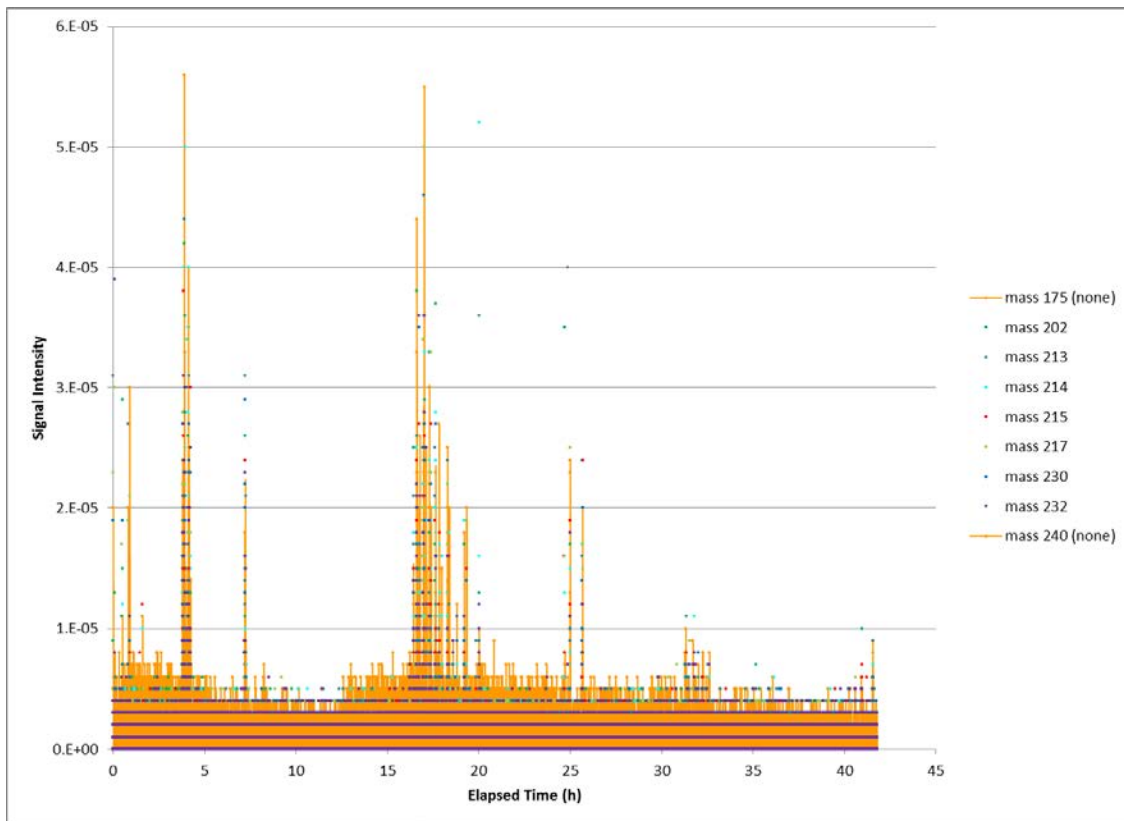


**Figure 3-19: Dimethylmercury Mass Signal Intensities Compared to Background**

Run GN60

The FTIR was operated during this run, but the mass spectrometer (MS) was not. Data after the end of the run is just measurement of stagnant sample in sampling system.

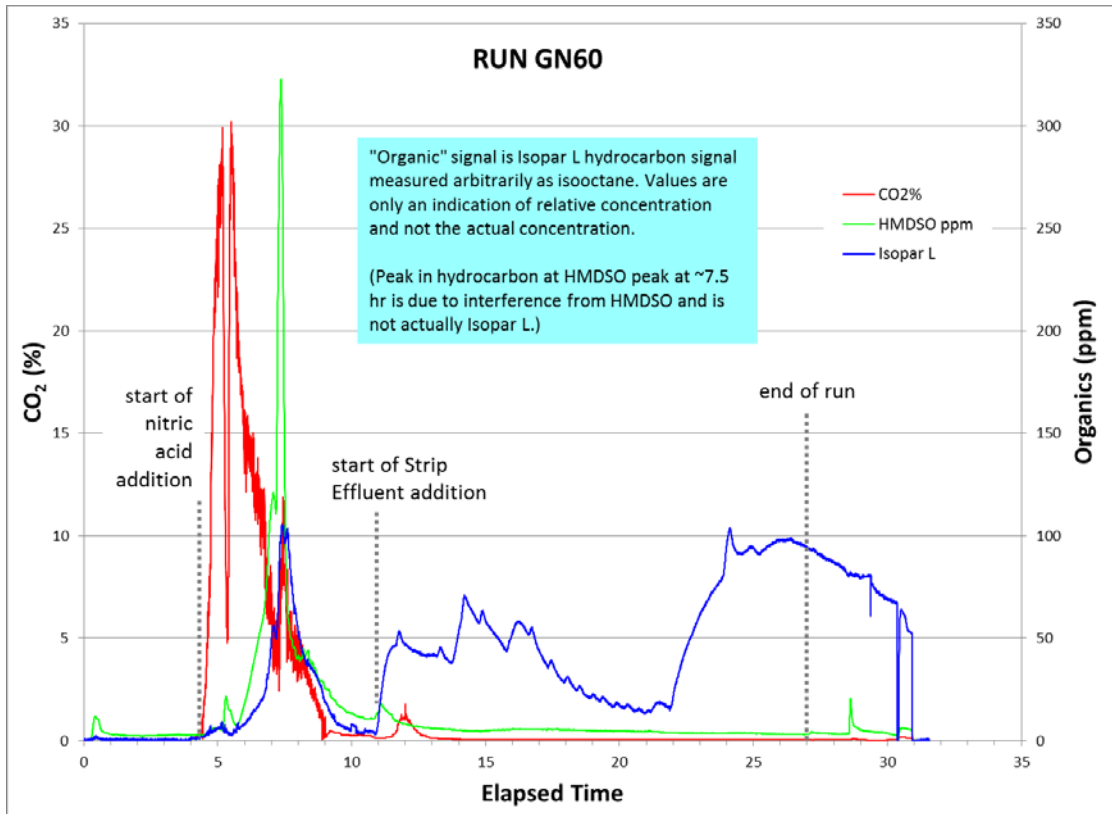


**Figure 3-20: GN60 Isopar, HMDSO, and CO<sub>2</sub> Concentration**

CO<sub>2</sub>, NO, NO<sub>2</sub>, and N<sub>2</sub>O (labeled N<sub>y</sub>O<sub>x</sub> on the y-axis) were monitored by the FTIR throughout the runs. The data from GN60 is plotted in Figure 3-21. Note big narrow NO peak (8.5%) at boiling after acid addition. This coincides with the depletion of oxygen measured by the GC.

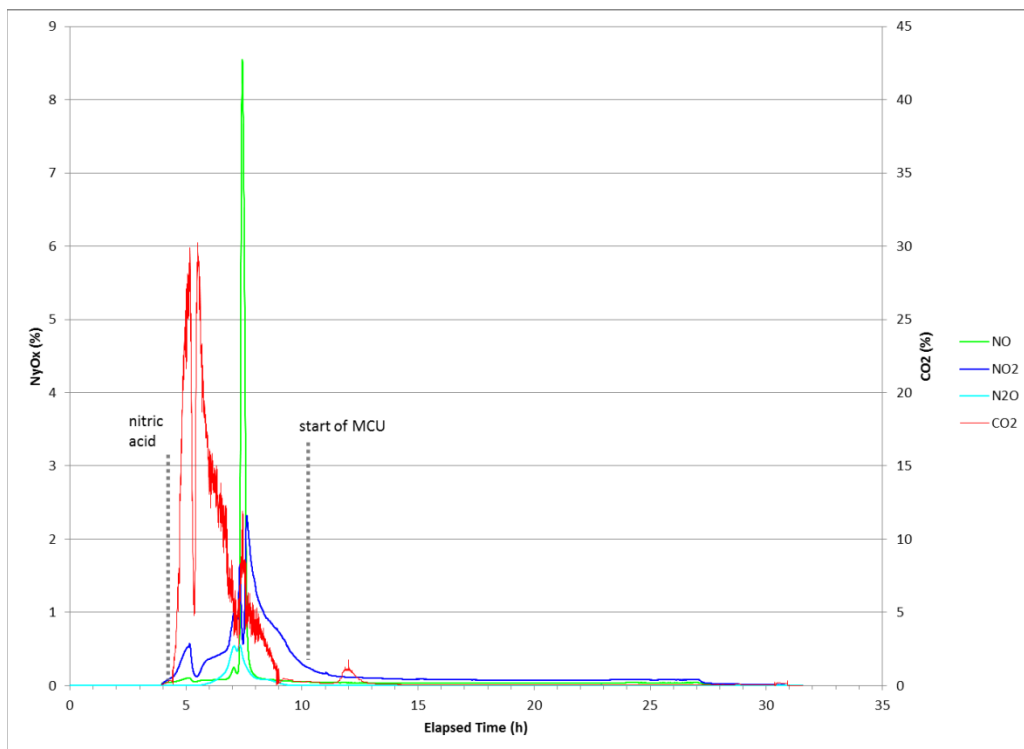


**Figure 3-21: GN60 NO, NO<sub>2</sub>, N<sub>2</sub>O, and CO<sub>2</sub> Concentration**

Run GN61

The FTIR was offline throughout the run (valving error). The pump was brought online and briefly sampled the residual sample in the sample line, then turned off and sampled residual sample. The MS was used to measure the intensity of mass 57 (C<sub>4</sub>H<sub>9</sub>) fragments of hydrocarbons (most abundant fragment of most C8-C13 isoparaffins). Several other masses were also sampled. Note that only relative intensities were measured, not actual concentrations. (Assuming a reasonable sensitivity value of 0.2 for the organic signals results in the calculated MS concentrations being of the correct order of magnitude compared to the FTIR values.)

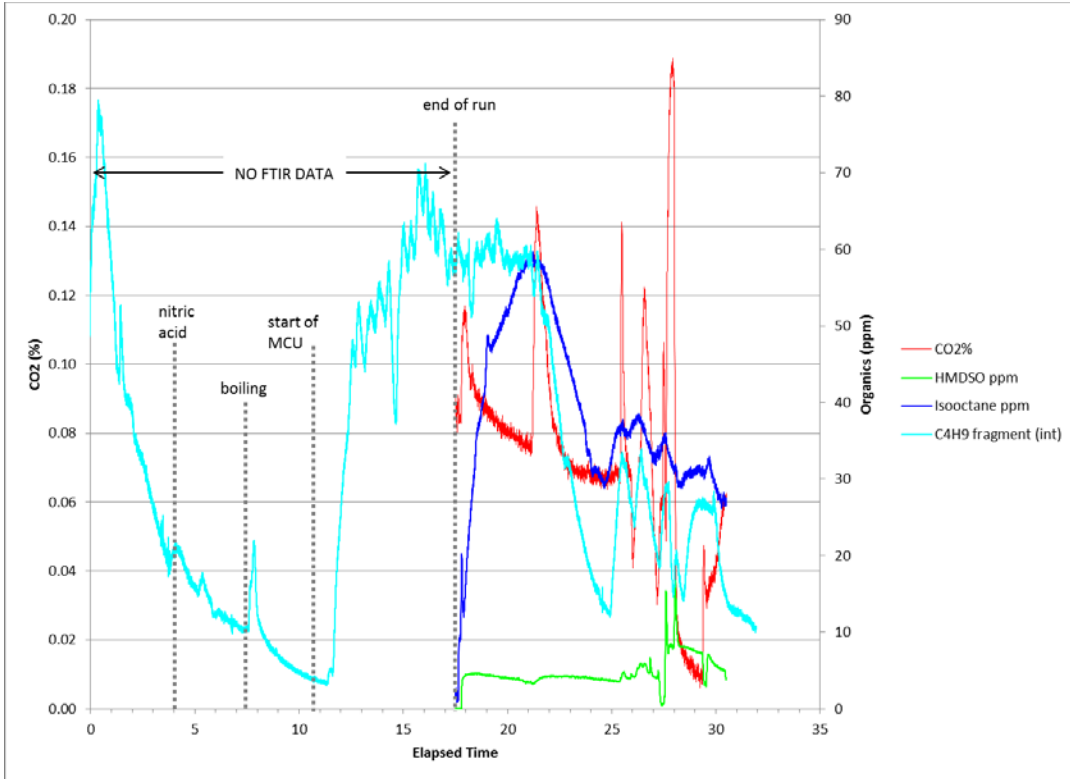


**Figure 3-22: GN61 HMDSO, Isooctane, C<sub>4</sub>H<sub>9</sub> fragment, and CO<sub>2</sub> Concentration**

The large hydrocarbon peak at time ~0.5 h appears to be Isopar™ L from the heel being boiled off. Note that after the end of the run, the MS and FTIR hydrocarbon signals follow the same trends. The MS signal always varies more than the FTIR signal, but does so at the same time. It is speculated that the FTIR sample volume of 200 mL and low flow make the concentrations spread out compared to the MS. The MS values should be more representative of the actual values.

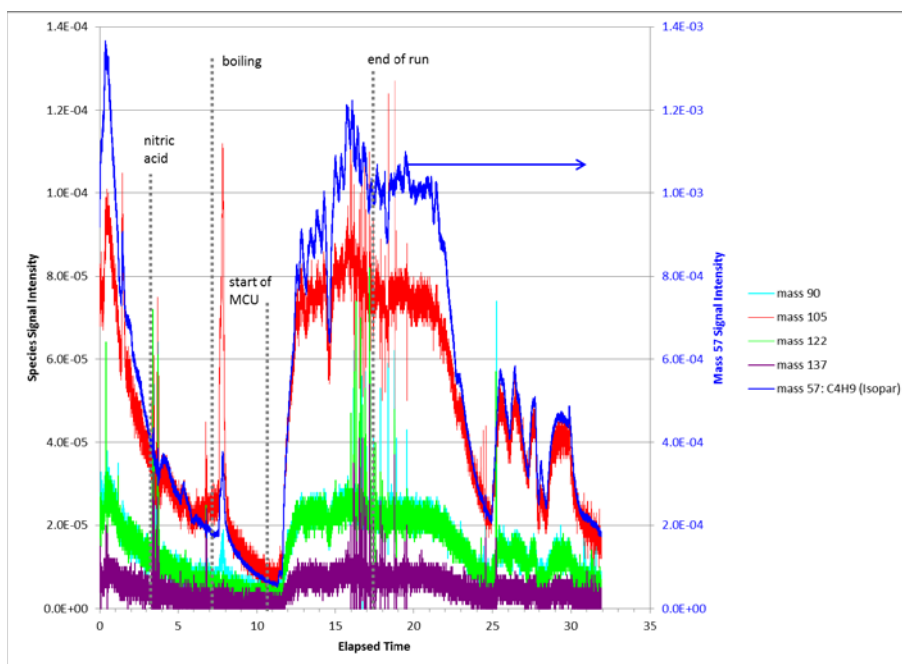


**Figure 3-23: GN61 Mass Spec Masses 50, 57, 105, 122, and 137**

Figure 3-23 compares the signals at mass 57, which is the  $C_4H_9$  fragment of Isopar™ L to the signals at several other masses. The other masses had been chosen in the belief that they would give zero signal and be an indication of the signal noise. This was done for comparison to signals that might indicate dimethylmercury. However, these signals were found to track the mass 57 signal very well, indicating that they are probably due to components of the Isopar™ L or the modifier component Cs-7SB or the Suppressor. Note that these signals are 1-2 orders of magnitude below the mass 57 signal. The signal at mass 122 could correspond to 4-sec-butylphenol, which has been shown to be a breakdown product of the Cs-7SB modifier.<sup>15</sup>

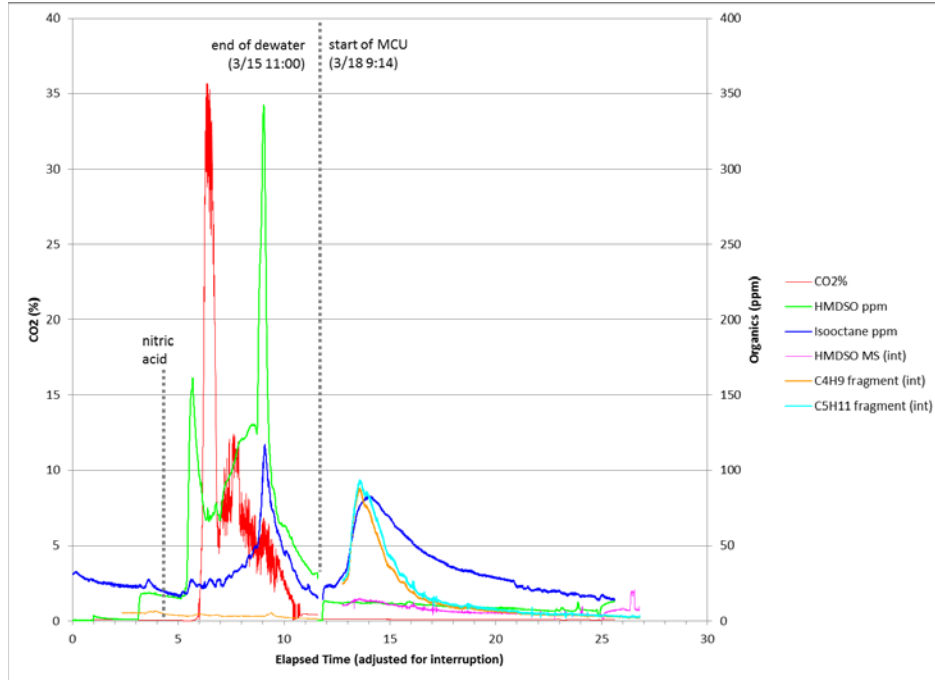
The signal at mass 90 could be trimethylsilanol, which is a known decomposition product of the antifoam; however, the fact that it exactly follows the mass 57 signal is not expected.

The signals at masses 105 and 137 are harder to explain. Isoparaffins have no signals at these masses. These masses could correspond to various methyl siloxy compounds that are similar to fragments of the 747 antifoam, but do not appear to be close enough in structure to be likely (all contain methoxy  $-OCH_3$  groups that are not present in antifoam). The mass 105 signal is about 10% of the mass 57 signal.

It would be useful in the future testing with solvent to run the MS and FTIR to measure the decomposition products.

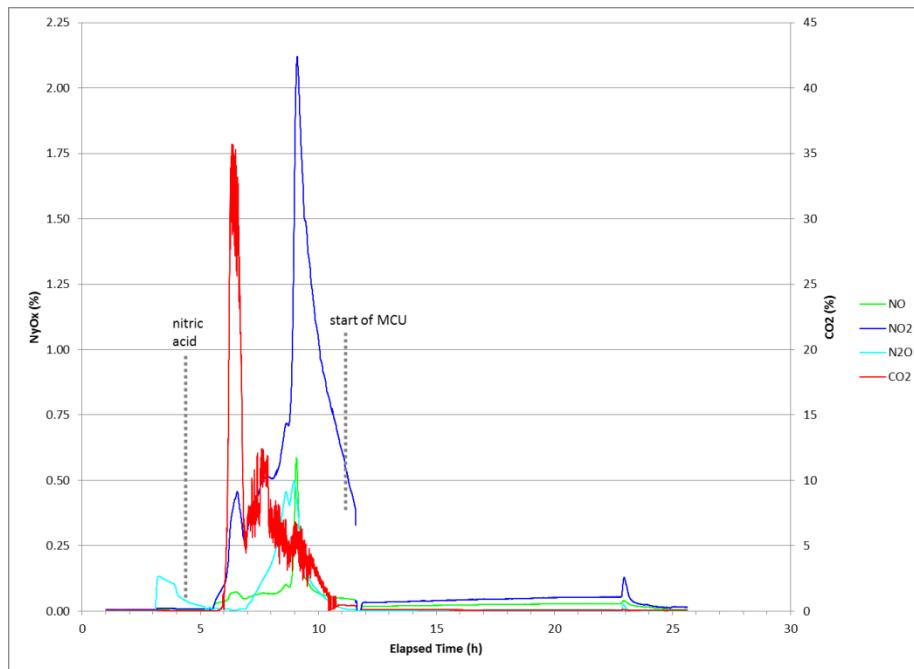
#### Run GN62

Figure 3-24 shows the concentrations from FTIR data and MS intensity data adjusted to approximately match the FTIR data. The intensities of the  $C_4H_9$  and  $C_5H_{11}$  fragments by MS match well.



**Figure 3-24: GN62 Isopar, Isooctane, C<sub>4</sub>H<sub>9</sub>, C<sub>5</sub>H<sub>11</sub>, HMDSO, and CO<sub>2</sub> Concentration**

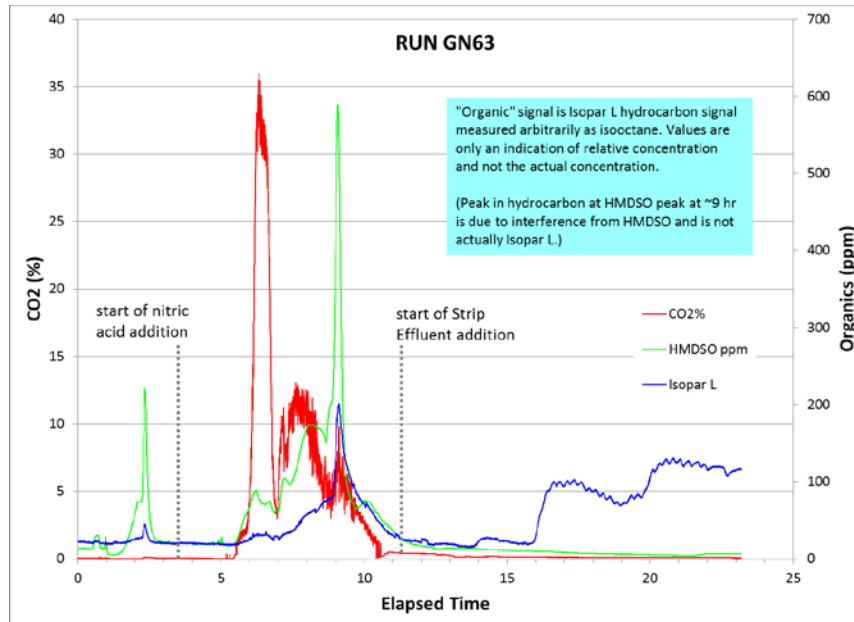
Figure 3-25 plots the NO, NO<sub>2</sub>, N<sub>2</sub>O and CO<sub>2</sub> data from the FTIR. The peak at boiling is mostly NO<sub>2</sub> rather than NO as in GN60. The NO<sub>2</sub> concentration is lower in GN 62 (~2% NO<sub>2</sub>) than GN60 (8.5% NO). The GN62 peak is also wider – maybe ~same moles. A wide NO<sub>2</sub> peak would reflux more HNO<sub>3</sub> back into SRAT and result in higher nitrite to nitrate conversion or less apparent nitrate destruction or both.



**Figure 3-25: GN62 FTIR NO, NO<sub>2</sub>, N<sub>2</sub>O, and CO<sub>2</sub> Concentration**

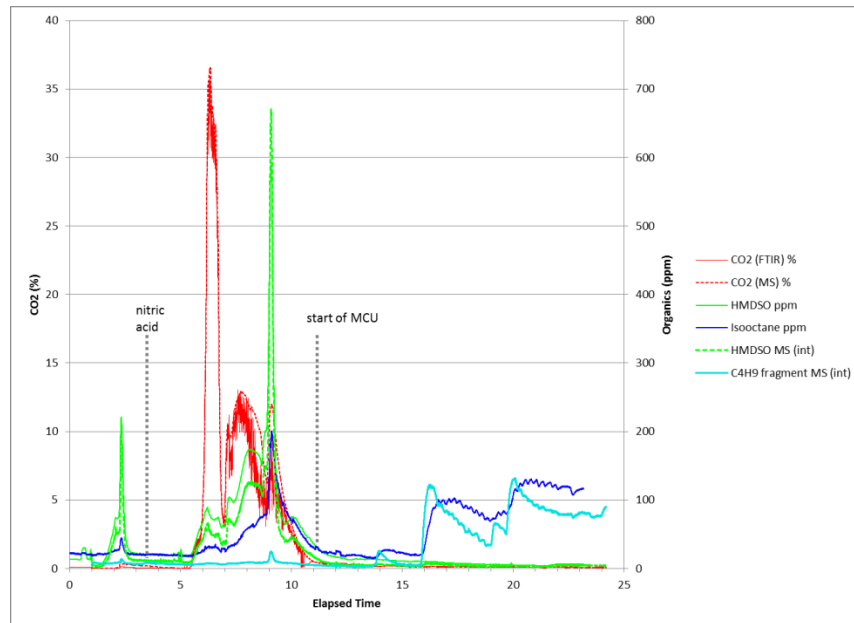
GN63

Similar data was collected during GN63. Figure 3-26 summarizes the FTIR HMDSO, Isopar-L, and CO<sub>2</sub> concentrations below.



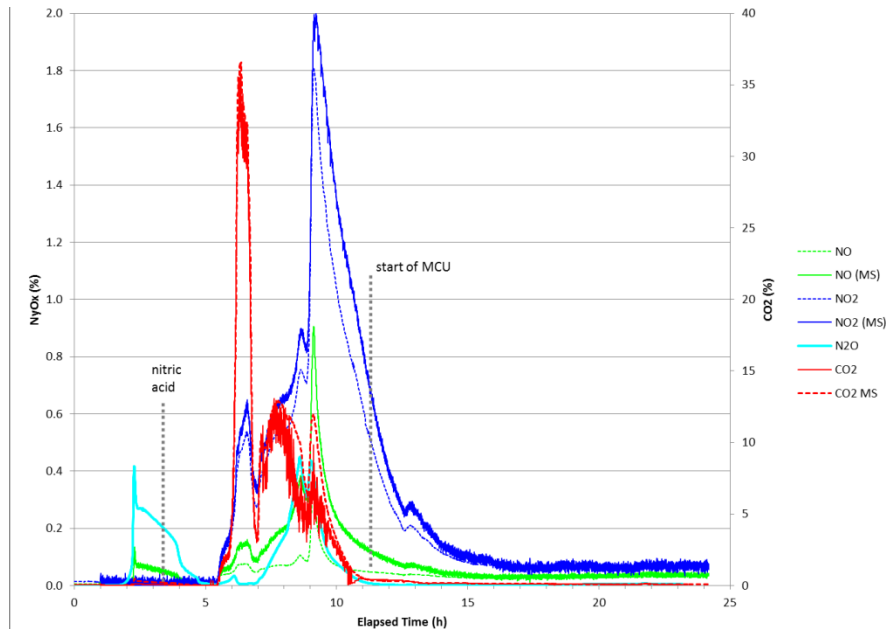
**Figure 3-26: GN63 HMDSO, Isopar-L, and CO<sub>2</sub> Concentration**

Figure 3-27 compares the FTIR and MS data. CO<sub>2</sub> by MS is quantitative and matches FTIR very well. HMDSO by MS was adjusted to match FTIR – values agree very well. Isopar™ L C<sub>4</sub>H<sub>9</sub> fragment by MS similar to FTIR, but more sharply shaped.



**Figure 3-27: GN63 Isopar, Isooctane, C<sub>4</sub>H<sub>9</sub>, G<sub>3</sub>H<sub>11</sub>, HMDSO, and CO<sub>2</sub> Concentration**

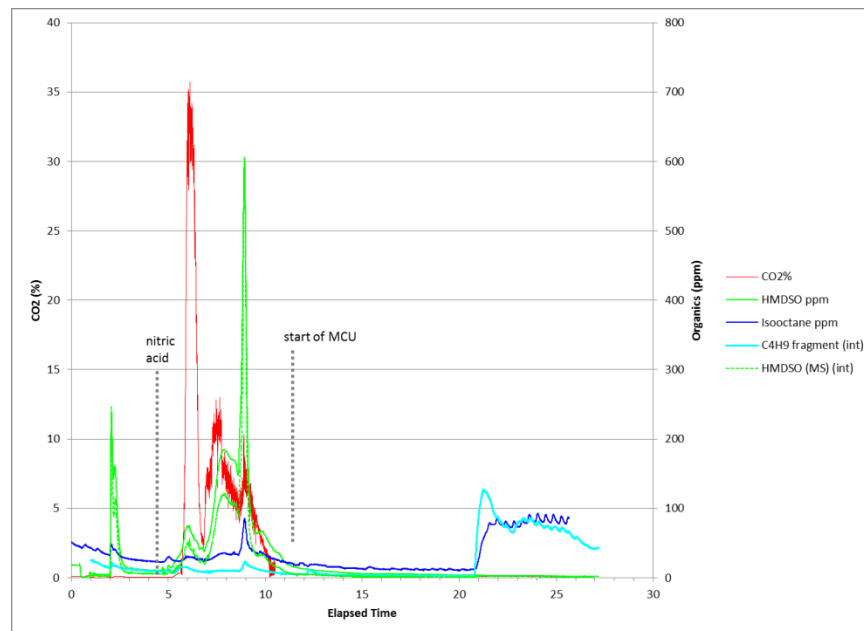
Figure 3-28 compares FTIR and MS  $\text{CO}_2$ ,  $\text{N}_2\text{O}$ ,  $\text{NO}$ , and  $\text{NO}_2$ . Again, there was a low, wide  $\text{NO}_2$  peak rather than sharp a  $\text{NO}$  peak. Note  $\text{N}_2\text{O}$  and a bit of  $\text{NO}$  peak during ARP addition. See similar for GN62.



**Figure 3-28: GN63  $\text{NO}$ ,  $\text{NO}_2$ ,  $\text{N}_2\text{O}$ ,  $\text{N}_y\text{O}_x$ , and  $\text{CO}_2$  Concentration**

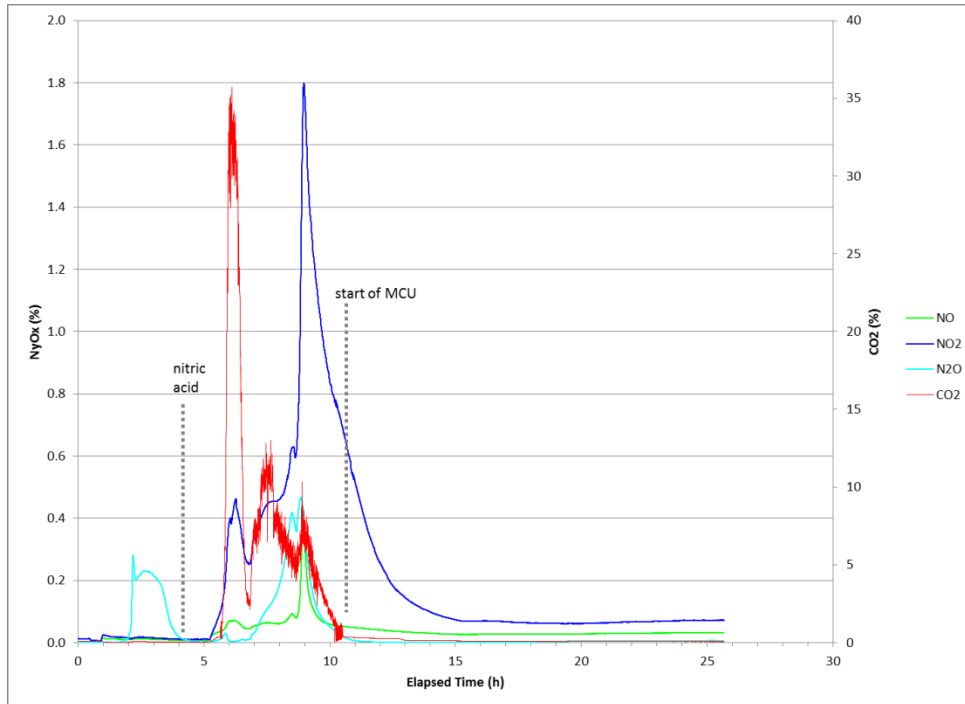
#### GN64

Figure 3-29 is a graph of  $\text{CO}_2$ , HMDSO, Isopar™ L. The HMDSO concentrations match well and the Isopar™ L matches qualitatively.



**Figure 3-29: GN64 Isopar, Isooctane,  $\text{C}_4\text{H}_9$ ,  $\text{G}_5\text{H}_{11}$ , HMDSO, and  $\text{CO}_2$  Concentration**

Figure 3-30 summarizes the FTIR and adjusted MS data NO, NO<sub>2</sub>, N<sub>2</sub>O, and CO<sub>2</sub>. The CO<sub>2</sub> and NO<sub>x</sub> are similar to the other runs with heels, which had a low, wide NO<sub>2</sub> peak.



**Figure 3-30: GN64 NO, NO<sub>2</sub>, N<sub>2</sub>O, and CO<sub>2</sub> Concentration**

### 3.1.5 GN60-64 pH

The pH profile was very similar in all SRAT cycles. The pH dropped during heatup to boiling before the ARP addition. The pH increased from about 9.8 to 10.2 during the ARP addition phase. The pH dropped from 10.2 to about 5.5 during nitric acid addition and decreased to about four by the end of glycolic acid addition. The pH rose to about 4.5 during the dewater phase and then stayed relatively constant during the MCU addition. The pH profile is included below in Figure 3-31.

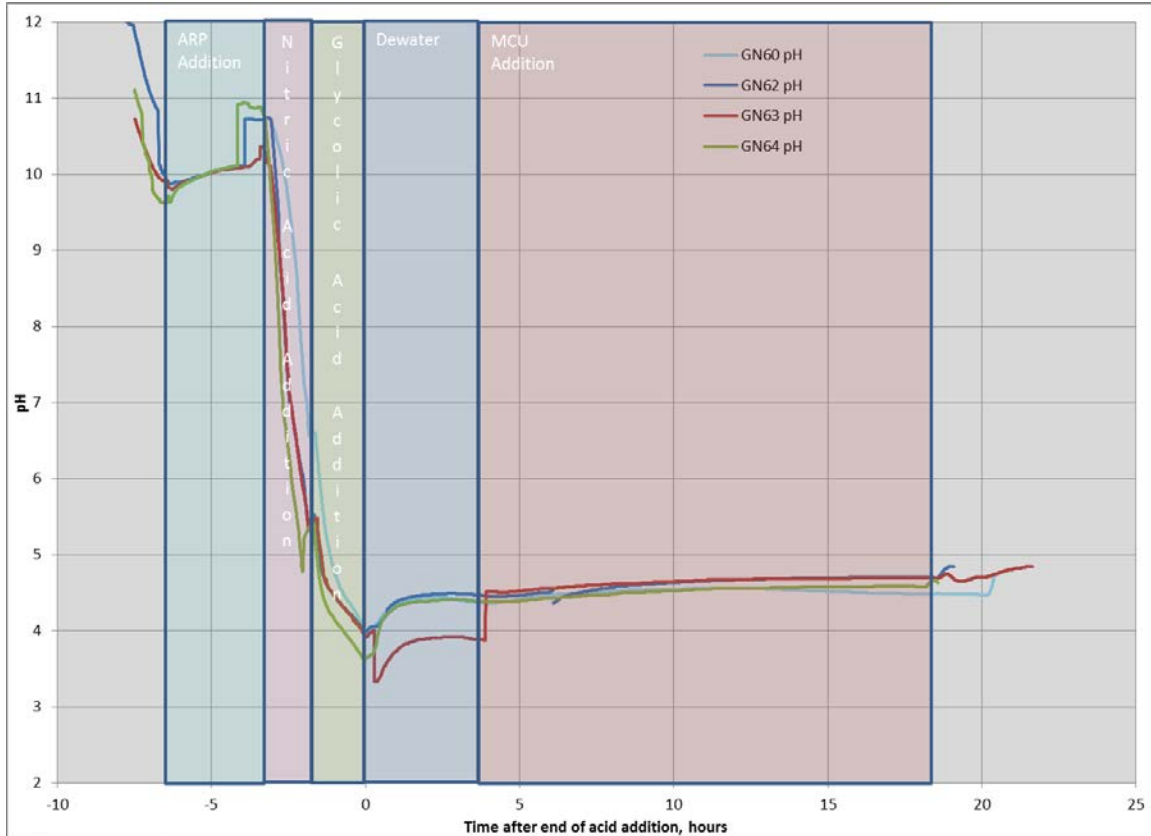


**Figure 3-31. SRAT Cycle pH Profile**

### 3.1.6 GN60-64 ARP

All five SRAT cycles included a segment where the ARP simulant was added at boiling. This occurred at the beginning of the SRAT cycle and lasted for three hours. The ARP was added at 4.2 ml/min to the SRAT with a boilup rate of 4.2 ml/min. This is equivalent to a 1,800 gallon ARP addition at 10 gpm and 5000 lb/hr steam flow. Note that the total base concentration of the ARP simulant was 0.467 M, compared to 0.444 M for the sludge simulant.

The ARP addition period is a time of minimal reactions, just the addition of caustic ARP product to caustic sludge. The condensate produced is very clear and near neutral (condensate can be very acidic during acid addition, dewater, and strip effluent addition). During this period, the condensate returning through the condenser and MWWT will clean the particulate mercury off the condenser tubes and MWWT.

No foaming was noted during the ARP addition, although foaming is noted during ARP addition in DWPF. Most of the ARP addition foamovers in DWPF occur at the end of the ARP addition. Once the ARP addition is stopped, the 5,000 lb/hr steam flow is no longer needed to heat the ARP feed to boiling and evaporate the water. This is equivalent to rapidly increasing the steam flow. If foaming is an issue, a foamover is likely within minutes of stopping the ARP addition. An example of this is shown in Figure 3-32. At the end of ARP addition, the ARP pump was turned off. The temperature of the condensate exiting the condenser and draining to the MWWT jumped from 30 °C to 45 °C before the heat was turned off at approximately -3 hours. The temperature of the condensate exiting the condenser and draining to the MWWT jumped to 45 °C again at the initiation of boiling and slowly declined for the next three hours. The condenser return

temperature is essentially the same during boiling. Note that the SRAT condenser is likely oversized in the experimental rig so the temperature spikes might be larger in DWPF.

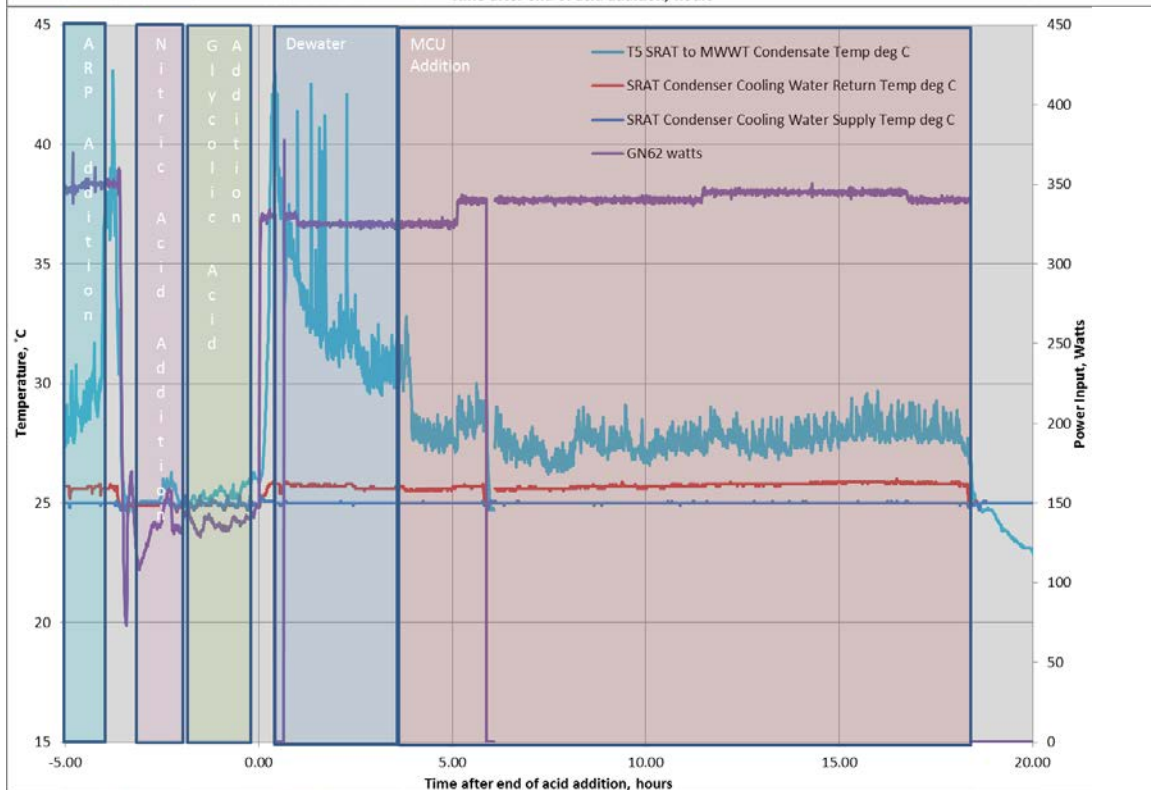
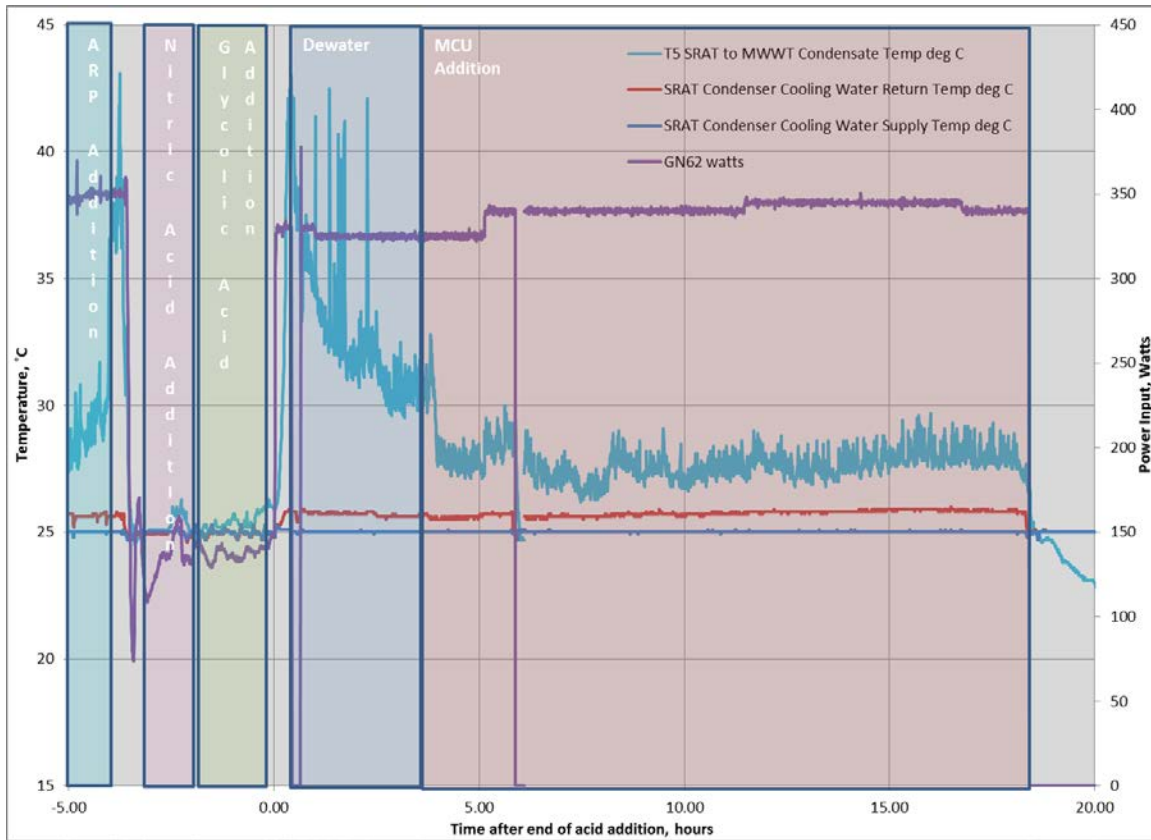


### Figure 3-32. GN62 SRAT Cycle Condenser Temperature Profile

**Recommendation:** A good practice is stopping steam flow when the ARP pump is turned off and/or ramping down the ARP flowrate. This prevents the surge in offgas as the flow is turned off.  
**Recommendation:** It is recommended to test the viability of adding nitric acid before adding the ARP product. The nitric acid reduces the pH to approximately seven, where the antifoam is much more stable and effective at a more neutral pH.

#### 3.1.7 GN60-64 MCU

All five SRAT cycles included a segment where the MCU Strip Effluent simulant was added at boiling. This occurred after the SRAT dewater was complete and lasted for fifteen hours. The Strip Effluent simulant was added at 4.2 ml/min with a boilup rate of 4.2 ml/min. The Strip Effluent stream was created by combining a 0.01 M (0.03 N) boric acid solution at 4.2 ml/min with a 0.0435  $\mu\text{L}/\text{min}$  solvent stream to produce an 87 mg/kg solvent concentration. This is equivalent to a 10,000-gallon MCU Strip Effluent addition at 10 gpm and 5000 lb/hr steam flow. The solvent was blended to match the solvent composition after switching to the MaxCalix solvent.

There were some difficulties in maintaining a constant solvent concentration throughout the strip effluent addition phase. The syringe pump has options of 0.04 or 0.05  $\mu\text{L}/\text{min}$ , so the solvent was added at 0.05  $\mu\text{L}/\text{min}$  and the solvent addition was complete prior to the boric acid solution. In addition, the solvent pump was bumped several times causing a small surge in flow as technicians were ensuring that the syringe pump was operating properly. It is also very hard to start the solvent flow concurrent with the boric acid solution flow as any space between the syringe and pump could take up to an hour to close and begin pumping solvent. Therefore, there were several deviations from the planned, constant feed rate but it likely did not affect the results of this test.

It should also be noted that there is no analytical technique for the BobCalix or MaxCalix in the solvent so only the isopar and modifier were analyzed.

A mass balance was completed and the results are summarized in Table 3-11. The isopar mass balance demonstrates that all of the isopar is volatilized in the SRAT and exits through the offgas system so none is present in the SRAT product or melter feed. The modifier mass balance was ten times the amount added was noted in the sample analyses. The data showed that approximately 90% of the modifier was stripped out during SRAT boiling and was collected in the dewater (SMECT). Another 5% was detected in the SRAT product, although this is likely to be removed by steam stripping during the SME cycle so little likely remains in the melter feed. Analysis of the modifier should be completed using High-Performance Liquid Chromatography in future testing.

**Table 3-11. Solvent Component Mass Balance**

Source	Solvent, mg	Isopar, mg	Modifier, mg
Solvent Added	1,661	1,080	216
ARP Dewater		0	74
SRAT Dewater		0	179
MCU Dewater		0	1,493
Offgas		748	54
SRAT Product		0	178
Other		55	2
Total Mass Balance		803	1,980

3.1.8 *GN60-64 SRAT Heating Rod Heat Transfer*

Two rods used for providing the heat for processing. These rods also have thermocouples and measure the amps and volts supplied during heating. This allows the calculation of a heat transfer coefficient, a measure of how efficiently the heat is transferred to the slurry. Heating rods are used in our testing because they are very similar to steam coils and thus have a way to track the fouling of the rods. In previous testing, the rods fouled<sup>16</sup> during processing in a similar manner to the coil fouling that has been seen in DWPF.

The measured heat transfer coefficient increased from about 0.15 to 0.17 W/cm<sup>2</sup>/°C during acid addition. The heat transfer increased slightly at the beginning of boiling and stayed steady throughout the rest of the SRAT cycle. Even more importantly, the heat transfer trend was very similar from run to run so based on these readings and the visual inspection after the last run was completed, there was no fouling noted in the SRAT cycles. The heat transfer coefficient data is summarized in Figure 3-33.

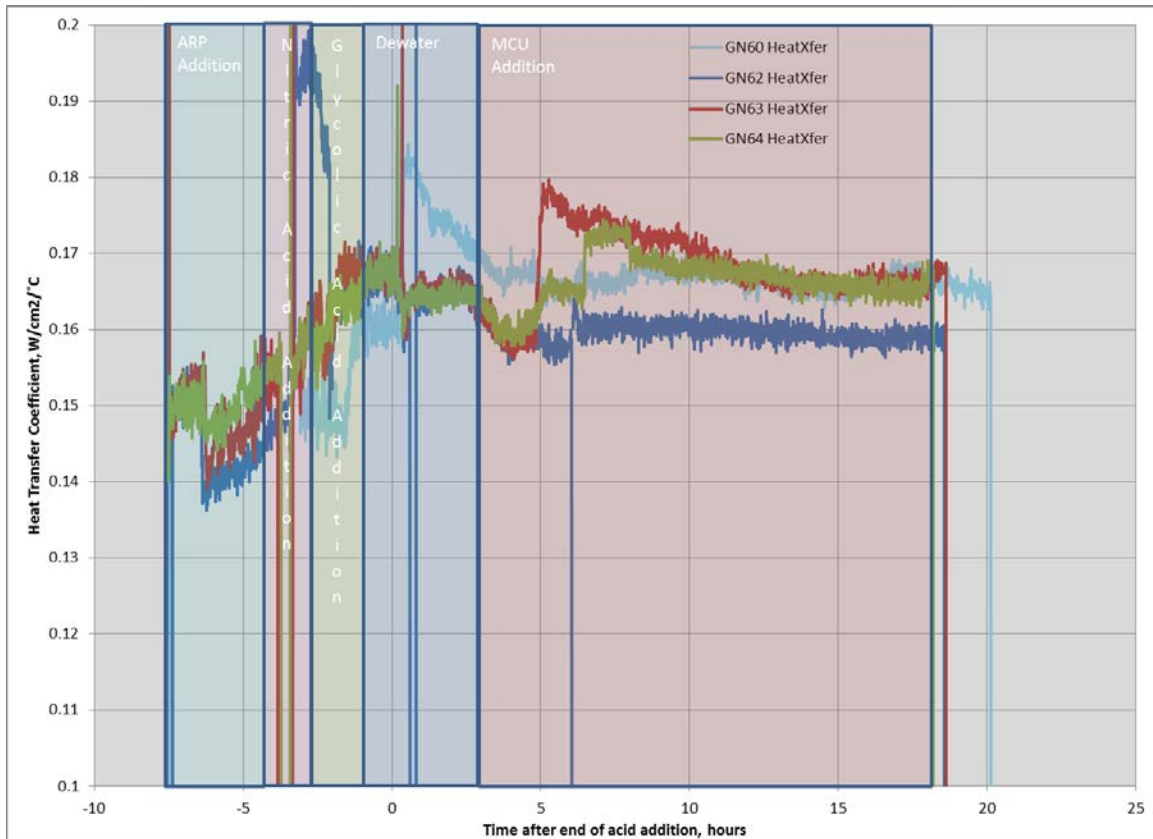


**Figure 3-33. SRAT Heat Transfer Coefficient Profile**

The temperature to the heating rods is another measure of fouling. If the power input has to be increased to maintain the desired boilup, it is evidence that fouling may be occurring. Increasing power to the rods increases the rod temperature and accelerates fouling. To prevent the rod temperature from increasing above the DWPF steam coil temperature, a control loop was added to control the heating rod temperature below the 160°C possible at 80 psig steam.

In the first of the five back-to-back experiments, the power input was changed at least five times to maintain the desired boilup rate. However, the rest of the experiments, used the settings from the previous run and had little problem controlling the boilup rate (Figure 3-34). The identical power curves indicate no differences in reaction chemistry. No sign of coil fouling was noted in these five SRAT cycles.

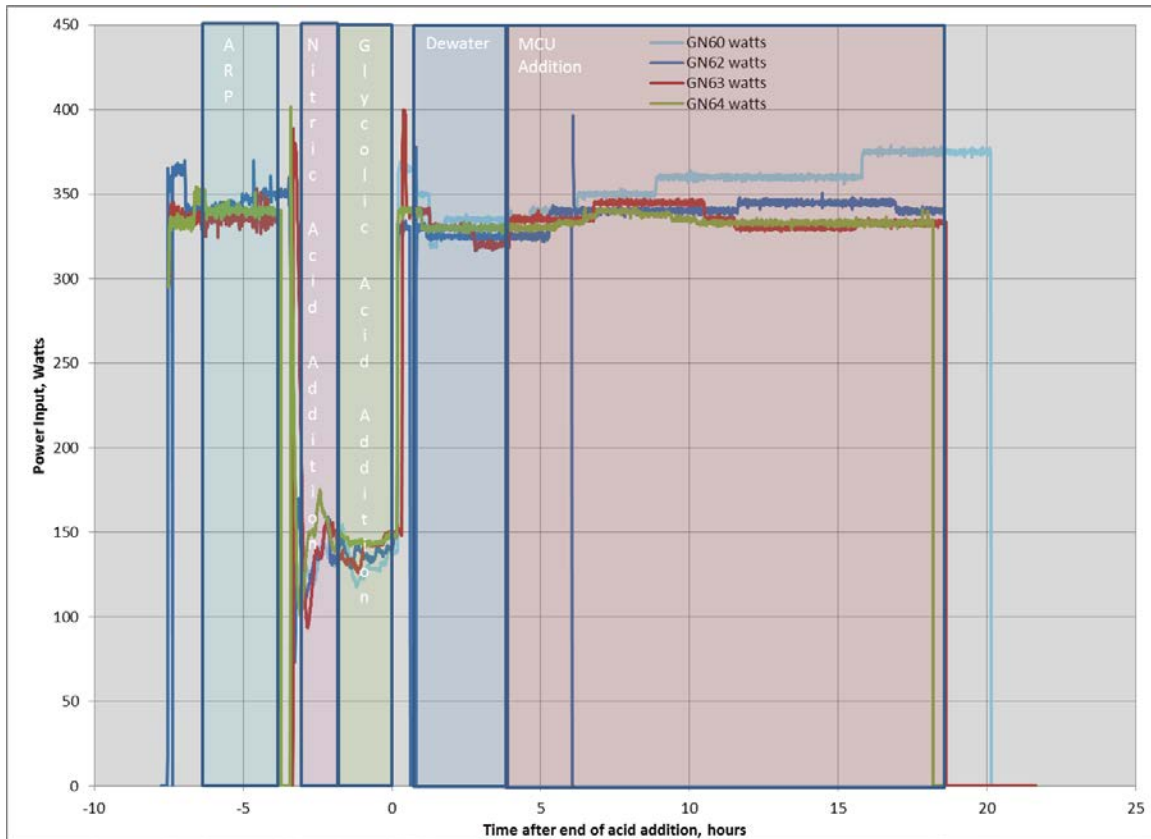


**Figure 3-34. SRAT Power Input Profile**

### 3.1.9 GN60-64 REDOX

SRAT Product samples were pulled from runs GN60, GN62 and GN64. A portion of the SRAT product was combined with sufficient Frit 418 and vitrified in a crucible. The resulting glass was analyzed for REDOX. The REDOX target for these runs was 0.2. The measured REDOX was  $0.55 \text{ Fe}^{+2}/\Sigma\text{Fe}$  for GN60,  $0.46 \text{ Fe}^{+2}/\Sigma\text{Fe}$  for GN62, and  $0.50 \text{ Fe}^{+2}/\Sigma\text{Fe}$  for GN64

### 3.1.10 GN60-64 Ammonia Scrubber

The ammonia scrubber used in this testing is not prototypic of DWPF. All condensate from the DWPF SRAT, SME and FAVC drains to the SMECT and is recirculated through all three ammonia scrubbers. In this testing, 750 mL of a 0.01 M nitric acid solution (pH 2, 620 mg/L nitrate) is recirculated through the SRAT ammonia scrubber. The condensate generated is drained to sample bottles and is not recirculated through the ammonia scrubbers. In the case of a foamover, the slurry would be collected in the condensate sample bottle and is not recirculated through the scrubber. As a result, the ammonia scrubber is virtually solids free. However, it does scrub anions such as nitrate from the offgas. An ammonia scrubber sample was pulled at the completion of run GN64. The sample was analyzed and the results are summarized in Table 3-12.

**Table 3-12. Ammonia Scrubbers Sample Results**

Source	Analysis	Units
$\text{NH}_4^+$	<10	mg/L
$\text{F}^-$	<10	mg/L
$\text{Cl}^-$	<10	mg/L
$\text{NO}_2^-$	<10	mg/L
$\text{NO}_3^-$	40,500	mg/L
$\text{C}_2\text{H}_3\text{O}_3^-$	22	mg/L
$\text{SO}_4^{2-}$	20	mg/L
$\text{C}_2\text{O}_4^{2-}$	<10	mg/L
$\text{HCO}_2^-$	22	mg/L

The nitrate concentration, 40,500 mg/L was 65.3 times higher than starting solution. The ammonia scrubber did not remove ammonia from the offgas system as no ammonia was detected in the ammonia scrubber solution. Either no ammonia was produced or the ammonia remained soluble in the SRAT product.

### 3.1.11 GN60-64 Lessons Learned

What should be done differently in future back-to-back SME cycles? Testing can always be improved upon and the following are the author's thoughts on what changes might be prudent in future back-to-back SRAT testing:

1. Complete the SRAT cycles using the same recipe as a previous successful experiment. In these experiments, the REDOX was high and this could have been prevented by completing a series of SRAT cycles first and using the conditions from the optimum experiment for the back-to-back experiments. In addition, the product from the optimum experiment could serve as the heel so that each experiment would include a heel.
2. Videotaping the experiments throughout is also recommended. This would help to identify when foamovers happen and help to understand the collection of mercury in the MWWT. In addition, making sure a camera was present in the lab for still photos is essential in documenting interesting observations.
3. The presence of ARP and MCU strip effluent make a huge difference in processing. These should be included in future experiments as much as possible. However, the organic added with the strip effluent likely has no impact on processing and could be eliminated. The solvent was added to the kettles as planned in only two of the five experiments so its elimination would also simplify the experiments without losing significant processing information.
4. This testing was completed at design basis conditions. Future testing should be completed at prototypic processing conditions. This will lengthen the testing but will be more realistic as it would duplicate the time at temperature, which affects antifoam degradation, antifoam addition amount, anion destruction, and steam stripping.
5. Varying the conditions for the five runs will allow gathering more information in an attempt to better understand DWPF SRAT processing. Runs GN61-64 were identical. For example, varying the SRAT dewater amount would allow testing at various slurry rheologies to help in understanding rheological impacts such as fouling of coils.
6. Digestion and analysis of the collected MWWT mercury would help in determining the mass of Hg collected. The mass of mercury is likely overestimated, as the assumption is that it is elemental Hg. For example, if some of the mercury is present as calomel ( $\text{Hg}_2\text{Cl}_2$ ) or mercuric oxide, the Hg mass can be overestimated by 15%. Although the

mercury is dried out in the dessicator, there is likely some water, sludge solids and antifoam present with the mercury. In addition, identification of the forms of mercury is also suggested.

### 3.2 GN65-68 Back to Back SME Simulations using GN SRAT Product Blend and Frit 418

No GN Flowsheet experiments have been completed utilizing a heel and no back-to-back experiments have been completed prior to this set of experiments. In all previous GN experiments, each experiment began with a clean SRAT/SME vessel and clean offgas equipment (SRAT/SME condenser and FAVC). In this series of experiments, the first SME cycle (GN65) began with clean glassware, 3,000 g of SRAT product (Table 2-2) and no heel. The rest of the experiments (GN66-68) started with 750 g of SME heel from the previous experiment and 2,250 g of SRAT product. The time line for the runs is summarized in Table 3-13.

**Table 3-13. SME Processing Time Line**

Process Step	GN65	GN66	GN67	GN68
SME Boil#1	3/12/2013 16:40	3/13/2013 21:08	3/19/2013 13:50	3/20/2013 22:15
Decon Dewater #1	3/12/2013 18:46	3/13/2013 23:08	3/19/2013 15:42	3/21/2013 0:19
SME Boil#2	3/12/2013 19:23	3/13/2013 23:39	3/19/2013 16:15	3/21/2013 1:05
Decon Dewater #2	3/12/2013 21:23	3/14/2013 1:39	3/19/2013 18:10	3/21/2013 2:52
SME Boil#3	3/12/2013 22:01	3/14/2013 2:16	3/19/2013 18:50	3/21/2013 3:33
Decon Dewater #3	3/12/2013 23:56	3/14/2013 4:17	3/19/2013 20:36	3/21/2013 5:20
SME Boil#4	3/13/2013 0:28	3/14/2013 4:50	3/19/2013 21:25	3/21/2013 6:13
Decon Dewater #4	3/13/2013 2:33	3/14/2013 6:50	3/19/2013 23:15	3/21/2013 8:10
SME Boil#5	3/13/2013 3:05	3/14/2013 7:40	3/19/2013 23:58	3/21/2013 8:55
Decon Dewater #5	3/13/2013 5:00	3/14/2013 9:40	3/20/2013 1:50	3/21/2013 10:50
SME Boil#6	3/13/2013 5:28	3/14/2013 10:15	3/20/2013 2:40	3/21/2013 11:25
Decon Dewater #6	3/13/2013 7:26	3/14/2013 12:10	3/20/2013 4:55	3/21/2013 13:11
SME Boil#7	3/13/2013 9:05	3/14/2013 12:55	3/20/2013 9:04	3/21/2013 13:55
Frit Dewater #1	3/13/2013 10:25	3/14/2013 14:08	3/20/2013 10:30	3/21/2013 15:41
SME Boil#8	3/13/2013 11:07	3/14/2013 14:50	3/20/2013 11:10	3/21/2013 16:01
Frit Dewater #2	3/13/2013 14:03	3/14/2013 16:50	3/20/2013 13:53	3/21/2013 17:01
Can Blast Processing Time, hrs	14.8	15.0	15.1	14.9
Frit Dewater Processing Time, hrs	6.6	4.7	9.0	3.8

Due to breakage of the kettle in experiment GN66, run GN67 also started with a new kettle. The kettle in GN66 broke due to a design flaw in the Teflon cup between the glassware and agitator shaft. The frit eroded the cup's Teflon completely away and the agitator shaft nicked the glassware, leading to the breakage. The cup was redesigned after run GN66 and a new, stronger, thicker plastic cup, and a straighter shaft was used for the final two runs.

#### 3.2.1 GN65-68 SME Product

The slurry sample results for the four runs are summarized in Table 3-14, Table 3-15, and Table 3-16. The supernate sample results for the four runs are summarized in Table 3-17 and Table 3-18.

**Table 3-14. SME Product Slurry Cation Composition, wt % Calcined Solids**

Analyte	GN65	GN66	GN67	GN68
Al	5.795	5.73	5.455	5.455
B	1.430	1.455	1.390	1.365
Ba	0.069	0.0285	0.028	0.0275
Ca	0.649	0.6275	0.645	0.6505
Cr	0.0745	0.0555	0.0595	0.053
Cu	0.0465	0.0415	0.048	0.0425
Fe	8.395	8.095	8.025	7.865
K	0.08	0.065	0.0545	0.055
Li	2.175	2.19	2.085	2.06
Mg	0.4455	0.4325	0.4395	0.4535
Mn	1.17	1.155	1.17	1.165
Na	8.99	8.985	9.19	9.86
Ni	0.5205	0.511	0.5185	0.5085
S	0.0845	0.0855	0.1015	0.0915
Si	23.5	23.4	23.2	24.05
Sn	0.0235	0.017	0.018	0.018
Ti	0.121	0.022	0.0155	0.016
Zn	0.02	0.02	0.0205	0.02
Zr	0.0515	0.0545	0.0475	0.045

**Table 3-15. SME Product Slurry Anion Results**

Analyte	GN65	GN66	GN67	GN68
F	<500	<500	<500	<500
Cl <sup>-</sup>	546	490	411	401
NO <sub>2</sub> <sup>-</sup>	<500	<500	<500	<500
NO <sub>3</sub> <sup>-</sup>	60,050	57,400	48,700	49,450
C <sub>2</sub> H <sub>3</sub> O <sub>3</sub> <sup>-</sup>	26,050	26,350	22,050	29,050
SO <sub>4</sub> <sup>2-</sup>	1,640	1,435	1,190	1,320
C <sub>2</sub> O <sub>4</sub> <sup>2-</sup>	2,860	2,080	1,795	2,910
HCO <sub>2</sub> <sup>-</sup>	1,185	1,090	539	1,455
PO <sub>4</sub> <sup>3-</sup>	<500	<500	<500	<500

**Table 3-16. SME Product Solids, pH and Density Compositions**

<b>Analyte</b>	<b>GN65</b>	<b>GN66</b>	<b>GN67</b>	<b>GN68</b>
Total Solids, wt %	52.55%	50.50%	42.95%	41.25%
Insoluble Solids, wt %	39.70%	38.15%	32.75%	31.65%
Calcined Solids, wt %	40.95%	39.35%	33.50%	32.15%
Soluble Solids, wt %	12.85%	12.35%	10.20%	9.60%
pH	4.84	4.85	4.74	4.65
Slurry Density, g/mL	1.4406	1.3798	1.2853	1.2022
Supernate Density, g/mL	1.1505	1.1379	1.10325	1.0956

**Table 3-17. SME Product Supernate Cation Composition, mg/L**

<b>Analyte</b>	<b>GN65</b>	<b>GN66</b>	<b>GN67</b>	<b>GN68</b>
Al	344.5	210	296.5	283.5
B	38.45	38.5	31.9	26.3
Ba	4.745	3.275	3.445	2.87
Ca	3994.5	4095	2760	2590
Cr	12.4	8.685	5.995	7.81
Cu	40.75	35.75	27.3	29.85
Fe	2411	1360	1390	1290
K	723.5	561	471	380
Li	280	289	261	177
Mg	2809	2560	1825	1660
Mn	7441	6415	1800	4460
Na	42450	42850		27900
Ni	1936	1710	1260	1210
Pd	<0.100	<0.100	<0.100	<0.100
Rh	13.35	10.3	7.455	7.86
Ru	113.5	98.85	73.6	72.35
S	989	777	545	506
Si	76.15	69.2	49.55	56.85
Sn	8.5	6.73	3.935	4.835
Ti	<0.100	<0.100	<0.100	<0.100
Zn	27.65	22.9	14.8	15.95
Zr	18.5	10.1	8.29	10.8

**Table 3-18. SME Product Supernate Anion Composition, mg/L**

Analyte	GN65	GN66	GN67	GN68
F <sup>-</sup>	<500	<500	<500	<500
Cl <sup>-</sup>	1120	923	735	513
NO <sub>2</sub> <sup>-</sup>	<500	<500	<500	<500
NO <sub>3</sub> <sup>-</sup>	122,000	110,000	85,800	76,350
C <sub>2</sub> H <sub>3</sub> O <sub>3</sub> <sup>-</sup>	55,950	45,000	34,800	34,650
SO <sub>4</sub> <sup>2-</sup>	3,075	2,780	1,970	2,090
C <sub>2</sub> O <sub>4</sub> <sup>2-</sup>	2,210	2,205	1,590	1,650
HCO <sub>2</sub> <sup>-</sup>	1,900	NM	NM	1,210
PO <sub>4</sub> <sup>3-</sup>	<500	<500	<500	<500

**Table 3-19. SME Product Anion Solubility, %**

Analyte	GN65	GN66	GN67	GN68
F <sup>-</sup>	NM	NM	NM	NM
Cl <sup>-</sup>	108	102	109	79.8
NO <sub>2</sub> <sup>-</sup>	NM	NM	NM	NM
NO <sub>3</sub> <sup>-</sup>	106	104	107	96
C <sub>2</sub> H <sub>3</sub> O <sub>3</sub> <sup>-</sup>	113	93	96	74
SO <sub>4</sub> <sup>2-</sup>	98	105	101	99
C <sub>2</sub> O <sub>4</sub> <sup>2-</sup>	40.5	57.6	54.0	35.4
HCO <sub>2</sub> <sup>-</sup>	84.0	NM	NM	51.9
PO <sub>4</sub> <sup>3-</sup>	NM	NM	NM	NM

**Table 3-20. SME Product Cation Solubility, %**

Analyte	GN65	GN66	GN67	GN68
Al	0.76	0.51	0.99	1.01
B	0.34	0.37	0.42	0.37
Ba	0.88	1.59	2.24	2.03
Ca	78.78	90.14	77.86	77.26
Cr	2.13	2.16	1.83	2.86
Cu	11.22	11.90	10.35	13.63
Fe	3.68	2.32	3.15	3.18
K	116	119	157	134
Li	1.65	1.82	2.28	1.67
Mg	80.70	81.76	75.56	71.03
Mn	81.40	76.72	27.99	74.29
Na	60.44	65.88	0.00	54.91
Ni	47.61	46.22	44.22	46.17
S	150	126	98	107
Si	0.04	0.04	0.04	0.05
Sn	4.63	5.47	3.98	5.21
Ti	BDL	BDL	BDL	BDL
Zn	17.69	15.82	13.14	15.48
Zr	4.60	2.56	3.18	4.66

### 3.2.2 GN65-68 Dewater Samples

Dewater samples were pulled from the condensate collected during the simulation of six canister blasts and two process frit additions. The purpose of these samples was to track the concentrations of anions and cations from run to run. Visually, the samples looked very clear.

The samples were analyzed for both anions by IC and cations by ICP-AES by PSAL. All anions (F<sup>-</sup>, Cl<sup>-</sup>, NO<sub>2</sub><sup>-</sup>, NO<sub>3</sub><sup>-</sup>, C<sub>2</sub>H<sub>3</sub>O<sub>3</sub><sup>-</sup>, SO<sub>4</sub><sup>2-</sup>, C<sub>2</sub>O<sub>4</sub><sup>2-</sup>, HCO<sub>2</sub><sup>-</sup> and PO<sub>4</sub><sup>3-</sup>) were below the 100 mg/L detection limit. Only Si was present at a concentration above 2 mg/L. Si was very low in the frit dewater (<1.00 to 3.66 mg/L). The Si was much higher in the canister dewater sample varying from 39.4-141 mg/L. As was discussed in the SRAT processing, this is an antifoam degradation product, not the result of frit leaching. Al, Ca, and Cu were above their detection limit of 0.1 mg/L in almost all samples. The cation results are summarized in Table 3-21.

**Table 3-21. In process Dewater Analysis by ICP-AES, mg/L**

Sample Element	Composite Decon Dewater				Composite Frit Dewater			
	GN65	GN66	GN67	GN68	GN65	GN66	GN67	GN68
Al	0.907	0.939	0.907	0.781	0.898	0.928	0.907	1.034
Ba	<0.100	<0.100	<0.100	<0.100	<0.100	<0.100	<0.100	<0.100
Ca	0.851	0.866	0.812	1.11	0.798	0.800	0.823	0.992
Cd	<0.100	<0.100	<0.100	<0.100	<0.100	<0.100	<0.100	<0.100
Cr	<0.100	<0.100	<0.100	<0.100	<0.100	<0.100	<0.100	<0.100
Cu	0.236	0.231	0.168	<0.100	0.199	0.190	0.166	<0.100
Fe	<0.100	<0.100	<0.100	<0.100	<0.100	<0.100	<0.100	<0.100
Gd	<0.100	<0.100	<0.100	<0.100	<0.100	<0.100	<0.100	<0.100
K	<10.0	<10.0	<10.0	<10.0	<10.0	<10.0	<10.0	<10.0
Li	<10.0	<10.0	<10.0	<10.0	<10.0	<10.0	<10.0	<10.0
Mg	<0.100	<0.100	<0.100	<0.100	<0.100	<0.100	<0.100	<0.100
Mn	<0.100	<0.100	<0.100	<0.100	<0.100	<0.100	<0.100	<0.100
Na	<1.00	<1.00	<1.00	<1.00	<1.00	<1.00	<1.00	<1.00
Ni	<0.100	<0.100	<0.100	<0.100	<0.100	<0.100	<0.100	<0.100
P	<0.100	<0.100	<0.100	<0.100	<0.100	<0.100	<0.100	<0.100
Pb	<0.100	<0.100	<0.100	<0.100	<0.100	<0.100	<0.100	<0.100
S	<0.100	<0.100	<0.100	<0.100	<0.100	<0.100	<0.100	<0.100
Si	61.800	39.350	42.450	141.00	<1.00	<1.00	2.370	3.660
Sn	<0.100	<0.100	<0.100	<0.100	<0.100	<0.100	<0.100	<0.100
Ti	<0.100	<0.100	<0.100	<0.100	<0.100	<0.100	<0.100	<0.100
Zn	<0.100	<0.100	<0.100	<0.100	<0.100	<0.100	<0.100	<0.100
Zr	<0.100	<0.100	<0.100	<0.100	<0.100	<0.100	<0.100	<0.100

### 3.2.3 GN65-68 In Process Supernate Samples

A sample was pulled from the slurry, then centrifuged after the completion of dewater after the second, fourth and sixth canister blasts. A sample was pulled after the process frit dewater was complete. The purpose of these samples was to look for solubility changes from run to run. The samples were analyzed by PSAL for both anions by IC and cations by ICP-AES. The anions results are summarized in Table 3-22. The cation results are summarized in Table 3-23.

In each run, the formate (Figure 3-35) was highest when the sample was pulled after the second canister blast. Then the concentration dropped with each subsequent blast. The incoming SRAT product for each run contained 3,250 mg/kg formate, so the formate was slowly destroyed in the SME cycle with minimal hydrogen generation. The samples pulled during dewater had added sodium hydroxide to quench the chemical reactions, although the SME product sample did not. It is likely that there was some formate generation after the SME cycle was complete (between the time the sample was pulled and when it was analyzed weeks later). The glycolate concentration (Figure 3-36) was fairly constant throughout the SME cycle.

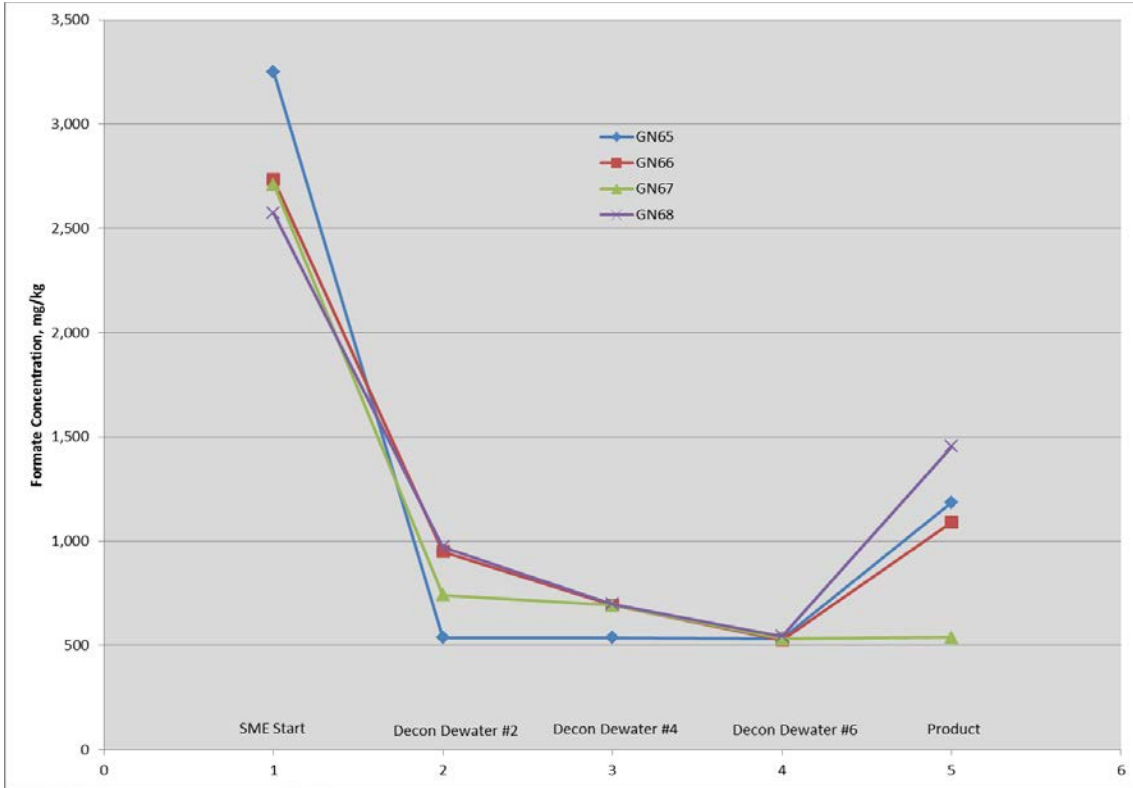


Figure 3-35. SME Formate Concentration, mg/kg

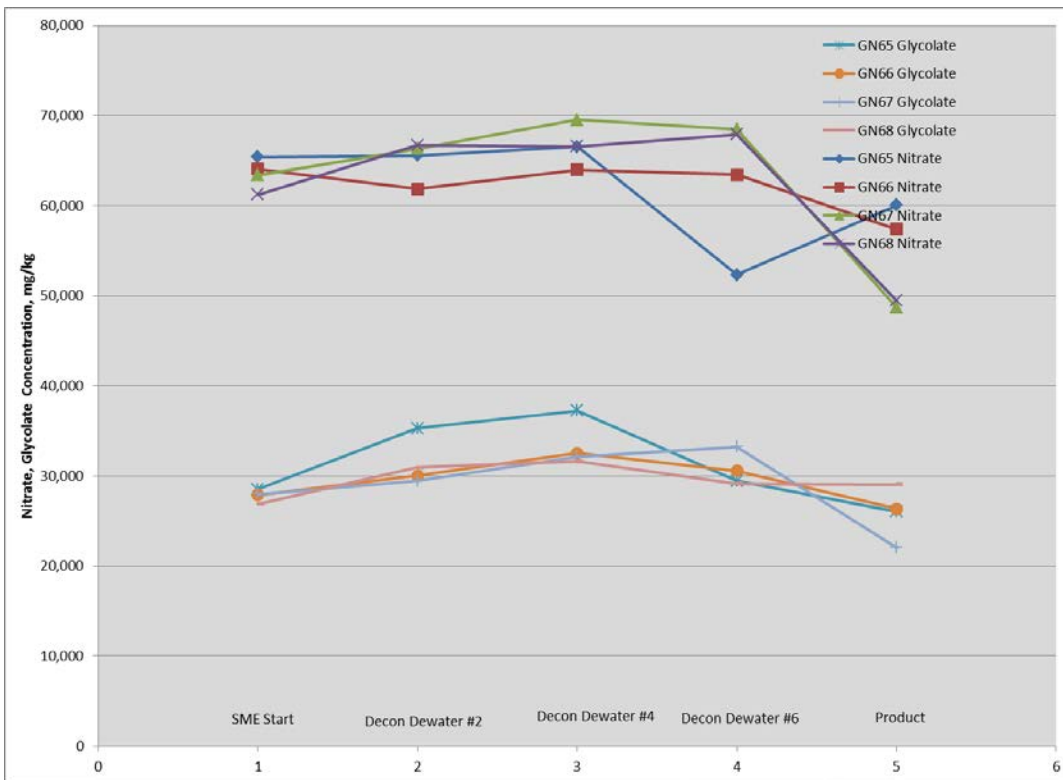


Figure 3-36. SME Nitrate, Glycolate Concentration, mg/kg

**Table 3-22. In Process Supernate Analysis by IC, mg/L**

Analyte	GN65	GN65	GN65	GN66	GN66	GN66	GN67	GN67	GN67	GN68	GN68	GN68
	2 canisters	4 canisters	6 canisters									
F <sup>-</sup>	<500	<500	<500	<500	<500	<500	<500	<500	<500	<500	<500	<500
Cl <sup>-</sup>	562	612	480	482	514	503	535	505	505	499	482	495
NO <sub>2</sub> <sup>-</sup>	<500	<500	<500	<500	<500	<500	<500	<500	<500	<500	<500	<500
NO <sub>3</sub> <sup>-</sup>	32,900	34,700	27,600	27,900	30,300	28,700	27,400	29,900	31,100	28,800	29,500	27,300
C <sub>2</sub> H <sub>3</sub> O <sub>3</sub> <sup>-</sup>	61,100	62,100	49,100	57,600	59,700	59,500	61,700	64,900	64,200	62,100	62,100	63,700
SO <sub>4</sub> <sup>2-</sup>	1,630	1,730	1,450	1,450	1,600	1,630	1,530	1,490	1,410	1,470	1,500	1,550
C <sub>2</sub> O <sub>4</sub> <sup>2-</sup>	1,690	2,020	1,580	2,510	2,790	1,880	1,790	2,250	2,020	1,710	1,830	1,990
HCO <sub>2</sub> <sup>-</sup>	<500	<500	<500	885	645	493	691	645	499	905	650	510

**Table 3-23. In Process Supernate Analysis by ICP-AES, mg/L**

	<b>GN65</b>	<b>GN65</b>	<b>GN65</b>	<b>GN66</b>	<b>GN66</b>	<b>GN66</b>	<b>GN67</b>	<b>GN67</b>	<b>GN67</b>	<b>GN68</b>	<b>GN68</b>	<b>GN68</b>
<b>Element</b>	<b>Decon Dewater #2</b>	<b>Decon Dewater #4</b>	<b>Decon Dewater #6</b>									
Al	685	487	377	443	320	288	537	363	313	461	387	339
Ba	4.96	4.53	4.14	4.70	4.80	4.98	3.96	4.46	4.33	4.23	4.30	4.57
Ca	3,500	3,520	2,890	3,570	4,010	4,850	2,930	3,370	3,150	3,090	3,150	3,030
Cr	21.4	14.7	10.6	17.7	12.2	9.32	19.6	11.0	8.8	15.9	11.5	9.35
Cu	54.8	36.7	30.8	50.6	25.9	22.8	41.7	31.6	25.6	47.5	36.1	31.4
Fe	2,680	2,840	2,070	1,340	793	1,110	1,180	2,390	2,160	1,970	2,040	2,010
K	522	533	456	446	470	480	373	469	474	384	414	413
Li	<10.0	<10.0	37.4	66.0	77.8	91.6	67.8	101	108	65.8	75.5	82.0
Mg	2,090	2,070	1,750	2,210	2,210	2,230	1,640	1,990	1,940	1,770	1,810	1,770
Mn	6,040	5,910	4,970	5,910	5,810	5,730	4,730	5,440	5,200	5,030	4,960	4,770
Na	30,200	31,100	26,700	35,800	36,700	37,500	26,300	32,700	32,500	29,700	30,500	30,400
Ni	1,560	1,460	1,230	1,530	1,500	1,480	1,240	1,410	1,370	1,320	1,300	1,260
P	0.543	0.510	0.487	<1.00	<1.00	<1.00	<0.100	<0.100	<0.100	<0.100	<0.100	<0.100
S	699	710	621	617	656	656	448	544	543	492	518	515
Si	57.2	51.1	45.1	63.8	61.8	61.2	47.6	49.4	47.2	61.5	59.3	57.0
Sn	11.0	8.40	6.46	9.81	8.14	6.73	8.05	5.60	4.86	7.55	6.11	5.40
Ti	<0.100	<0.100	<0.100	<0.100	<0.100	<0.100	<0.100	<0.100	<0.100	<0.100	<0.100	<0.100
Zn	23.4	22.2	18.7	22.7	20.9	20.0	17.3	16.7	15.6	17.7	16.5	16.0
Zr	36.3	25.5	17.9	23.2	14.6	12.5	24.9	16.3	13.5	21.8	16.9	14.0

### 3.2.4 GN66-68 Post Run FAVC, and SMECT samples

Samples were pulled at the completion of each run from the SMECT (nitric acid circulated through ammonia scrubber), and FAVC. The samples were analyzed by IC for anions and ICP-AES for cations. The results are summarized in the following subsections.

#### 3.2.4.1 GN65-68 Post Run FAVC Sample Results

The FAVC sample is a very small sample (3-5 g) that is historically high in nitric and reducing acids. Only Si had a concentration above 10 mg/L, with a concentration from 27.5-111 mg/L. This is likely an antifoam degradation product. Because of the small sample size and large anion concentration, only the glycolate anion was quantified in the sample. The glycolate concentration ranged from 292,000 mg/L to 378,000 mg/L. This sample was also analyzed by AD for ammonium, with no ammonium detected (<10 mg/L).

#### 3.2.4.2 GN65-68 Post Run SMECT Sample Results

The SMECT samples are expected to be very low in anions and cations, unless there has been a foamover. Si had the highest concentration from <1-141 mg/L. This is likely an antifoam degradation product. Aluminum, calcium, and copper were detected in all runs but were below 1 mg/L.

None of the anions was above the 100-ppm detection limit.

### 3.2.5 GN65-68 Offgas

Unlike the SRAT cycles, only the GC was used to monitor helium, hydrogen, oxygen, nitrogen, carbon dioxide, and nitrous oxide throughout the runs.

The hydrogen was low throughout the testing with a maximum hydrogen concentration of 0.018 volume %, just after initiating boiling after the 6<sup>th</sup> can blast for run GN67. In each run, the hydrogen peaked at each onset of boiling. The average hydrogen concentration was about 0.012 volume %, 0.3% of the Lower Flammability Limit (LFL) of 4-volume % in air. A graph summarizing the data is included in Figure 3-37.

The carbon dioxide was low compared to SRAT processing. The highest CO<sub>2</sub> concentration was just after the initiation of boiling in run GN65. Like the hydrogen, the CO<sub>2</sub> peaked each time boiling was initiated, although each peak was lower than the last during any run. The CO<sub>2</sub> concentration dropped from about 2-volume % at the beginning of the SME cycle to about 0.5 volume % by the completion of each SRAT cycle. A graph summarizing the data is included in Figure 3-38.

There is no evidence that appreciable oxygen is being consumed in the SME cycle, although there might be a small oxygen decrease at initiation of boiling. A graph of oxygen versus nitrogen should give the same curve if not oxygen is being consumed. The data is compared in Figure 3-39 for Run GN67.

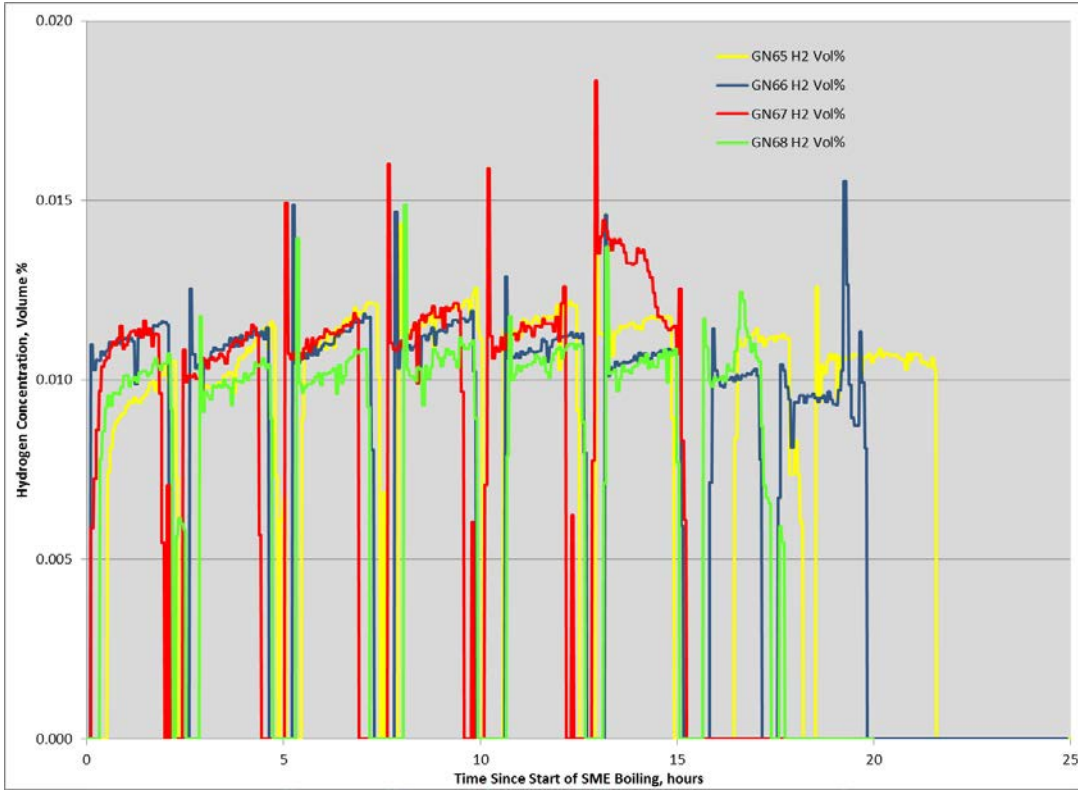


Figure 3-37: SME Measured Hydrogen Concentration, volume %

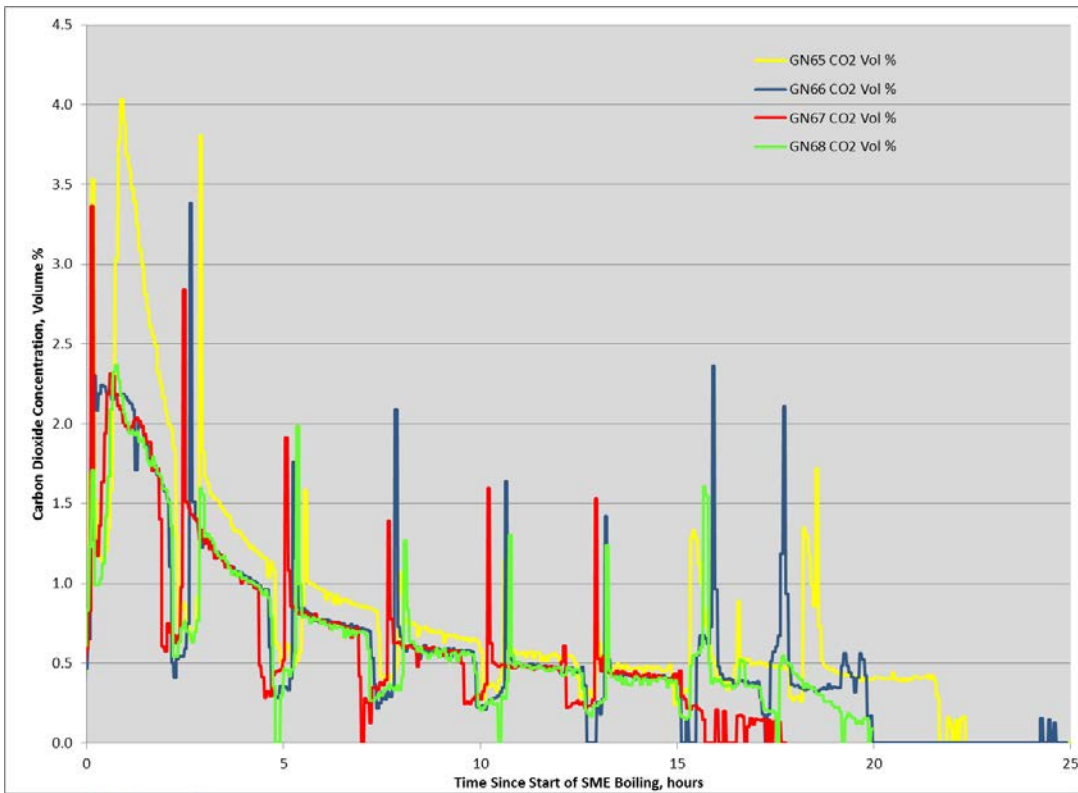
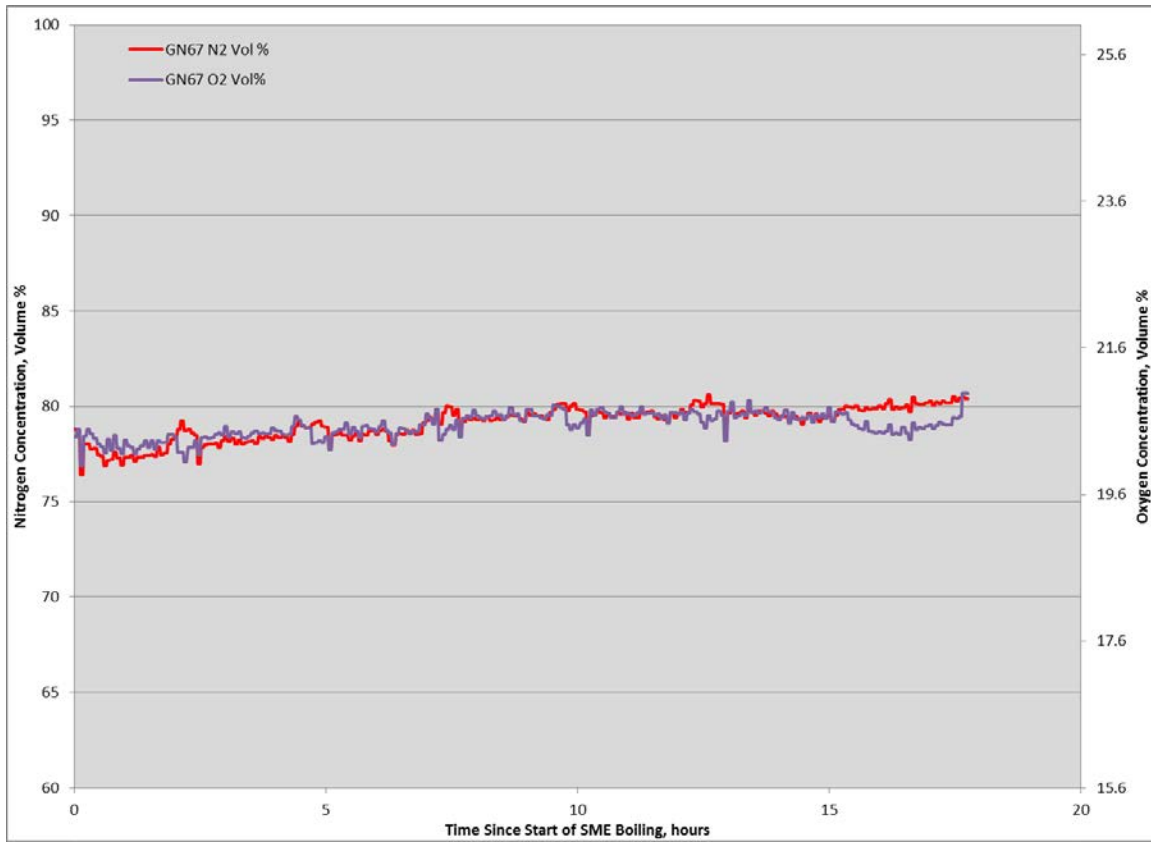


Figure 3-38: SME Measured Carbon Dioxide Concentration, volume %



**Figure 3-39: SME Nitrogen versus Oxygen Concentration, volume %**

**Table 3-24: Peak Offgas Generation Rates (lb/hr)**

<b>RUN</b>	<b>Peak CO<sub>2</sub></b>	<b>Peak NO</b>	<b>Peak N<sub>2</sub>O</b>	<b>Peak H<sub>2</sub></b>
GN65	27.9	0.176	BDL	0.0041
GN66	22.1	0.171	0.730	0.0049
GN67	21.5	0.145	0.850	0.0076
GN68	15.4	0.144	0.541	0.0039

Figure A-6 through Figure A - 9 of Appendix A contains plots of the GC data from the individual runs.

### 3.2.6 GN65-68 pH

The pH increased slowly during processing, from a pH of 4 to a pH of 4.5 based on the online pH meter. The lab measured pH or the SRAT product blend was 4 and the SME product pH varied from 4.65 to 4.85. The pH peaks each time boiling is initiated and then decreases. The most concentrated runs (GN65 and GN66) both had strange pH behavior during the final concentration phase after the 2<sup>nd</sup> frit addition (time of maximum concentration). The data is summarized in Figure 3-40.

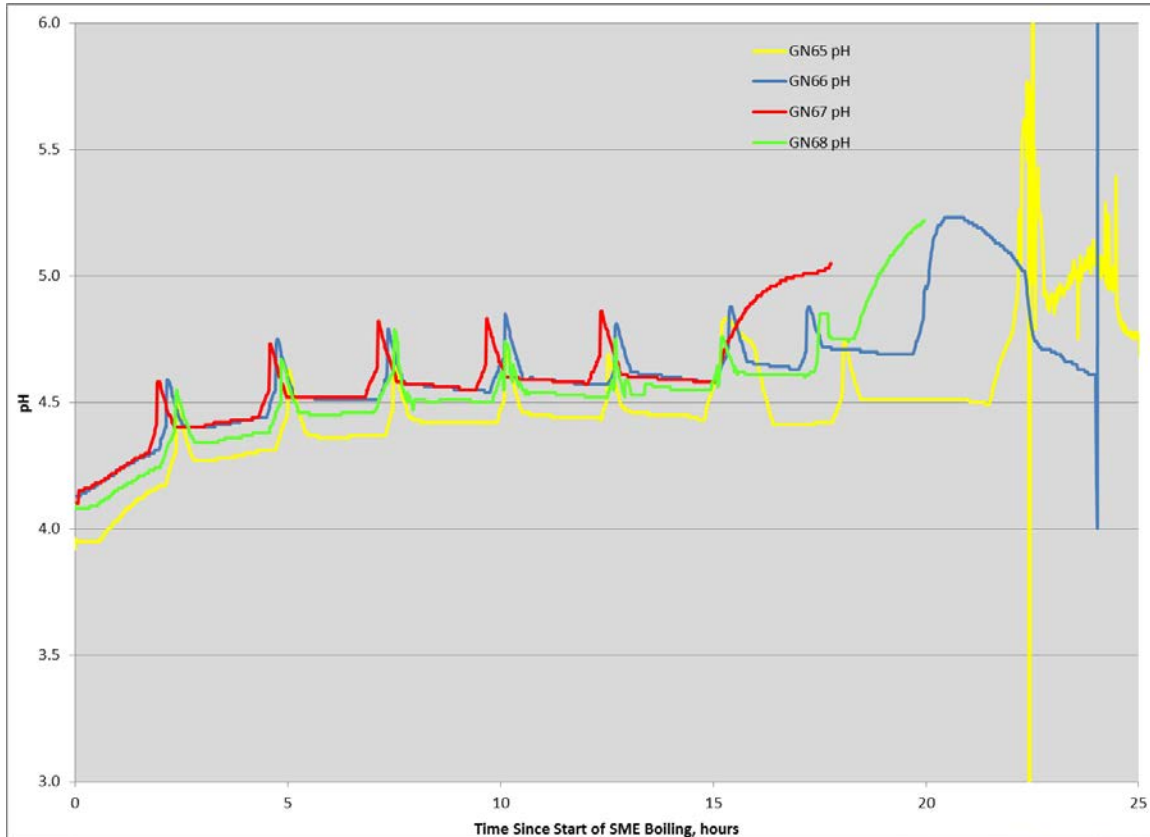


**Figure 3-40: SME cycle pH**

### 3.2.7 GN65-68 SME Heating Rod Heat Transfer

The same type of heating rods were used during SME processing as the SRAT cycles. The measured heat transfer coefficient varied from about 0.14 to 0.15 W/cm<sup>2</sup>/°C throughout the SME processing. This is a little lower than the SRAT processing but it should be noted that different sludge was used in the SRAT and SME cycles. The heat transfer coefficient data is summarized in Figure 3-41.

Three fouling incidents are highlighted on Figure 3-41. The first was GN66, one of the rods fouled, the heat transfer coefficient drops to half (0.06 W/cm<sup>2</sup>/°C), the heat was turned off from that rod, and the fouling was removed by processing. The second is GN67, one of the rods fouled, the heat transfer coefficient drops to half (0.06 W/cm<sup>2</sup>/°C), the heat was turned off from that rod, and the fouling was removed by processing. The third was GN68, one of the rods fouled, the heat transfer coefficient drops to half (0.06 W/cm<sup>2</sup>/°C), the heat was turned off from that rod. After fouling in Run GN67, the rod was removed and the fouled rod material was extracted. A photo of the material is included in Figure 3-42.

When an experimental heating rod fouls, it heats up (usually just rod T8). The temperature controller will adjust by cutting back the Watts to both rods to prevent the fouling. The fouled rod has very low heat transfer and most of the heat from the rod is used to dry out the deposit and make heat transfer even worse. Unplugging the rod stops that rod from continuing to bake on and create a brick around the heating rod. It also gives the rod time to recover as was noted that the fouling was removed by processing. In our experiments, the hotter of the two rods is responsible for very little of the heat transfer with the cooler rod doing the bulk of the heating.

In DWPF, the coils likely foul using the same principles. As portions of the coil foul, heat transfer is poor. The steam controller's response is to open the steam valve (increase steam pressure), which returns the steam flow to the target and raises the temperature in the coil. This has two results, the steam flow does go up but the temperature inside the coil also goes up (since the pressure of the steam is now higher), which dries the deposit and makes heat transfer through the fouled section of the coil even lower. The fouling is likely to expand as the steam temperature increases. Eventually, the steam valve is 100% open and the steam flow cannot be maintained. The steam flow drops off to nothing, as the steam is not being condensed in the coil.

**Recommendation:** A good practice to minimize coil fouling is to monitor the steam pressure and steam flow. There should be a direct correlation between flow and pressure. When it takes more pressure to get the same flow, the slurry is either very thick or the coils are starting to foul.

**Recommendation:** Another good practice is to calculate the steam coil heat transfer coefficient and monitor this during boiling. It would be expected to show the same pattern as Figure 3-41 with the heat transfer coefficient decreasing slightly as the slurry is concentrated but recovering to the same value after each decon blast or frit slurry addition.

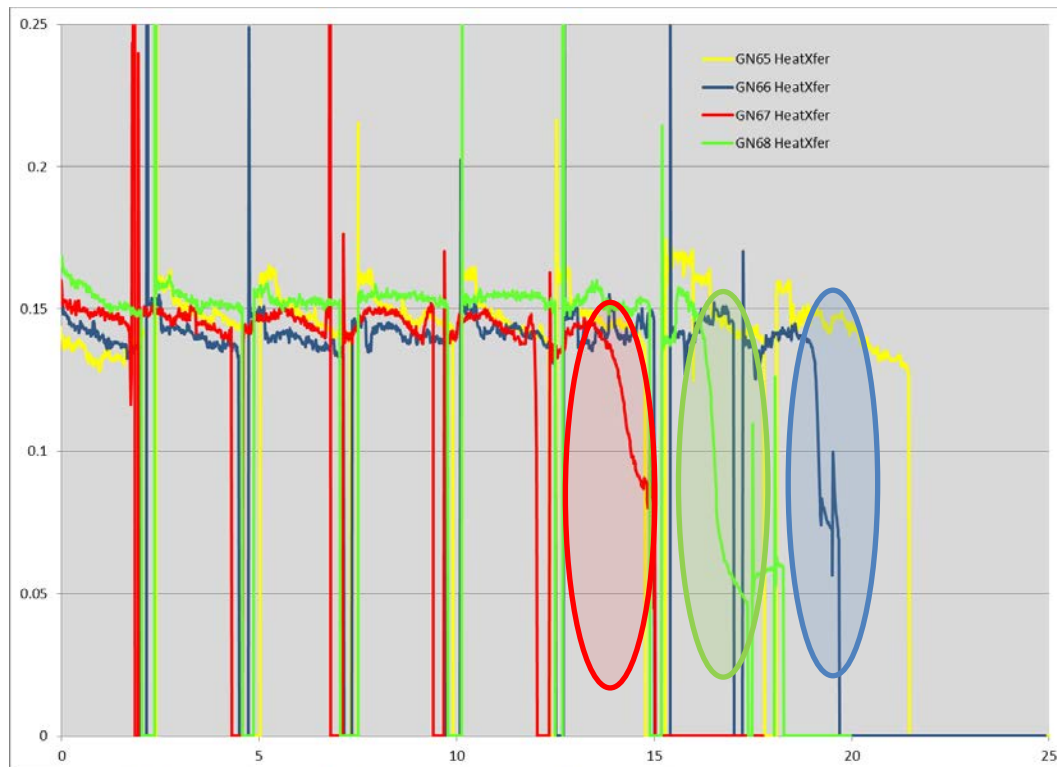


**Figure 3-41: SME Cycle Heat Transfer Coefficient Profile**



**Figure 3-42: SME Cycle Fouled Rod Deposits**

### 3.2.8 GN65-68 SME Foaming

The plan for antifoam addition during these SME cycles was to add 100 mg/kg antifoam before initiating boiling, and then add antifoam only as needed to control foam. The SME cycles lasted approximately 24 hours at boiling, much shorter than a typical DWPF SME cycle due to design basis boilup rates. It was expected that at least two 100 mg/kg antifoam additions would be needed for each SME cycle. The following summarizes the foam related incidents during the runs.

Additional antifoam was added only during the last SME cycle (GN68) to control foaming. GN68 included three extra 100 mg/kg additions of foam over a two-hour period, just after the start of boiling at the beginning of the SME cycle (decon blast #1). This was the most dilute of the four runs, ending the SME cycle at 41.25 wt % total solids.

Run GN67 also had a small foamover, which was not witnessed by the technicians. This occurred soon after the initiation of boiling after the first frit addition. Significant foam was also noted in GN67 after the initiation of boiling after the third can blast. This was another dilute run, ending the SME cycle at 42.98 wt % total solids.

No additional antifoam additions or notes about foaming were record for runs GN65 and GN66.

### 3.2.9 GN65-68 SME Anion Destruction

The anion destruction was calculated for each of the four SME cycles. The results are summarized in Table 3-25.

**Table 3-25. SME Cycle Anion Destruction**

<b>Anion</b>	<b>GN65</b>	<b>GN66</b>	<b>GN67</b>	<b>GN68</b>
Formate	43.7	34.7	58.2	13.0
Glycolate	1.7	-14.9	-4.8	-47.1
Oxalate	-60.2	-17.4	-21.7	-109.7
Nitrate	1.3	-9.0	-4.8	-9.9

3.2.10 *GN65-68 SME REDOX*

The REDOX was measured on first and last of the four SME products. The results are summarized in Table 3-26. Note that there was no REDOX target, the REDOX was controlled by the SRAT product blend that was used.

**Table 3-26. SME REDOX**

<b>Anion</b>	<b>GN65</b>	<b>GN68</b>
Measured REDOX	0.275	0.224

3.2.11 *GN65-68 Ammonia Scrubber*

An ammonia scrubber sample was pulled after each run. Each sample was analyzed and the results are summarized in Table 3-27. No ammonia was detected in any of the samples.

**Table 3-27. Ammonia Scrubbers Sample Results**

<b>Source</b>	<b>GN65</b>	<b>GN66</b>	<b>GN67</b>	<b>GN68</b>	<b>Units</b>
NH <sub>4</sub> <sup>+</sup>	<10	<10	<10	<10	mg/L

No detectable ammonia was scrubbed from the offgas by the SME ammonia scrubber. The ammonia scrubber did not remove ammonia from the offgas system as the SME pH is approximately five, and the ammonium is tied up as ammonium nitrate in the slurry.

3.2.12 *GN65-68 Lessons Learned*

What should be done differently in future back-to-back SME cycles? Testing can always be improved upon and the following are the author's thoughts on what changes might be prudent in future back-to-back SME testing:

1. Complete a REDOX measurement prior to completing the first run.
2. Videotaping the experiments throughout is also recommended. This would help to identify when foamovers happen. In addition, making sure a camera was present in the lab for still photos is essential in documenting interesting observations.
3. This testing was completed at design basis conditions. Future testing should be completed at prototypic processing conditions. This will lengthen the testing but will be more realistic as it would duplicate the time at temperature, which affects antifoam degradation, antifoam addition amount, anion destruction, and steam stripping.
4. Varying the conditions for the back-to-back runs will allow gathering more information in an attempt to better understand DWPF SME processing. The GN66-68 runs were

planned to be identical. For example, varying the waste loading or solids concentration in the SME heel would allow testing at various slurry rheologies to help in understanding rheological impacts such as fouling of coils.

## 4.0 Conclusions

Five back-to-back Sludge Receipt and Adjustment Tank (SRAT) cycles and four back-to-back Slurry Mix Evaporator (SME) cycles were successful in demonstrating the viability of the nitric/glycolic acid flowsheet. The testing was completed in FY13 to determine the impact of process heels (approximately 25% of the material is left behind after transfers). In addition, back-to-back experiments might identify longer-term processing problems. The testing was designed to be prototypic by including sludge simulant, Actinide Removal Product simulant, nitric acid, glycolic acid, and Strip Effluent simulant containing Next Generation Solvent in the SRAT processing and SRAT product simulant, decontamination frit slurry, and process frit slurry in the SME processing. A heel was produced in the first cycle and each subsequent cycle utilized the remaining heel from the previous cycle. Lower SRAT purges were utilized due to the low hydrogen generation. Design basis addition rates and boilup rates were used so the processing time was shorter than current processing rates.

Significant processing findings identified in the five SRAT cycles include:

- Low hydrogen generation (<0.0005 lb/hr hydrogen peak, <0.077% of SRAT limit of 0.65 lb/hr). This is 0.25% of the Lower Flammability Limit.
- Complete destruction of nitrite in SRAT cycle
- Stable SRAT slurry pH post acid addition (<5)
- Several small foamovers were noted
- No fouling of heating rods (similar to steam coils)
- There was less elemental mercury and more dark crystalline mercury recovered in subsequent cycles. Some of the mercury, likely a mercury film on a gas bubble, floated and some bypassed the Mercury Water Wash Tank without being collected. This has not been noted in previous simulant testing.
- No dimethyl mercury generation was detected by the mass spectrometer
- Hexamethyldisiloxane, an antifoam degradation product, was detected by the mass spectrometer and Fourier Transformed InfraRed analyzer. This may be useful in determining the effectiveness of the antifoam
- Oxygen was completely consumed in 3 of the 5 cycles, just after initiating boiling
- The REDOX measured in the glass product made by combining the SRAT product with frit at 36% waste loading was 0.46 – 0.55  $\text{Fe}^{2+}/\Sigma\text{Fe}$ , much higher than the 0.1 target.
- No detectable ammonia was removed by the Ammonia Scrubber

Significant processing findings identified in the four SME cycles include:

- Low hydrogen generation (<0.0076 lb/hr hydrogen peak, 3.4% of SME limit of 0.228 lb/hr). This is 0.63% of the Lower Flammability Limit.
- Stable pH throughout SME processing (<5)
- The heating rods (similar to steam coils) were fouled by thick deposits during the later decon water evaporation and frit dewater stages of the SME cycle.
- The REDOX measured in glass made from SME Product was (0.22 – 0.28  $\text{Fe}^{2+}/\Sigma\text{Fe}$ ). There was no REDOX target for the SME cycles as the ratio of oxidants and reductants was established by the SRAT product used for this testing. No nitric acid or glycolic acid was used in this testing.
- No detectable ammonia was removed by the Ammonia Scrubber

## 5.0 Recommendations

### *Recommendations for Improving R&D testing*

- Complete the SRAT cycles using the same recipe as a previous successful experiment. In these experiments, the REDOX was high and this could have been prevented by completing a series of SRAT cycles first and using the conditions from the optimum experiment for the back-to-back experiments. In addition, the product from the optimum experiment could serve as the heel so that each experiment would include a heel.
- Videotaping the experiments throughout is also recommended. This would help to identify when foamovers happen and help to understand the collection of mercury in the MWWT. In addition, making sure a camera was present in the lab for still photos is essential in documenting interesting observations.
- This testing was completed at design basis conditions. Future testing should be completed at prototypic processing conditions. This will lengthen the testing but will be more realistic as it would duplicate the time at temperature, which affects antifoam degradation, antifoam addition amount, anion destruction, and steam stripping.
- Varying the conditions for the five runs will allow gathering more information in an attempt to better understand DWPF SRAT processing. Runs GN61-64 were identical. For example, varying the SRAT dewater amount would allow testing at various slurry rheologies to help in understanding rheological impacts such as fouling of coils.
- Digestion and analysis of the collected MWWT mercury would help in determining the mass of Hg collected. The mass of mercury is likely overestimated, as the assumption is that it is elemental Hg. For example, if some of the mercury is present as calomel ( $\text{Hg}_2\text{Cl}_2$ ) or mercuric oxide, the Hg mass can be overestimated by 15%. Although the mercury is dried out in the dessicator, there is likely some water, sludge solids and antifoam present with the mercury. Identification of the forms of mercury is also suggested.
- DWPF rarely transfers mercury or drains the Mercury Water Wash Tank. Consider returning the contents of the Mercury Water Wash Tank after previous run to better simulate processing conditions instead of starting with a clean vessel and distilled water.
- The presence of ARP and MCU strip effluent make a huge difference in processing. These should be included in future experiments as much as possible. However, the organic added with the strip effluent likely has no impact on processing and could be eliminated. The solvent was added to the kettles as planned in only two of the five experiments – in two of the experiments it was added too slowly and then sped up and in a third experiment the syringe pump was bumped, adding the remaining contents faster than planned. Elimination of the solvent feed would also simplify the experiments without losing significant processing information.

### *Recommendations to improve the project or plant operations*

- An improved REDOX equation is needed to produce melter feed with the appropriate REDOX ratio.
- At the conclusion of ARP and strip effluent additions, the steam flow should be reduced to keep from overheating vessel contents. This is likely the cause of some foamovers in DWPF.
- A good practice to minimize coil fouling is to monitor the steam pressure and steam flow. There should be a direct correlation between flow and pressure. When it takes more pressure to get the same flow, the slurry is either very thick or the coils are starting to foul.

- Another good practice is to calculate the steam coil heat transfer coefficient and monitor this during boiling. It would be expected to decrease slightly as the slurry is concentrated but recovering to the same value after each decon blast or frit slurry addition.

## 6.0 References

- <sup>1</sup> Pickenheim, B.R., M.E. Stone, *SRAT Alternative Reductant Feasibility Assessment – Phase I*, SRNL-STI-2009-00120, Savannah River National Laboratory, Aiken, SC, February 2009.
- <sup>2</sup> Pickenheim, B.R., M.E. Stone, J.D. Newell, *Glycolic-Formic Acid Flowsheet Development*, SRNL-STI-2010-00523, Rev 0, Savannah River National Laboratory, Aiken, SC, November 2010.
- <sup>3</sup> Lambert, D.P., B.R. Pickenheim, M.E. Stone, J.D. Newell, D.R. Best, *Glycolic - Formic Acid Flowsheet Final Report for Downselection Decision*, SRNL-STI- 2010-00523, Rev 1, Savannah River National Laboratory, Aiken, SC, March 2011.
- <sup>4</sup> Lambert, D.P., M.E. Stone, J.D. Newell, D.R. Best, J.R. Zamecnik, *Glycolic-Nitric Acid Flowsheet Demonstration of the DWPF Chemical Process Cell with Sludge and Supernate Simulants*, SRNL-STI-2012-00018, Rev 1, Savannah River Site, Aiken, SC 29808 (2012).
- <sup>5</sup> Fellingner, T. L., *Phase II – Nitric-Glycolic Acid Testing*, HLW-DWPF-TTR-2013-0003, Rev 0, Savannah River Site, Aiken, SC 29808 (2012).
- <sup>6</sup> Lambert, D.P., *Task Technical and Quality Assurance Plan for Phase II CPC Testing for Nitric-Glycolic Flowsheet Development*, WSRC-RP-2012-00762, Rev. 0, Savannah River Site, Aiken, SC, 29808 (2012).
- <sup>7</sup> Koopman, D. C., A. I. Fernandez, and B. R. Pickenheim, *Preliminary Evaluations of Two Proposed Stoichiometric Acid Equations*, SRNL-L3100-2009-00146, Savannah River Site, Aiken, SC, 29808 (2009).
- <sup>8</sup> Stone, M. E., *Lab-Scale CPC Equipment Set-up*, SRNL-ITS-2006-000742011-00127, Savannah River Site, Aiken, SC 29808 (2011).
- <sup>9</sup> SRNL L29 Manual, Procedure ITS-0094, Rev. 7, *Laboratory Scale Chemical Process Cell Simulations*, SRNL, Aiken, SC, 29808.
- <sup>10</sup> Lambert, D.P., “GN60-64 ARP/MCU Heel Study”, Experiment O7787-00055-03, SRNL E-Notebook (Production); Savannah River National Laboratory, Aiken, SC 29808 (2013).
- <sup>11</sup> Lambert, D.P., “GN65-68 SME Heel Study”, Experiment O7787-00055-05, SRNL E-Notebook (Production); Savannah River National Laboratory, Aiken, SC 29808 (2013).
- <sup>12</sup> Best, D.R., *Anion Analysis by Ion Chromatography for the Alternate Reductant Program for the Defense Waste Processing Facility*, SRNL-STI-2010-00389, Savannah River National Laboratory, Aiken, SC, June 2010.
- <sup>13</sup> Manual L29, Procedure ITS-0052, Rev. 2, *Heat Treatment of Waste Slurries for REDOX ( $Fe^{2+}/\Sigma Fe$ ) and Chemical Composition Measurement*.
- <sup>14</sup> Koopman, D. C., *Noble Metal Chemistry and Hydrogen Generation during Simulated DWPF Melter Feed Preparation*, WSRC-STI-2008-00002, SRNL, Aiken, SC, 29808 (June 2008).
- <sup>15</sup> Peterson, R. A. White, T. L., Crump, S., Delmau, L. H., *Solvent Extraction External Radiation Stability Testing*, WSRC-TR-2000-00413, Savannah River Site, Aiken, SC 29808 (November 2000).
- <sup>16</sup> Lambert, D.P., M.E. Stone, J.D. Newell, D.R. Best, J.R. Zamecnik, *Glycolic-Nitric Acid Flowsheet Demonstration of the DWPF Chemical Process Cell with Sludge and Supernate Simulants*, SRNL-STI-2012-00018, SRNL, Aiken, SC, 29808 (August 2012).

## **Appendix A. Offgas Data**

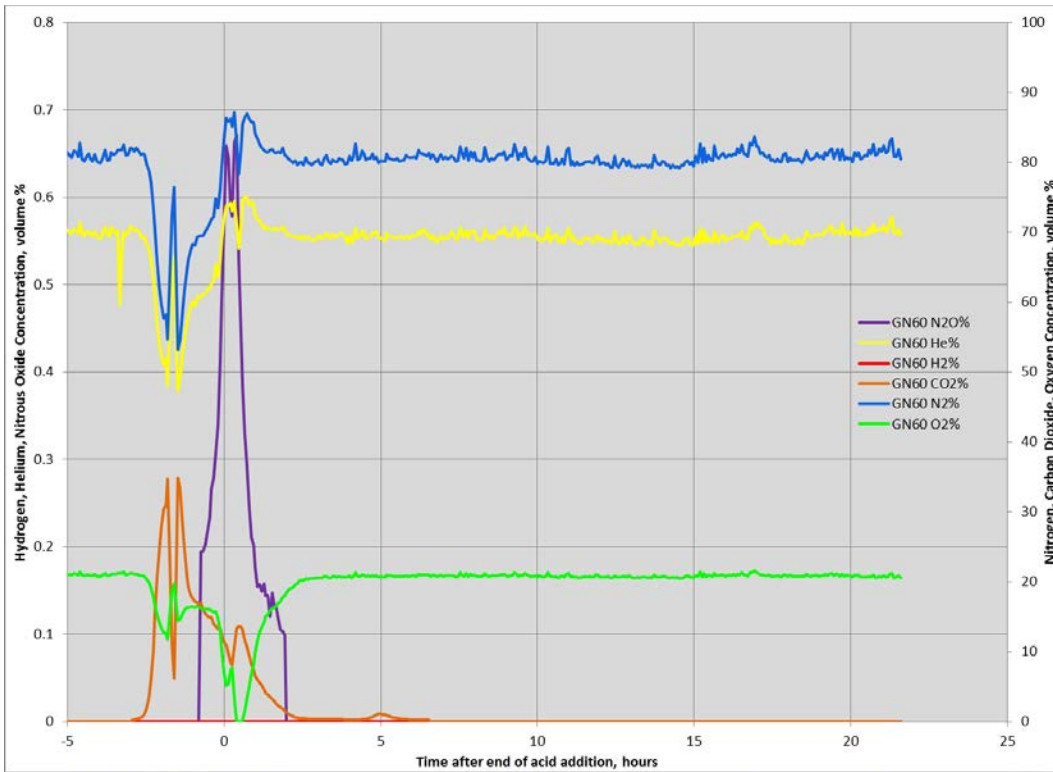


Figure A-1. GN60 Offgas Data

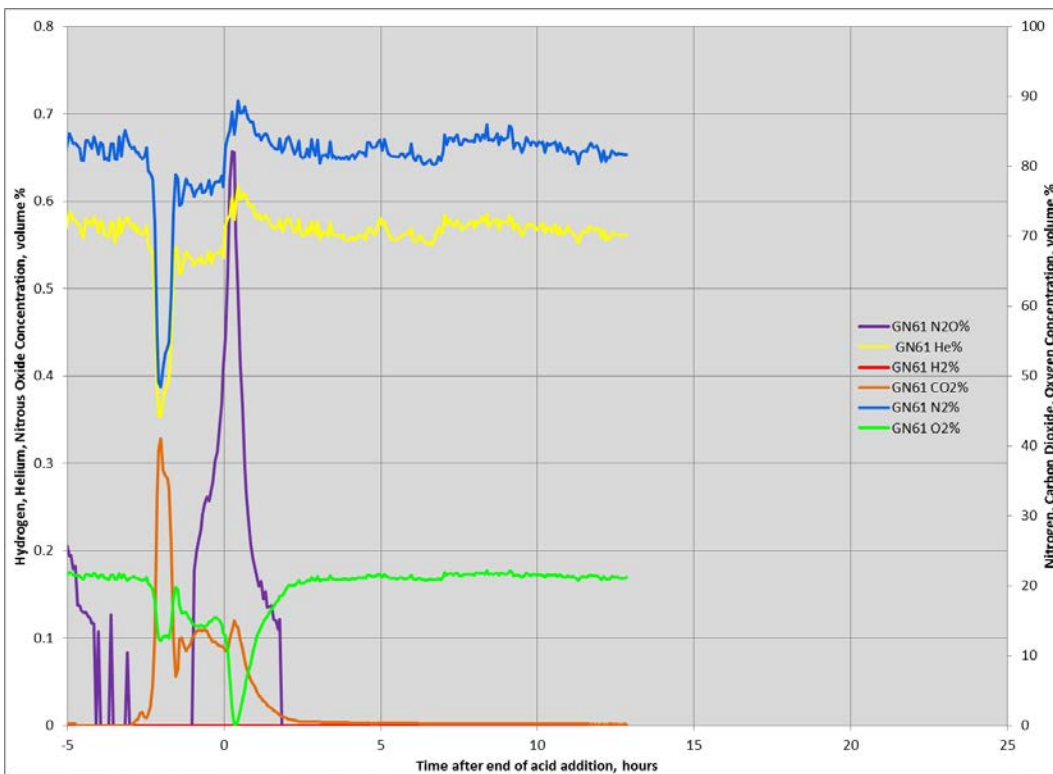


Figure A-2. GN61 Offgas Data

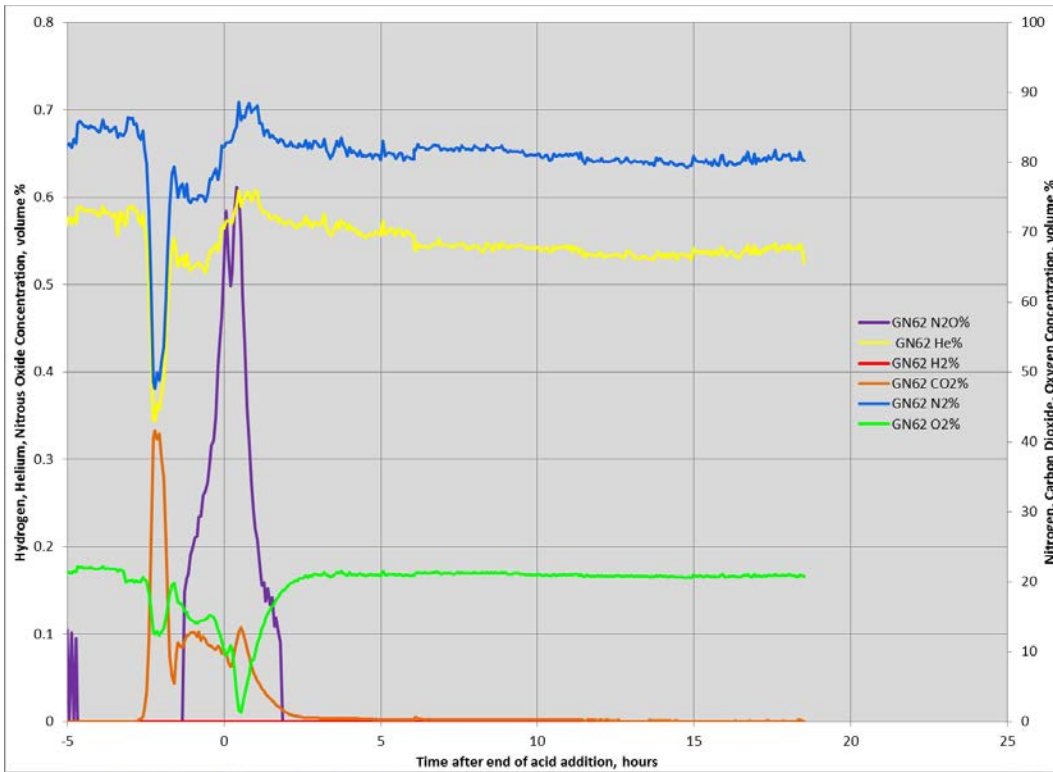


Figure A-3. GN62 Offgas Data

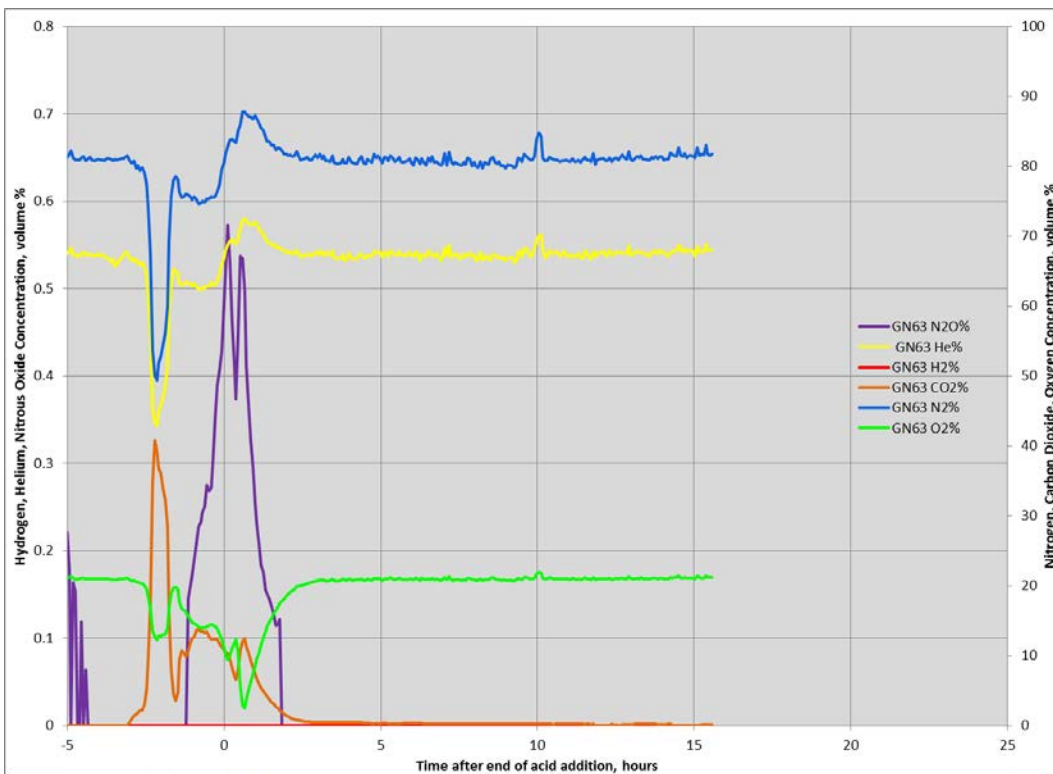


Figure A-4. GN63 Offgas Data

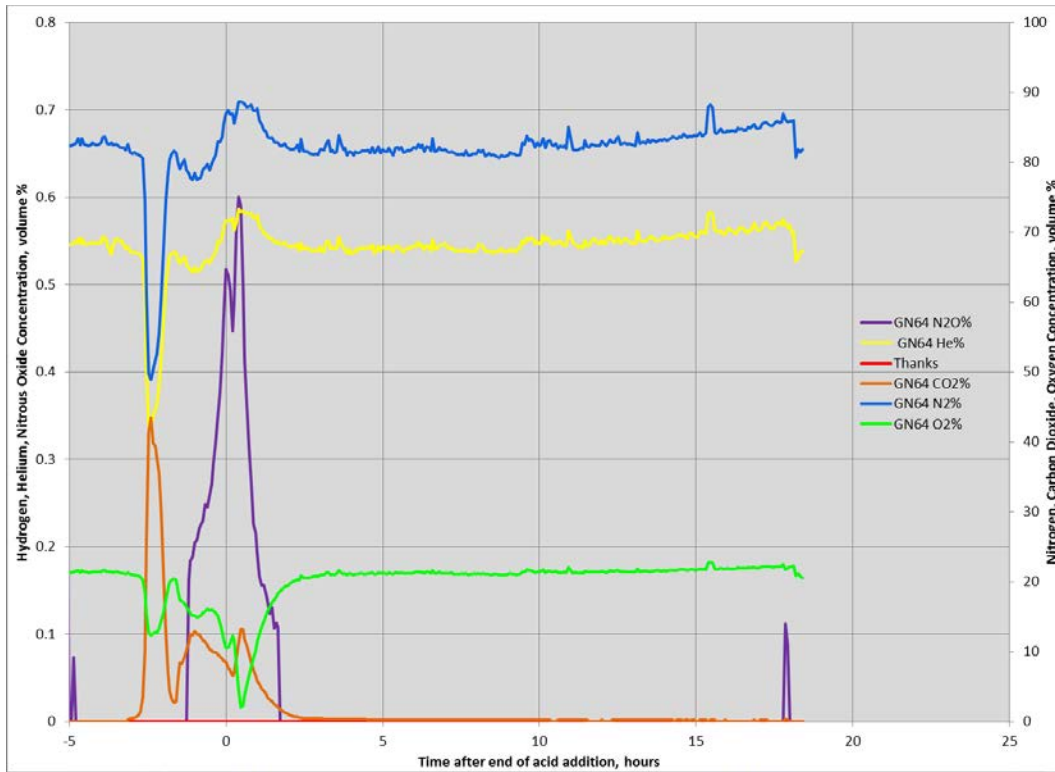


Figure A-5. GN64 Offgas Data

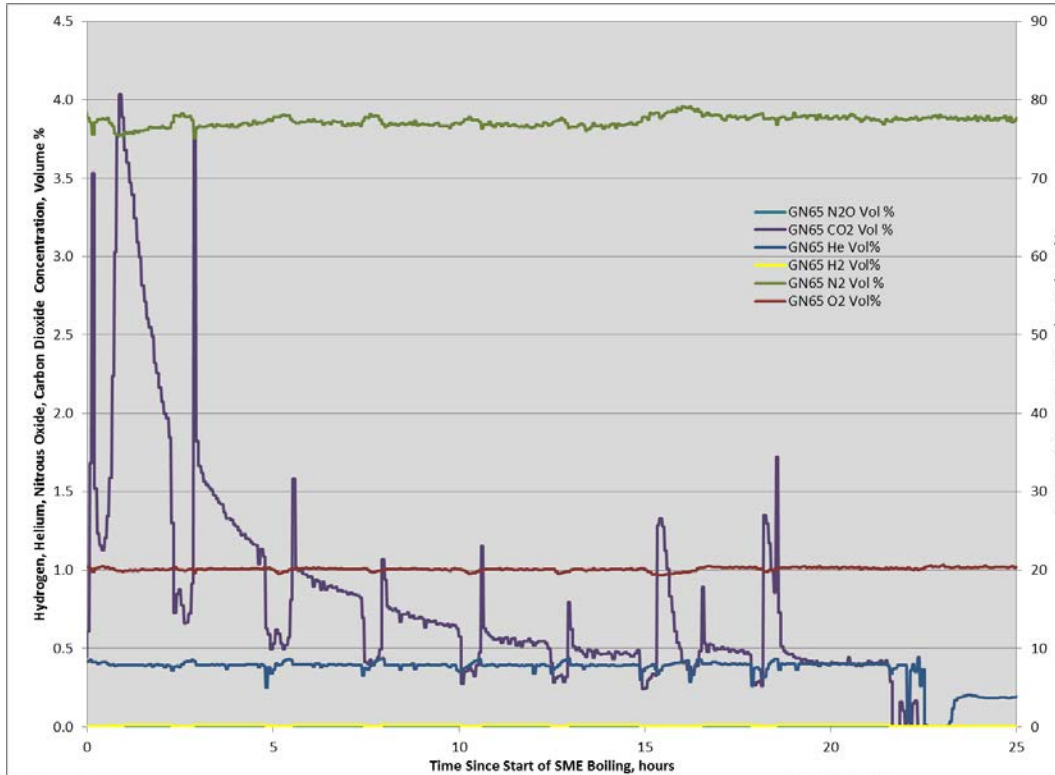


Figure A-6. GN65 Offgas Data

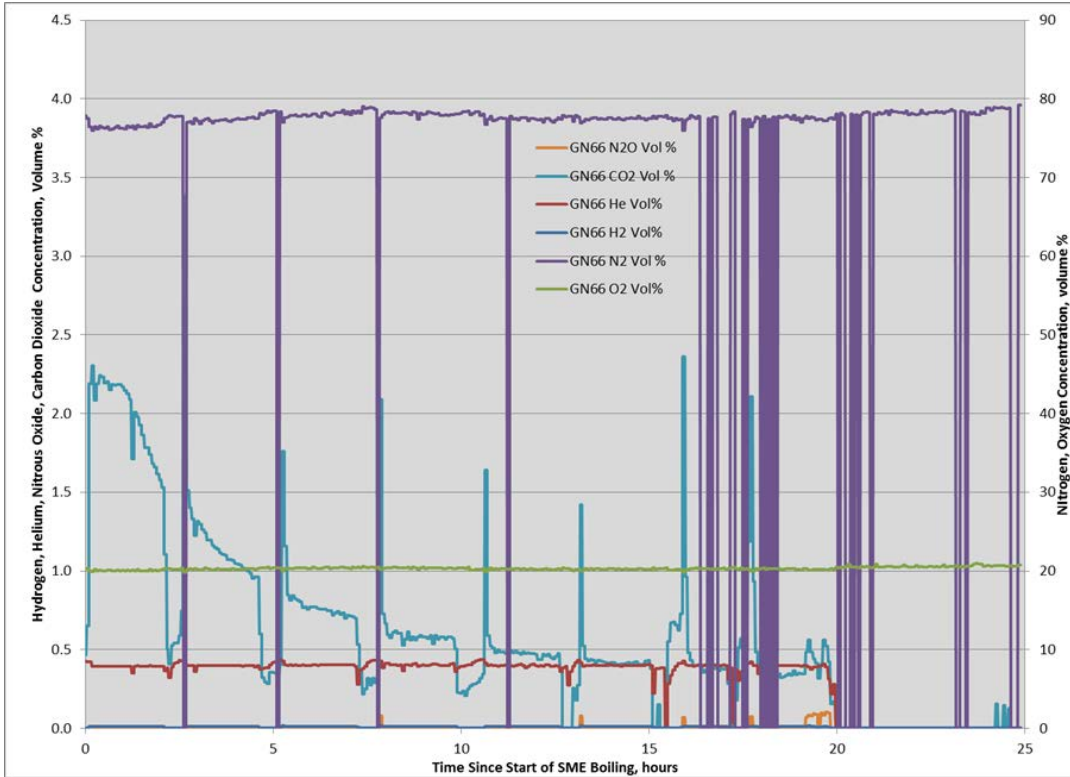


Figure A-7. GN66 Offgas Data

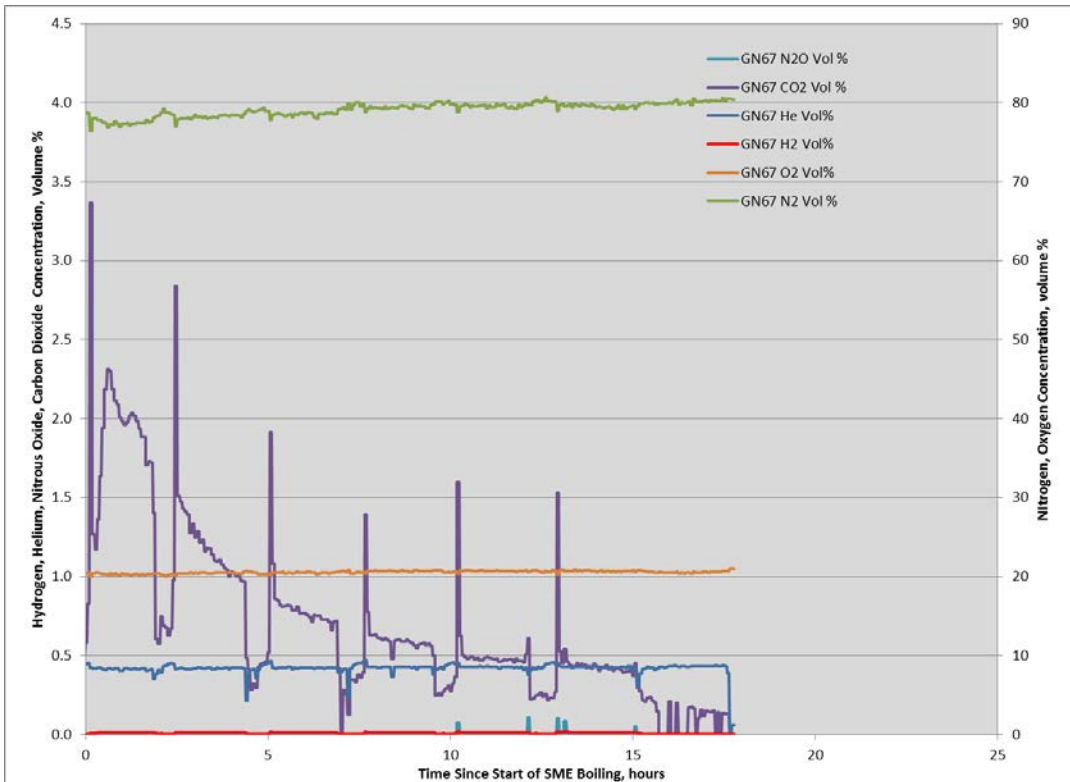


Figure A-8. GN67 Offgas Data

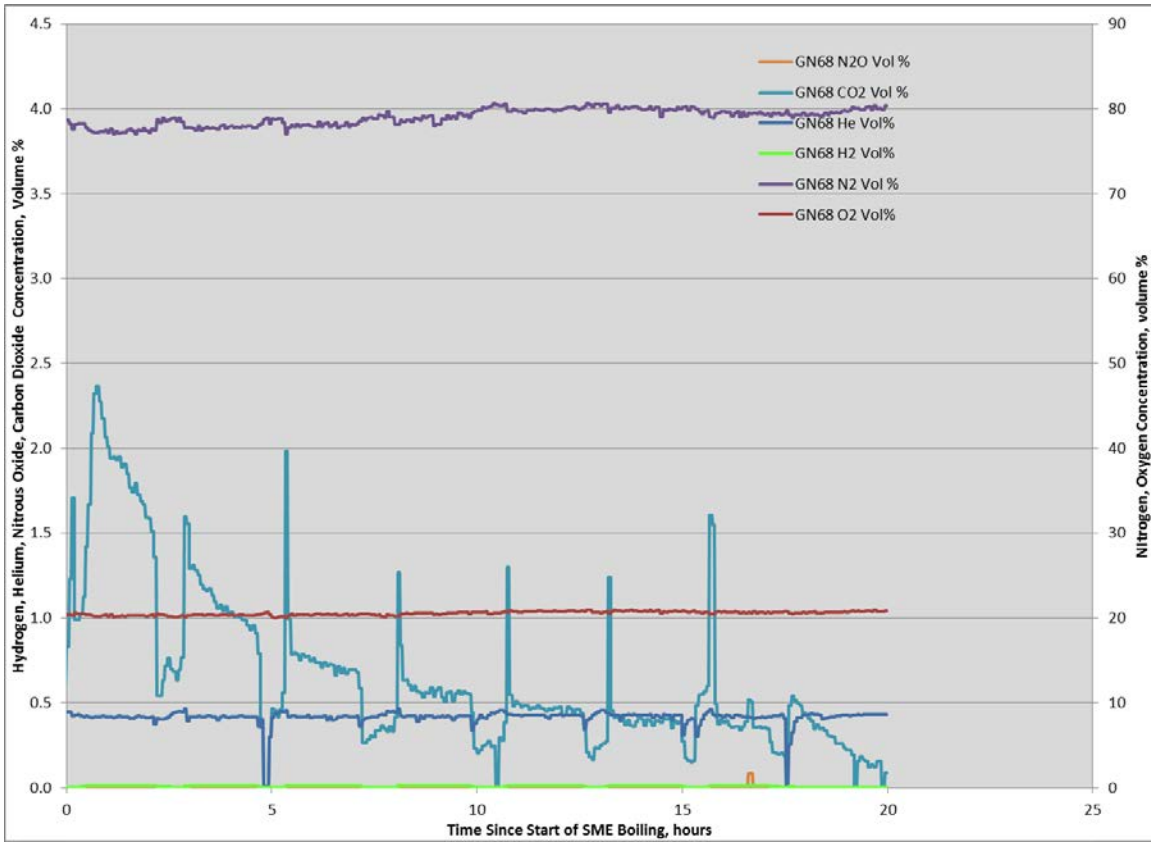


Figure A-9. GN68 Offgas Data

**Distribution:**

T. B. Brown, 773-A  
D. H. McGuire, 999-W  
S. D. Fink, 773-A  
C. C. Herman, 999-W  
E. N. Hoffman, 999-W  
S. L. Marra, 773-A  
F. M. Pennebaker, 773-42A  
Records Administration (EDWS)  
C. J. Bannochie, 773-42A  
E. J. Freed, 704-S  
D. C. Sherburne, 704-S  
J. M. Bricker, 704-30S  
T. L. Fellingner, 704-26S  
J. M. Gillam, 766-H  
B. A. Hamm, 766-H  
E. W. Holtzscheiter, 704-15S  
J. F. Iaukea, 704-27S  
M. T. Keefer, 766-H  
D. D. Larsen, 766-H  
D. K. Peeler, 999-W  
J. W. Ray, 704-S  
H. B. Shah, 766-H  
A. V. Staub, 704-27S  
M. E. Stone, 999-W  
J. D. Newell, 999-W  
J. R. Zamecnik, 999-W  
D. P. Lambert, 999-W  
D. J. Martin, 241-152H  
M. W. Geeting, 241-152H  
T. A. Le, 766-H  
A. R. Shafer, 704-27S  
C. K. Chiu, 704-27S  
S. E. Campbell, 241-152H  
S. P. Mcleskey, 241-152H  
B. A. Gifford, 704-56H  
R. M. Wolfenden, 704-56 H  
K. L. Lang, 704-27S  
P. R. Jackson, DOE-SR, 703-46A  
K. H. Subramanian, 766-H  
J. Best, 999-W